Flexible electronics: novel substrates and transducers

by

Lingju Meng

A thesis submitted in partial fulfillment of the requirements for the degree of

Doctor of Philosophy

in

Solid State Electronics

Department of Electrical and Computer Engineering

University of Alberta

Abstract

Flexible electronics integrate functional electronic devices on paper and plastic substrates, and fill niches complementary to silicon electronics in applications where bending and stretching of devices are required or preferred. Yet, most flexible devices are still more or less facing performance and cost issues. Here, in this thesis, I focused on solving these problems by applying novel substrates and introducing new working mechanisms of transducers which can be categorized into 4 sub-projects in 4 chapters.

First, the fabrication and characterization of silver (Ag) nanoparticle-based strain sensors on the water-soluble nanofibril paper, a cellulose nanocrystal (CNC) produced flexible film, by stencil lithography were shown. This is the first demonstration of using polydimethylsiloxane (PDMS) stencils to pattern metal electrodes on water-soluble substrates. For the large London dispersion force between the PDMS stencil and the flexible substrate, the stencil can conformably cover the substrate and prevent metal diffusion into the area under the stencil when metal electrodes are patterned on water-soluble nanofibril papers. PDMS stencil lithography avoids damage to the cellulose nanofibril paper, which conventional photolithography processes lead to, without compromising the resolution in patterning metal electrodes. Our strain sensors have a high sensitivity with a gauge-factor of over 50 in strain testing, which is the highest among reported strain sensors fabricated on water-soluble substrates.

Additionally, a substrate modification strategy by using chlorine (Cl) to achieve both trap-site suppression and a hydrophilic surface was proposed. The chlorine can effectively passivate the surface dangling bonds and charged hydroxyl groups while creating a hydrophilic surface. On this modified substrate, the contact angle between the water droplet and the silicon dioxide (SiO_2) substrate can be as small as 20° and this strategy is also feasible for other polymer and inorganic substrates. For a proof-of-concept demonstration, we fabricated a lead sulfide (PbS) colloidal quantum dot (CQD) ink-based field-effect transistor on a Cl-passivated substrate, and the device showed a mobility as high as $4.36 \times 10^{-3} cm^2/V \cdot s$, which indicates effective trap-site suppression. This device also enables the potential of the Cl-passivated substrates for CQD inks with water or other polar solvents.

Furthermore, a new class of sensors, digital microelectromechanical (MEM) sensors, for wearable technologies was designed and fabricated. Our digital MEM sensors were implemented with the PDMS bridge on flexible substrates, and provided digital signal outputs based on electrical insulating-to-conducting transitions. By engineering the PDMS bridge structure, we could tune the sensitivity of the digital MEM sensor for various applications. These digital MEM sensors were used in bending tests: they were integrated on glove fingers and used to detect gestures. These sensors were also used as force sensors: they were used on human wrists to monitor heart rates. The device was experimentally found to maintain its performance level even after 10000 cycles of bending or pressing. The digital output of our devices allows a higher tolerance for device fabrication to be set. Furthermore, our devices can be engineered for desired specifications in various potential applications.

Ultimately, CQD touch sensors employing PDMS triboelectric films were demonstrated. The electrical response of touching activity is enhanced by incorporating CQD field-effect transistors (FETs) into the device architecture. Thanks to the use of the CQD thin film as a current amplifier, the field-effect CQD touch sensor shows a fast response to various touching materials, even being bent to a large curvature. It also shows a much higher output current density compared to a PDMS triboelectric touch sensor.

Preface

This thesis is an original work by Lingju Meng under the supervision of Dr. Xihua Wang at Department of Electrical and Computer Engineering, University of Alberta.

Chapter 2 of this thesis has been published as L. Meng, S.M. Mahpeykar, Q. Xiong, B. Ahvazi, & X. Wang, "Strain sensors on water-soluble cellulose nanofibril paper by polydimethylsiloxane (PDMS) stencil lithography". RSC Advances, 6(88), 85427-85433, 2016. I was responsible for experimental design, device fabrication, data analysis and drafting manuscript. S.M. Mahpeykar was involved in device fabrication. B. Ahvazi led the group that synthesized CNC and X. Wang was the corresponding author and conceived this project. All authors are involved in manuscript editing.

Chapter 3 of this thesis has been published as L. Meng, T. Zeng, Y. Jin, Q. Xu & X. Wang, "Surface-Modified Substrates for Quantum Dot Inks in Printed Electronics". ACS Omega, 4(2), 4161-4168, 2019. I conceived and planned this project, designed and carried out the experiments, analyzed the data and drafted the manuscript. T. Zeng developed the ink synthesis process. Y. Jin and Q. Xu assisted in all experiments and X. Wang was the corresponding author and supervised the whole project. All authors are involved in manuscript editing.

Chapter 4 of this thesis has been published as L. Meng, S. Fan, S.M. Mahpeykar & X. Wang, "Digital microelectromechanical sensor with an engineered polydimethylsiloxane (PDMS) bridge structure". Nanoscale, 9(3),

1257-1262, 2017. I planned this project, designed and carried out the device fabrication and characterization experiments, analyzed the data and drafted the manuscript. S. Fan developed the heart rate detection device. S.M. Mahpeykar assisted in the device fabrication and X. Wang was the corresponding author and conceived and supervised the whole project. All authors are involved in manuscript editing. This work involves data collection of flexible sensors attached on human body (authors themselves) in the research lab. Upon discussion with the Research Ethics Office at the University of Alberta, it's confirmed that this work does not constitute human participant research that requires REB review. Thus, ethics approval is not required.

Chapter 5 of this thesis has been published as L. Meng, Q. Xu, S. Fan, C.R. Dick & X. Wang, "Field-effect enhanced triboelectric colloidal quantum dot flexible sensor". Applied Physics Letters, 111(18), 183103, 2017. and L. Meng, Q. Xu, L. Dan & X. Wang, "Single-walled carbon nanotube based triboelectric flexible touch sensors", IEEE/TMS Journal of Electronic Materials, 2019. I conceived and planned this project, designed and carried out all the experiments, analyzed the data and drafted the manuscript. Q. Xu assisted in device fabrication. L. Dan designed the mechanical testing experiments and X. Wang also contributed in conceiving this project and supervised the whole project. All authors are involved in manuscript editing.

To the heroes marching towards the Sea of Stars
For inspiring me in my journey.

You can know the name of a bird in all the languages of the world, but when you're finished, you'll know absolutely nothing whatever about the bird... So let's look at the bird and see what it's doing – that's what counts.

– Richard P. Feynman, Nobel Physics Prize Laureate.

Acknowledgements

Almost every legendary work possesses a great opening. This thesis is no way near a legendary work. So I'll just quote the great opening from Gabriel Garcia Marquez in *One Hundred Years of Solitude* to open my thesis.

Many years later, as he faced the firing squad, Colonel Aureliano Buendía was to remember that distant afternoon when his father took him to discover ice.

I don't know 20 or 30 years later, how I would think of the days when I first started my PhD career. But today, I still clearly remembered how I started it 6 years ago, how I make it here. I wouldn't say I am satisfied with what I've got. I made mistakes. Or I should say a lot of mistakes. But what really matters is the journey. Even if I did have a time capsule, I wouldn't rewind this 6 years. They make me who I am now.

Thank my supervisor, Dr. Xihua Wang. Many said picking a supervisor is like doing a lottery. But I don't think so. I trust my insight to others. Till now, I still do and I think I made the best choice I can. Sincere gratitude to Dr. Wang for the freedom he gives me in research. This freedom really builds me up, releases my potentials. I admire his patience, his views without prejudice towards everything. These are treasures in my life. Sincere thanks also go to my committee members, Dr. Douglas Barlage, Dr. Manisha Gupta, Dr. Hyun-Joong Chung and Dr. Woo Soo Kim.

Many thanks to my mom and dad. They supported me unconditionally

every time. They encouraged me to experience more and live a full life. They told me not to chase anyone else, just be the best me. Without their encouragements, I won't stick so long in my research career.

Thank my colleagues, Mr. Qiwei Xu, Mr. Qiuyang Xiong and Mr. Shicheng Fang. They helped me a lot in my research and always inspired me with their insights and optimism. My sincere thanks also go to other colleagues, Mr. Carson R. Dick, Dr. Seyed Milad Mahpeykar, Dr. Jue Wei, Dr. Xinmei Liu, Mr. Farsad Imtiaz Chowdhury, Ms. Shulan Xiao, Dr. Tao Zeng and Mr. Kaustubh Sinha.

My gratitude goes to my dearest friends, Dr. Chuangxin Lin, Dr. Qianli Ma, Dr. Zongyao Li, Ms. Zhengyu Ma, Mr. Yun Zhang and Mr. Jiangchen Li. They always support me when I was down.

My grand appreciation goes to Ms. Hui Wang, who always put my feelings at first and tolerated my stupid, mind-blowing ideas and bad temper. Thanks again for being my closest one. I know I'm like a hedgehog, which makes it not easy.

For those who have given me hard times, I still thank you. You make me who I am now.

The city of Edmonton never really caught my heart. I was a boy brought by a flight. But with time passing by, this town makes me feel like my second hometown. She calls up my tender feelings from heart. The great food in Sugarbowl and Biera and the summer time on Whyte Avenue and Jasper Avenue fascinate me a lot. The night lights in the University Hospital reminds me of those days when I was a child, saw my mom at her night shift. At last, thank the city of Edmonton.

Contents

List of Tables

List of Figures

List of Abbreviations

Ag	Silver
CNC	Cellulose nanocrystal
PDMS	Polydimethylsiloxane
Cl	Chlorine
SiO_2	Silicon dioxide
PbS	Lead sulfide
CQD	Colloidal quantum dot
MEM	Microelectromechanical
FET	Field-effect transistor
TFT	Thin film transistor
PECVD	Plasma-enhanced chemical vapor deposition
a-Si	Amorphous silicon
ITO	Indium-tin oxide
CTE	Coefficient of thermal expansion
WVTR	Water vapor transmission rates
LED	Light emitting diode
RMS	Root mean square roughness
OLED	Organic light emitting diode
OTR	Oxygen transimission rate
PET	Polyethylene terephthalate
PEN	Polyethylene naphthalate
PI	Polyimide
TCO	Transparent conducting oxides
FTO	Fluorine-doped tin oxide

AZO	Aluminum-doped zinc oxide
AMOLED	Active matrix organic light emitting diode
PEDOT:PSS	Poly(3,4-ethylenedioxythiophene) polystyrene sulfonate
TTF-TCNQ	Tetrathiofulvalene-7,7,8,8-tetracyanoquinodimethane
OTFT	Organic thin film transistor
CNT	Carbon nanotube
TMD	Transition metal dichalcogenide
BP	Black phosphorus
RF	Radio frequency
MOS	Metal-oxide-semiconductor
ALD	Atomic layer deposition
CyEPL	Cyanoethylpullulan
TFE	Thin-film encapsulation
FEOL	Front-end-of-line
BEOL	Back-end-of-line
PU	Polyurethane
EPLaR	Electronics on Plastic by laser release
SUFTLA	Surface-free technology by laser annealing
JILO	Joule heating induced lift-off technology
FlexUP	Flexible universal plane technology
P(VDF-TrFE)	Poly(vinylidene fluoride-trifluoroethylene)
PES	Polyethersulfone
BIPV	Building-integrated photovoltaics
CIGS	$Cu(In,Ga)Se_2$
PCE	Power-conversion efficiency
LCD	Liquid crystal display
FTIR	Fourier-transform infrared spectroscopy
XPS	X-ray photoelectron spectroscopy
EDX	Energy dispersive X-Ray analysis
MEMS	Microelectromechanical system

T-FET	Triboelectric field-effect transistors
DSL	Domestic substance list
DMF	N,N-dimethylformamide
AFM	Atomic force microscopy
SEM	Scanning electron microscopy
GF	Gauge factor
OTS	Octadecyltrichlorosilane
TMS	Transmission electron microscopy
ODE	1-octadecene
TMS2-S	Hexamethyldisilathiane
RFID	Radio-frequency identification
IZO	Indium zinc oxide
SWCNT	Single-walled carbon nanotube

Chapter 1

Introduction

1.1 What is flexible electronics?

Electronics deal with the emission, flow and control of electrons.[1] In order to engineer the behaviors of electrons, electrical circuits with various electronic components are usually involved. The electronic components can be divided into three categories: the active device, which can actively control the flow of electrons (diodes, transistors, optoelectronic devices, sensors etc.), the passive devices, which cannot control the flow of electrons (resistors, capacitors, inductors, transformers etc.) and interconnections.

In traditional electronics, almost all the electronic components are rigid, which means they lack the capabilities of being bent, folded, or even stretched. Except in some special scenarios, some interconnections are made to be flexible in order to save spaces such as the cables connected to computer/smartphone's motherboards. In contrast, in flexible electronics, these old concepts are all overturned in flexible electronics. "Flexible electronics—built on substrates like plastic or metallic foil—can be folded, wrapped, rolled, and twisted with negligible effect on its electronic function."[2] To meet this requirement, all the functional devices along with the substrates in a system, not just the interconnections, need to be flexible.

Till now, there have been some subcategories in flexible electronics emerging as hot areas. For example, stretchable electronics[3], which represents the

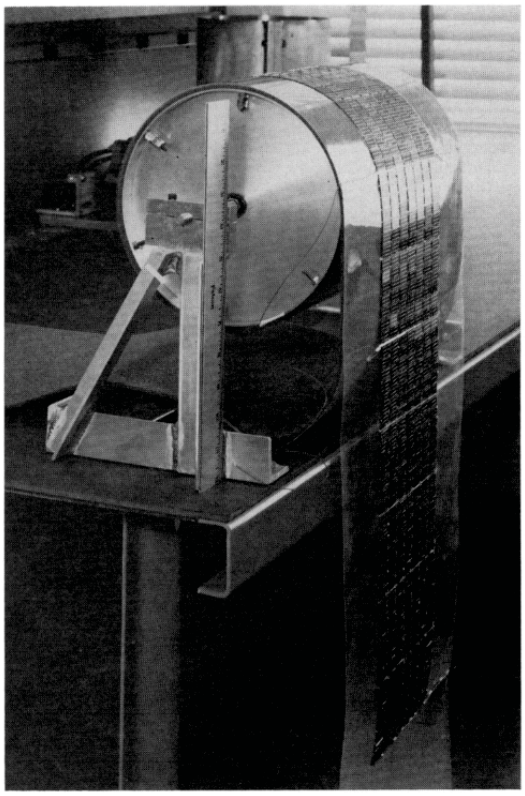

Figure 1.1: Flexible single crystal silicon solar cells by Ray in 1967. **Reprinted from [6] with permission from Institute of Electrical and Electronics Engineers (IEEE).**

electronic devices are not only flexible but also stretchable, and paper electronics[4], which specifically refers to electronic devices assembled on paper substrates. There are also some terms strongly associated and overlapped with flexible electronics but not being subcategories in flexible electronics, for example, printed electronics[5], which involves printing technology, a widely used technology in flexible electronics manufacturing.

1.2 The origination of flexible electronics

Flexible electronics is a time-honored field in electronics. It was born in the 1960s, in the middle of the cold war. The USA and USSR were competing in the 'space race' at that time. The space technologies were thrivingly developing. In 1967, Burt theoretically proved it is possible to change a spacecraft's orbit through continuous small thrusts from a electrical propulsion unit[7].

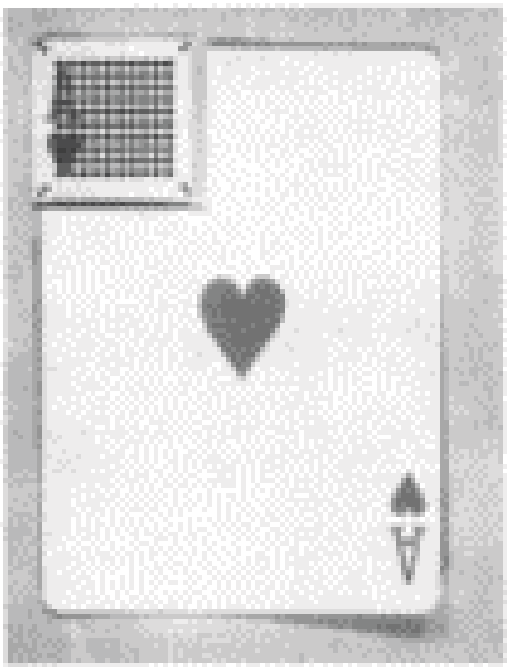

Figure 1.2: Flexible tellurium thin film transistors by Brody in 1967. **Reprinted from [9] with permission from John Wiley and Sons Inc.**

Since the thrusts needed for a spacecraft were small, solar cells emerged as the best option to power the electrical propulsion unit. Naturally, the 'space race' became the power source in solar cell research community during the cold war. Even today, tandem multi-junction solar cells are dominating in space technologies. In order to save the precious space in spacecrafts, researchers were thinking about making solar cells flexible and roll-able to better fit spacecrafts. Since every material will acquire flexibility when its thickness reaches some certain level, the first flexible electronic devices, flexible solar cells, were fabricated on plastic substrates with a thin single crystal silicon layer of $\sim$100 μm as shown in Fig. 1.1.[6], [8]

Following the demonstration of flexible solar cell, Brody and his colleagues developed the first flexible thin film transistors (TFTs) on various flexible substrates.[9], [10] However, both single crystal silicon or tellurium used in these reports were not intrinsically flexible materials. The flexible electronic devices in the 1960s were more of conceptual devices.

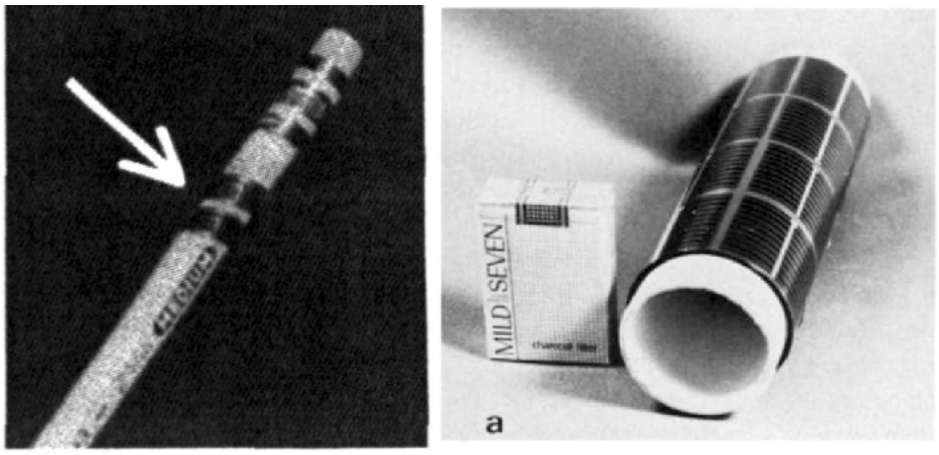

Figure 1.3: Left: flexible amorphous silicon TFT. **Reprinted from [11] with permission from Cambridge University Press.** Right: flexible amorphous silicon solar cell. **Reprinted from [12] with permission from Elsevier.**

The 1970s' energy crisis heavily stimulated the development of low-cost thin film solar cells. The large-scale utilization of plasma-enhanced chemical vapor deposition (PECVD) makes it possible to fabricate high-quality, stress-free amorphous silicon (a-Si) thin films.[13] Since a-Si's amorphous nature, it is a more flexible material than single crystal silicon. The PECVD-produced a-Si films largely reduced the internal stress compared to films produced by traditional heat-triggered CVD, giving the thin films more flexibility. Under these circumstances, a-Si based flexible solar cells on various substrates (stainless steel foil and plastic) had been made in the 1980s as shown the right panel in Fig. 1.3, which could exceed 6% efficiency[12], [14]. In 1995, Wagner developed a-Si based TFT on flexible steel foil substrate as shown in the left panel in Fig. 1.3[11]. Since then, as the technologies had already been mature, the research of flexible electronics in both industry and academia was on a highway.

Nowadays, flexible display technology is the jewel in the crown of flexible electronics. The flexible OLED technology has been commercialized. The details will be covered in the application section.

1.3 Materials for flexible electronics

1.3.1 Substrate materials

For substrate materials, not only the mechanical properties, but also other critical properties, especially the ones that are important in electronic devices need to be thought. They are listed below:

Optical properties: For photonic devices, the optical transparency is always crucial. Meanwhile, the interference caused by optical transparent thin film need to be minimized. What's more, birefringence in optical anisotropic materials is also needed to be minimized in most applications.

Surface roughness: Surface roughness has always been an important consideration in modern electronic devices since thin film fabrication is mostly done on smooth surfaces. In conventional electronics, the average roughness of industrial grade silicon wafer and indium-tin oxide (ITO) glass are as low as 0.2 nm and 0.5 nm, respectively.

Thermal properties: In device fabrication process or different usage scenarios, there may be high-temperature environment introduced. The first thing one needs to take into consideration is the vitrification. For a wide variety of flexible substrates, especially plastic substrates, there is no melting point. However, if the temperature exceeds the glass transition temperature, the material will go vitrification. Their physical and chemical properties will alter irreversibly. In this case, the processing and usage temperature should always be lower than the glass transition temperature, T_g. The other thermal property one needs to consider is the thermal expansion. If the coefficients of thermal expansion (CTEs) of the device layer and substrate don't match, extra internal stress will be introduced into the device which will cause device failure. There is one general rule for this which is $|\Delta CTE \times \Delta T| \leq 0.1-0.3\%$, where ΔCTE is the difference between coefficients of thermal expansion and ΔT is the temperature excursion during processing or using.

Chemical properties: Since the substrate is like 'half encapsulation' for the device, it should be resistant to permeation of water and oxygen in order to protect the device in some applications. In organic devices, water is the vicious killer. The widely quoted requirement for water vapor transmission rates (WVTRs) in organic TFTs and light emitting diodes (LEDs) of > 10000 h lifetime are $1 \times 10^{-3} g/m^2/day - 1 \times 10^{-1} g/m^2/day$ and $1 \times 10^{-6} g/m^2/day$. The substrate permeation rate of water must be below these values. What's more, the substrate should be chemically inert at least to the solvents which will be utilized in fabrication or usage process.[15] For example, ethanol, acetone etc.

Mechanical properties: As stated in the previous section, a flexible electronic device needs to maintain its performance at different bending, compressing or twisting working scenarios such as bending, compression or twisting. So a certain amount of Young's modulus is required for the flexible substrate to avoid device failure. For stretchable electronic devices, a smaller Young's modulus is required. The Young's modulus difference between the substrate and the device layer should also be designed in a certain degree to avoid potential device crack in extreme working conditions. What's more, the surface of the substrate needs to be hard enough to support devices.

Flexible substrates can be roughly categorized into: 1) Metal foil, 2) Polymer film, 3) Thin glass, 4) Paper.

As stated in the historical facts of flexible electronics, **metal foils** have been one of the earliest flexible substrates for electronic devices because of its easy accessibility. Metal foils are usually fabricated by hammering or rolling. When the thickness of the metal foil is below 125 μm, it will gain a certain degree of flexibility. Metal foils have their own advantages, especially regarding the thermal properties and chemical properties. Metal itself can endure a very high temperature. Its thermal expansion coefficient is small which will avoid

unwanted shrinkage during fabrication process. In addition, metal is a good conductor both thermally and electrically, which makes it a good candidate for flexible photovoltaic devices.

However, the shortcomings of metal foils are also obvious. First, it's opaque, which limits its applications in photonic devices. Second, surfaces of metal foils are usually very rough. For example, the RMS of an typical aluminum foil is usually over 1 μm.[16] This roughness will be an obstacle to construct thin films on it. However, there are strategies to overcome it. Such as polishing or planarized coating. Third, considering the chemical properties, metals will react with various chemicals especially acids and bases. This property will make a lot of semiconductor manufacturing techniques unavailable. At last, fatigue is also a problem of the metal foil substrates.[17]

There are a lot of metals which can act as substrates. The first and most widely used is steel. Since Brody's first TFT on steel foil substrate, there has been a lot of applications of flexible electronic devices constructed on steel foil substrate besides TFT[18], such as solar cells[19], LEDs[20] and even displays[21], [22]. In industry, STS304 and STS430 stainless steels are the most popular flexible substrates for flexible organic light emitting diode (OLED) displays and a-Si solar cells.[23], [24] Titanium foil is another popular flexible metal foil substrate especially in solar cell research community because its work function is low enough to form ohmic contact with highly doped n-type semiconductor like TiO_2 which means it can act as an electrode for solar cells. Dye-sensitized solar cell and perovskite solar cell all have been fabricated on flexible Ti foil before.[25], [26]

Polymer flexible substrates have drawn more and more attentions in flexible electronics research community in recent years. Polymer substrates consist various different classes of materials. Generally speaking, it will offer better optical transparency which will enable more photonic applications. The surface roughness can also be controlled in a very small range. The mechanical

properties are usually good for flexible electronic devices, like low Young's modulus, large ultimate tensile strength. However, regarding the thermal and chemical properties, there are still some issues. The coefficients of thermal expansion of polymer films are usually higher. The most important thing is, compared to metal foil, water and oxygen permeation is a big problem for polymer substrates. Their WVTR and oxygen transimission rate (OTR) are shown in Table. 1.1. So barrier encapsulation is usually required in industrial-grade organic flexible devices. The flexible encapsulation techniques will be covered in following subsections.

Polymer	**WVTR** ($g/m^2/day$)	**OTR** ($cm^3(STP)/m^2/day$)
PE	1.2–5.9	70–550
PP	1.5–5.9	93–300
PS	7.9–40	200–540
PET	3.9–17	1.8–7.7
PES	14	0.04
PEN	7.3	3
PI	0.4–21	0.04–17
PDMS	0.02	106

Table 1.1: Water and oxygen permeation rate for different flexible substrates.[27]–[32]

The most popular polymer substrates are **polyethylene terephthalate (PET)**, **polyethylene naphthalate (PEN)** and **polyimide (PI)**. PET and PEN are semi-crystalline polymers, while PI is an amorphous polymer. PET and PEN have similar molecular structures. They are transparent in visible light range. PET has a Young's modulus around 2.9 GPa. PEN has a slightly larger one around 4.4 GPa because the naphthalene in its structure in replacement of benzene in PET. They are both resistant to most ordinary solvents but their working temperatures are relatively low (150–200 °C). PI is the most popular polymer flexible substrate of which the most famous is the Kapton^{TM} brand from DuPont. It's the most outstanding polymer flexible substrate regarding all parameters. However, PI absorbs blue light which limits its application in photonic devices. The key parameters of these 3 substrates are summerized in Table. 1.2

	PET	**PEN**	**PI**
Optical property	Transparent	Transparent	Absorb blue light
Surface roughness	46 nm (Mylar)	20 nm (Teonex)	44 nm (Kapton^{TM} HN)
Thermal property	CTE: $30 - 65 \times 10^{-6}$ Working temp.: 115-170°C	CTE: 21×10^{-6} Working temp.: 155°C	CTE: $30 - 65 \times 10^{-6}$ Working temp.: >300°C
Chemical property	Good	Good	Good
Mechanical property	Young's modulus: 2.9 GPa Shear modulus: 2.2 GPa	Young's modulus: 4.4 GPa Shear modulus: 2.3 GPa	Young's modulus: 3.0 GPa Shear modulus: 2.7 GPa

Table 1.2: Key parameters of PET, PEN and PI.[13], [33]

Glass can also behave as a flexible substrate when its thickness is lowered to around 100 μm while it still inherits the advantages of conventional thick glass substrates. For example, its optical property is extraordinary for flexible electronic devices. If its thickness is less than 30 μm, the transmission can be >90%. Regarding the surface roughness, if polished properly, the RMS of thin glass substrate can be as small as 1 nm. Its thermal stability is also good both dimensionally and structurally. Just like thick glass, thin glass is also resistant to all common solvents. However, when it comes to its disadvantage, its mechanical properties need to be taken into consideration. Glass is a brittle material which will complicate material processing. So in industry, polymer coatings are usually laminated or printed onto the surface of glass to enhance its elasticity. Various research applications have been developed on thin glass substrate, especially optoelectronic devices, like lasers[34], solar cells[35], [36] and TFTs[37]. Yet the most important application of thin glass substrate in industry is substrates for large displays. However, the thickness of them is around 500 μm which means it's not flexible because the driven force in this area is 'lighter' and 'thinner'. However, due to needs for energy-saving, carbon-reducing and flexibility, glass substrates on large-area displays are becoming thinner and thinner. It can be expected to reach 200 μm in 10 to 20 years.[38]

Technically speaking, **paper and textiles** might not be perfect candidates for substrates in flexible electronic devices. They are not transparent, the surface is rough, they can't endure a lot of solvents. Especially for paper, the mechanical property is not ideal because it's not an elastic material. However, they have advantages which are almost unbeatable. They are cheap and can be directly fit in various using scenarios for IOT and wearable electronics applications.

The biggest problem in paper and textile electronics is the surface roughness problem. New device fabrication strategies can solve the thermal and chemical problems. This part will be covered in the manufacturing technology section. Paper and textiles are built by long fibers. There is no way to construct a smooth surface by those long fibers. In paper electronics, in order to conquer it, two methods are widely used. The first one is doing extra coatings. The coatings may consist a barrier layer such as latex for easy chemical processing and a smoothing layer like Kaolin to reduce surface roughness. The RMS of smoothed surface can be as low as 55 nm, which is competitive even compared to a polymer film.[39] The other approach is to replace the long cellulose fibers with cellulose nanocrysals or nanofibers. By using those small crystals to build a state-of-art paper for electronic applications, the roughness can be limited to a very low value.[40]–[42] For the textile, one doesn't really want to modify the surface because it's better to keep the fabric 'fabric'. One approach is to directly attach the flexible devices onto the surface of fabric materials.[43] The other one is about fabricating a new fabric which include the materials to build up the devices.[44] The pictures of these two types of sensors are shown below in Fig. 1.4. Nowadays, there are more advanced techniques to integrate electronic devices on paper or textile like μTransfer printing.[45]

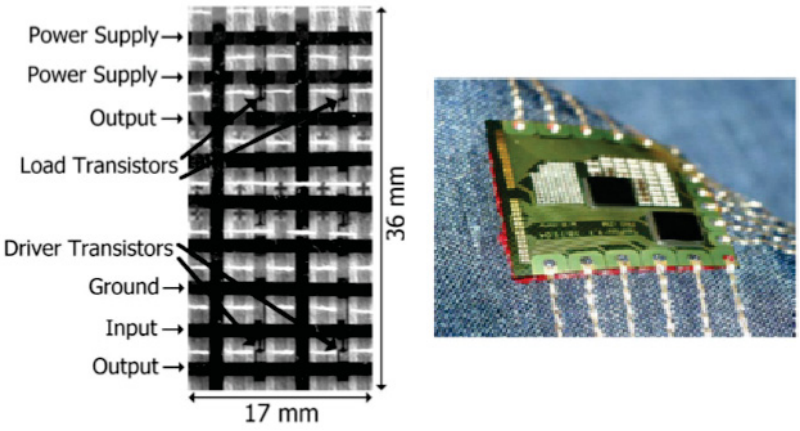

Figure 1.4: Left: woven on textile. **Reprinted form [44] with permission from Institute of Physics (IOP) publishing Ltd.** Right: Devices directly patched on textile. **Reprinted from [43] with permission from IEEE.**

1.3.2 Conducting materials

Conducting materials are an essential element in electronic devices. They are building blocks for contacts, electrodes and interconnects. Conducting materials can be generally categorized into inorganic conductors and organic conductors.

There are many **inorganic conductors**. The earliest flexible conductors are **metals**. Just like metal foils, metal thin films are also flexible. However, they are easy to generate cracks with some applied strain on metal thin films. What's more, metals are not transparent. Thus, **transparent conducting oxides (TCOs)** emerge as new candidates for flexible conductors. The TCOs are usually semiconductors. But after being highly doped to degenerate semiconductors, they will behave like metals. ITO is the most widely utilized TCO. However, indium is not an abundant element on Earth. The cost of ITO films is high. Therefore, the fluorine-doped tin oxide (FTO) and aluminum-doped zinc oxide (AZO) are also utilized in electronics in recent years. However, the mechanical properties of TCOs are not ideal for flexible electronics. Even though the electrodes on rigid touch screens are made from TCOs, but they can not be directly transplanted to flexible touch screen because they are too

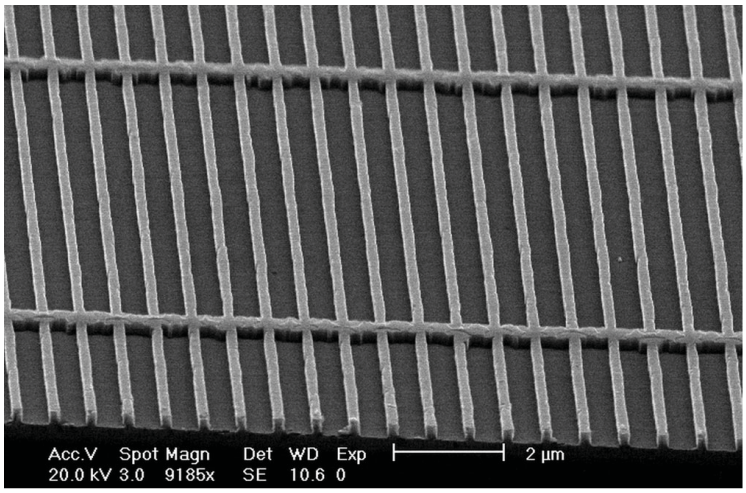

Figure 1.5: Aluminum mesh sturcture for touch panel. **Reprinted from [47] with permission from John Wiley and Sons Inc.**

brittle. By now, **metal mesh** is the best industrial grade solution. It has been used in Samsung's flexible active matrix organic light emitting diode (AMOLED) display with Y-OCTA technique. By patterning metals (Cu, Al etc.) in mesh-shape (micron-size mesh shape) as shown in Fig. 1.5, they can gain flexibility and transparency at the same time.[46]

Metal nanowire is another emerging new material for flexible electrodes. By forming nanoscale metal networks, which is even thinner compared to metal meshes, the film can acquire good transparency and elasticity. However, the stability and conductivity are a trade-off in this material. The capping ligands outside metal nanocrystals will lower the conductivity. Another class of materials for novel flexible electrodes is **carbon materials**, in which **graphene** and **carbon nanotube** are in the spotlight of both academia and industry. The graphene and carbon nanotube structures are shown in Fig. 1.6. Graphene is a single carbon layer with hexagonal structure. It is a 0-bandgap material and the carrier mobility is extremely high. Since graphene is a single-atom-layer material, its optical transmission is high. Carbon nanotube also has good conductivity and high transparency. However, these two materials are facing the same cost issue. There are some easy, low-cost synthesis methods. But a compromise in conductivity will exist.

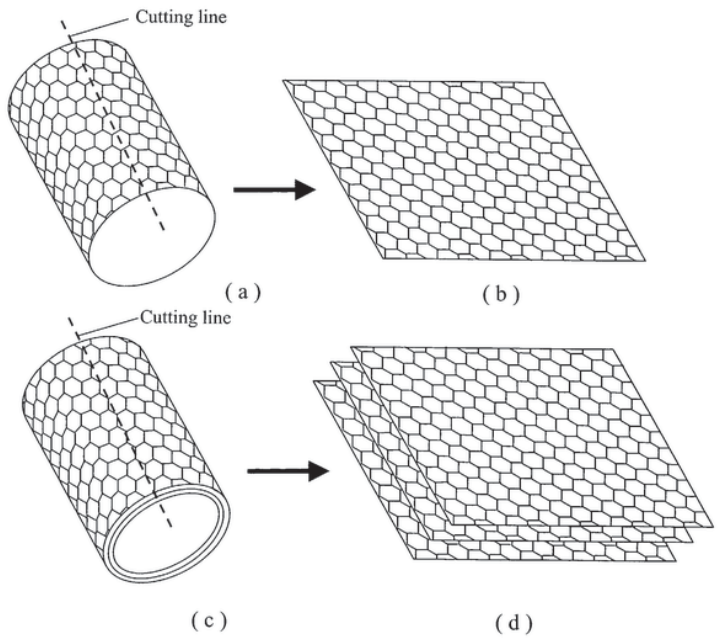

Figure 1.6: Sketches of graphene and carbon nanotube. **Reprinted from [48] under fair use provision.**

Organic conductors are elastic and transparent which make them a good candidate for flexible conductors. One type of conducting organic material is conducting by their unique molecular or crystalline structures. They are **polymer ionic electrolyte**, **conjugated polymer**, **charge-transfer complex** and **metal-chelation polymer**. The polymer ionic electrolyte conducts by ions, which limits its application in flexible electronics. The most popular organic conducting material is conjugated polymer. Conjugated polymers have π bond, which will de-localize carriers, making it conductive. **poly(3,4-ethylenedioxythiophene) polystyrene sulfonate (PEDOT:PSS)** is the most widely used conjugated polymer material. After proper treatment, it will acquire metallic properties. In this case, it has been widely employed as electrodes in photonic devices.[49]–[51] The charge-transfer complex usually consists at least two different molecules. These two types of molecules act as donor and acceptor and are weakly bonded to each other by covalent bonds. Some of them, like **tetrathiofulvalene-7,7,8,8-tetracyanoquinodimethane (TTF-TCNQ)**, have been used to fabricate

source and drain electrodes on organic thin film transistor (OTFT) and proven to have higher performance.[52] The metal-chelation polymer is made up by organic structures and metal ions. Its carrier transport mechanism also attibutes to the π bond. It has been proved to be a good conductive polymer, but there are still very few research about its application as flexible conductors. However, this material has a great potential because of its metal-organic structure, which makes it more stable than conventional organic materials.

The other type of organic conducting material is hybrid organic conductors. The hybridization strategy is usually to dope a conductive filler into a flexible polymer material. Hybrid conducting materials can date back decades ago. The conductive rubber electrode was filed as a patent in 1971.[53] Conductive PDMS was also reported in recent years.[54] Conductive hydrogels are emerging nowadays as another promising candidate for flexible conductors.[55], [56] Even micro-patternalble conductive hydrogel was also reported this year.[57]

Besides the advantages mentioned before, organic conductors have tunable Fermi levels. However, on the road to its large-scale application, the performance and air-stability are still the obstacles ahead.

1.3.3 Semiconducting materials

Similar as the conducting materials, there are also **inorganic semiconductor materials**. As stated in the conductor part, **TCOs** are a candidate for flexible semiconducting materials if not degenerated. **A-Si** is another flexible material which has already commercialized in flexible display backplane technology as mentioned before.

Besides these materials, **carbon materials** are also drawing considerable attentions. Carbon nanotube (CNT) is one of these materials which is considered to take torch from silicon beyond Moore's law. In 2017, IBM T.J. Watson Research Centre demonstrated high-mobility CNT FET and 5-stage

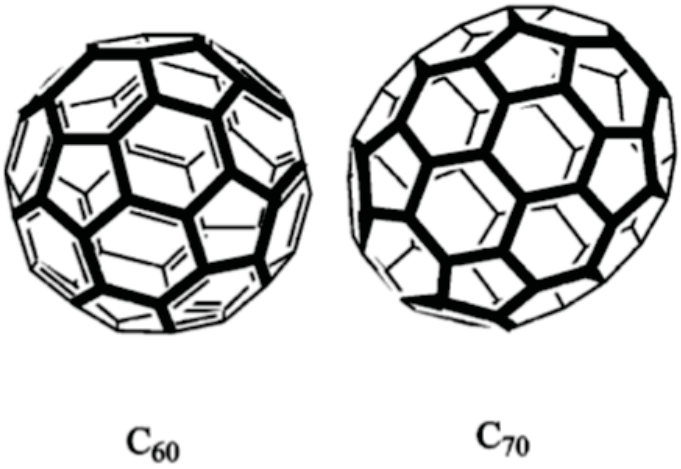

Figure 1.7: Structures of C60 and C70 fullerenes. **Reprinted from [58] with permission from Royal Society of Chemistry.**

CNT FET ring oscillator with an amazing working frequency of 2.8 GHz.[59], [60] The field-effect mobility of CNTs can exceed $10^5\ cm^2 \cdot V^{-1} \cdot s^{-1}$. It was introduced into flexible electronics more than 10 years ago. Up to medium-scale CNT integrated circuits have been demonstrated.[61], [62] Its application as the active matrix in OLED display has also been demonstrated.[63] Graphene is another carbon material. However, its bandgap is 0. But researchers have found ways to produce sizable bandgap in graphene by doping, stacking and making graphene to nanoribbons.[64] The semiconducting graphene has been employed in sensing devices like strain sensor and photodetector. However, as a high-mobility semiconducting material, its full potential lies in logic devices. The reported highest electro mobility tested in a graphene FET is over $10^5\ cm^2 \cdot V^{-1} \cdot s^{-}1$.[65] Due to this extremely high intrinsic mobility, graphene becomes a competitive candidate for 'beyond Moore's law' electronic materials. There is also reported inverter made by graphene which exhibit a gain of 1.9.[66] Fullerene is another class of carbon materials. It is an allotrope of carbon whose molecule consists of carbon atoms connected by single and double bonds so as to form a closed or partially closed mesh, with fused rings of five to seven atoms. Any fullerene is n-type semiconductor. C60 and C70 are the

two mostly investigated materials in fullerenes. Their structures are shown in Fig. 1.7. Fullerene was first predicted by Eiji Osawa at Toyohashi University of Technology in 1970. In 1985, researchers from University of Sussex and Rice University first created fullerene. Fullerene has been utilized in various flexible devices.[67] It should be noted that fullerene's potential in electronics, especially C60 and C70's, has been exploited in perovskite solar cells. C60 and C70 or their mixtures can be a good electron transport layer.[68] Consequently, this technique has been transferred to flexible perovskite solar cells.[69]

Low-dimensional materials attract a lot of attentions in both academia and industry, especially **0-dimensional materials** and **2-dimensional materials**. QDs are a class of semiconducting 0-dimensional materials. For a semiconductor crystal, if its particle size is smaller than its Bohr radius in all dimensions, it can be called a QD. QDs have a lot of advantages. They have sharp emission, solution processability. What's more, QDs have an extraordinary property, multi-exciton generation (MEG), which is especially important in solar energy harvesting. QDs have been utilized in various flexible devices, including FETs, displays[70], solar cells[71], sensors[72] etc. Flexible QD display is the most promising one in all those applications. Several tech giants, Samsung, LG and TCL, all released their prototype flexible QD displays. Graphene is the earliest 2D material. Since its discovery, there has been plenty of 2D materials emerging. A star class of material is transition metal dichalcogenide (TMD) monolayers, in which the most widely used is MoS_2 monolayer. MoS_2 monolayer is known for its huge on/off ratio as large as 10^7.[73] This privileged property renders it the potential to be applied in low-power electronic systems. There have been applications of flexible MoS_2 TFT as the backplane of LED display on wearable system.[74] Black phosphorus (BP) is another popular 2D material emerging in this research community because of its high mobility ($> 1000\ cm^2 \cdot V^{-1} \cdot s^{-1}$) and tunable bandgap (0.3eV-2eV).[75] There has been flexible BP transistors reported.[76] 2D materials were firstly fabricated by mechanical exfoliation. Now, CVD, which is an cost-effective, scalable process industry, is utilized to fabricate 2D materi-

als. In recent years, 2D-material inks were also invented, which enables R2R fabrication for 2D-material flexible electronic devices.[77]

The **organic semiconductors** have been introduced in the flexible organic conductor part.

1.3.4 Insulating materials

Insulating materials are important in radio-frequency (RF) devices and metal-oxide-semiconductor (MOS) structures. To evaluate the insulating material for flexible electronics, one not only needs to consider the flexibility, but also should pay more attentions to its **dielectric constant** and **interface defects**. High-dielectric-constant materials (high-κ) can effectively reduce the leakage current without compromising in thickness. The interface defects will trap and detrap carriers just like capacitors, but in a very low speed. So high density of interface defects will lower the operational speed of devices, especially TFTs. Like other functional material, the insulating materials can also be categorized into inorganics, organics and hybrids.

Inorganics are the most common ones in dielectric materials, like **SiO_2, Al_2O_3, ZrO_2 and HfO_2**. Their dielectric constants are listed below as shown in Table. 1.4:

Material	**Dielectric constant**
SiO_2	3.9
Al_2O_3	10.1
ZrO_2	25
HfO_2	25

Table 1.3: Comparison of dielectric constants of different inorganic materials.[78]

It can be seen that ZrO_2 and HfO_2 have much larger dielectric constants than others'. So these two materials are largely utilized in both academia and industry. But these oxides can not be fabricated by PVD. Because PVD produces too many defects and the grain size is too small. To one aspect, the grain boundaries and defects inside the crystal will lower its actual dielectric

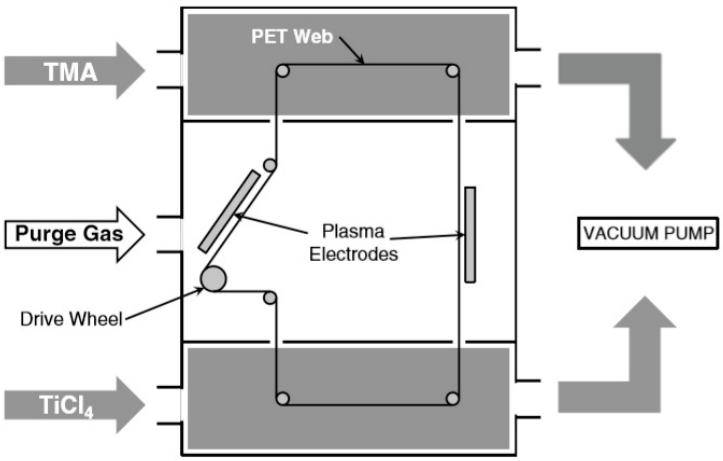

Figure 1.8: Schematic of a R2R ALD reactor. **Reprinted from [79] with permission from Elsevier.**

constant. To another aspect, the interface defects will largely lower the working frequency of the device. In this case, atomic layer deposition (ALD), a tool which can produce good lattice, is widely used to fabricate oxide insulating materials. However, ALD is costly and not compatible with a lot of mass-production process in flexible electronics. Recently, R2R ALD reactor (Fig. 1.8) was introduced into industry which makes ALD compatible with R2R printing and brings a bright future for ALD in flexible electronics.

Organic insulation materials have good flexibility and solution processablity which make them super compatible with flexible electronic fabrication process. They also have low density of defects. Their main problem is the low dielectric constant. It's shown in the table below:

It can be seen except cyanoethylpullulan (CyEPL), the dielectric constants are all pretty low, which will limit organics in low-voltage devices. It should be noted that Cytop^{TM}'s interface defect density is low enough to be compared to inorganics.

Hybrid materials

In order to acquire both fabrication compatibility and large dielectric constant, in recent years, researcher have tried ways to hybridize inorganic and organic materials. For example, $BaTiO_3$ nanoparticles can enhance the dielectric con-

Material	Dielectric constant
PVDF	6
PVA	5-10
PVP	3.1-4.2
PS	2.5
PDMS	2.6
PMMA	3.2-3.6
Parylene-C	3.15
CYTOP	2.1
CYEPL	12-18.5

Table 1.4: Comparison of dielectric constants of different organic materials.[5], [78], [80]

stant of polymers.[81]

1.3.5 Encapsulation materials

As mentioned before, almost all devices, especially organic and flexible devices need encapsulation to elongate devices' lifetime. For traditional rigid devices, the encapsulation is usually a glass lid or metal lid filled with nitrogen and CaO to avoid air and absorb moisture. However, it's not applicable on flexible devices. Fig. 1.9 shows 3 different flexible encapsulation strategies. Fig. 1.9a) shows a modified lid encapsulation method. The glass or metal lid can be thinned to fit flexible devices. Another approach is shown in Fig. 1.9b), the device can be sealed by a polymer cap with oxide barrier layer on top. However, because this technique is complicated especially the epoxy part, the tech giants like Samsung and LG all move to thin-film encapsulation as shown in Fig. 1.9c). The thin-film encapsulation is called TFE in which the most famous is the Barix^{TM} technique developed by Vitex as shown in Fig. 1.10. It's alternating layers of AlO_x and UV-crosslinked polymers which can effectively blockade oxygen and water while still maintain its flexibility. This technique is what Samsung is applying on their commercial OLED device. LG is doing a similar structure but by ink-jet printing technology from Kateeva. However, because of the appearance of R2R ALD technology. Both Samsung and LG are moving towards single barrier film of Al_2O_3 by R2R ALD which enables

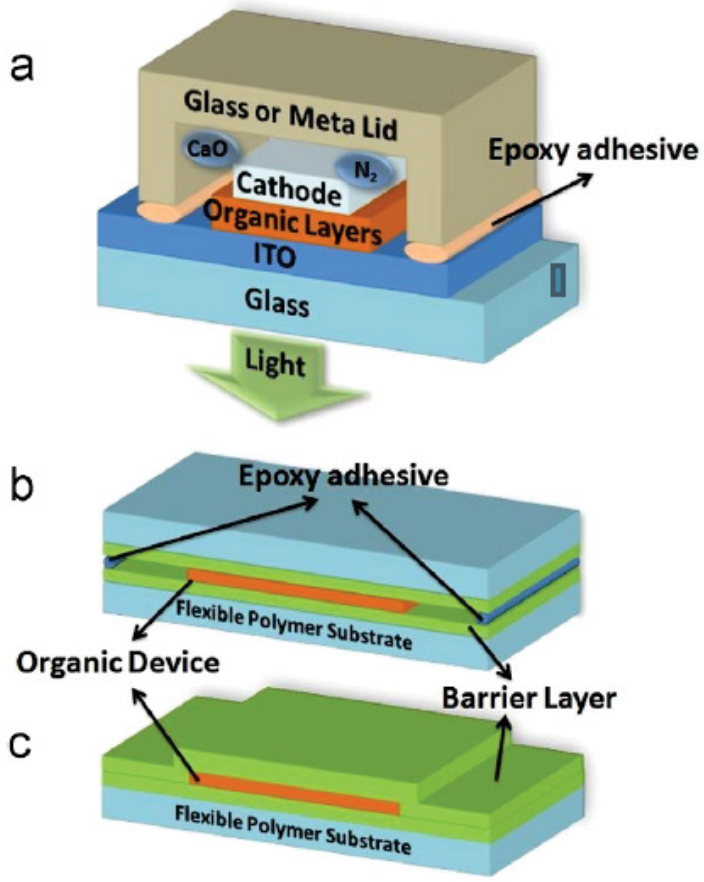

Figure 1.9: a) Glass lid encapsulation b) flexible barrier film encapsulation c)thin-film encapsulation. **Reprinted from [82] published by Elsevier under CC-BY 4.0 license.**

less cost and easy production.

1.4 Manufacturing technologies in flexible electronics

Traditional semicondutor manufacturing technologies consist two major process: the front-end-of-line (FEOL) process and back-end-of-line (BEOL) process. The FEOL process includes patterning, deposition, etching, ion-implantation, oxidization etc. while the BEOL includes packaging, interconnection etc. In these processes, patterning and deposition are the most important two. These are the main steps to create a device. The patterning techniques can be divided

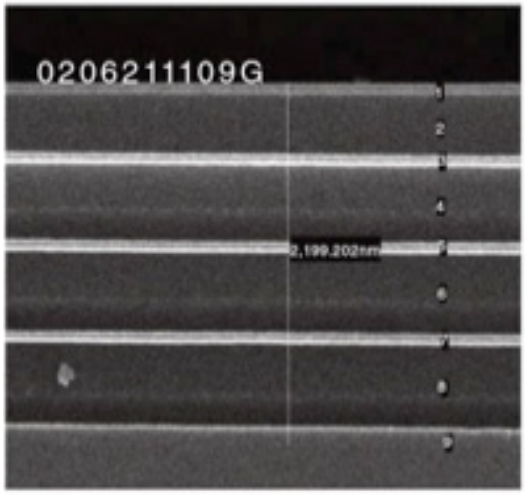

Figure 1.10: SEM image of the Barix^{TM} TFE. **Reprinted from [5] with permission from John Wiley and Sons Inc.**

into direct patterning and indirect patterning. Direct patterning can directly pattern the materials which are used to construct the device while the indirect patterning usually introduces an intermediate material to be patterned first, then the functional material will be transferred. Since direct patterning doesn't need an intermediate material, the deposition will be an additive manufacturing method while the indirect patterning is always associated with subtractive manufacturing. In this case, the manufacturing for flexible electronics can be categorized by patterning and deposition techniques: direct patterning+additive deposition (printing technologies) and indirect patterning+subtractive deposition (lithography technologies).

1.4.1 Printing technologies

The printing technologies can date back to more than 2000 years ago. But it hasn't been applied to electronic manufacturing until the recent decades. In 1994, Garnier reported an all-polymer FET with ink-jet printed graphite electrodes.[83]. A few years later, all-printed FETs have been developed by utilizing screen printing and ink-jet printing.[84], [85] The biggest advantage of printing is the cost and being scalable. Printing technologies abandoned the complex mask fabrication step, which saves material and shortens production

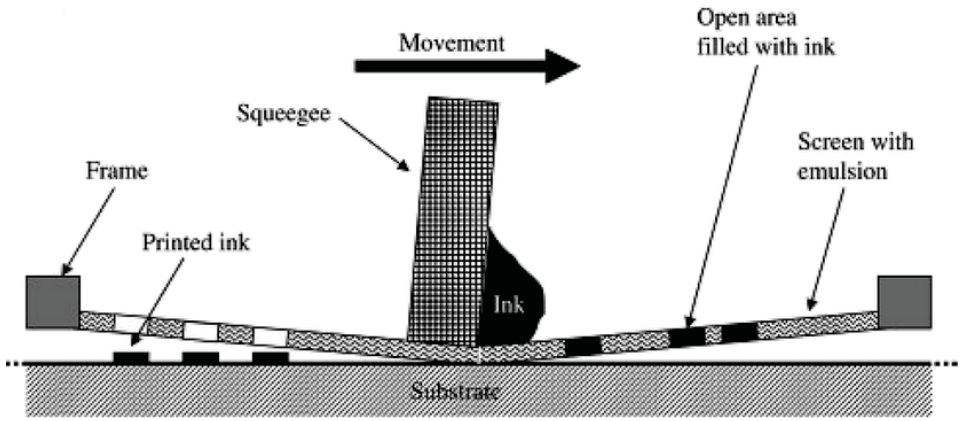

Figure 1.11: Schematic of screen printing process. **Reprintef from [86] with permission from Royal Society of Chemistry.**

cycles. They both contribute to lower device fabrication cost. Many printing techniques are compatible with R2R process which means they are scalable. However, the resolution is always a drawback in printing technologies.

Screen printing

Screen printing first appeared in China 1000 years ago. However, it hasn't been popular until the silk mesh was introduced into it in the 19th century. The screen printing is considered to be one of the most versatile printing techniques and it is also one of the earliest printing technique been introduced into electronics. The screen printing process is shown in Fig. 1.11. There will be a screen made by silk or stainless steel. The squeegee will move on the screen and squeeze the ink through the meshes so as to stick onto the substrate. The equipment for screen printing is cheap and simple and this process is totally compatible with R2R fabrication. But it requires inks which is not volatile and has some certain degree of viscosity. This makes the patterns printed by screen printing thick (10-100 μm). Now with some advanced techniques, screen printing can reach a resolution of 10 μm.

The biggest application of screen printing in electronics is the lining Ag electrodes on solar cells. By now, since the flexible TFT by screen printing, there has been tons of flexible electronic devices developed utilizing screen print-

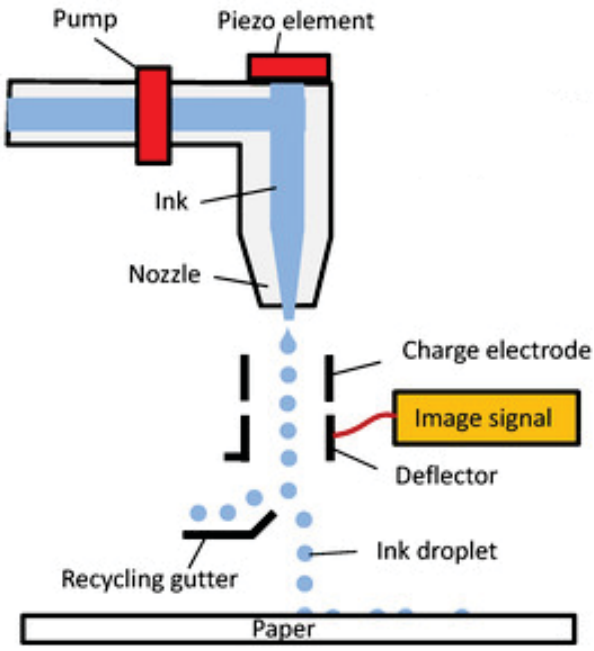

Figure 1.12: Schematic of ink-jet printing process. **Reprinted from [93] published by MDPI under CC-BY 4.0 license.**

ing. Since the screen-printed features are thick and large, usually, it's used to fabricate part of the device such as conductors[87], dielectrics[88] and passive devices[89]. Nowadays in academia, sensing devices[90] and even fully-screen-printed complex devices are developed[91]. In industry, with the introduction of advanced screen printing, fine lines and multilayer structures are enabled. As a result, fully-screen-printed electroluminescent device is fabricated.[92] In these works, besides traditional silk and steel screen, more novel screens, like silicon and polyester screens are also involved.

Ink-jet printing

Ink-jet printing is emerging as a promising strategy in flexible electronics. Compared to screen printing, the design is more simple and totally digital. The requirement for inks are also not so strict. Low viscosity inks are preferred in ink-jet printing. The working mechanism of ink-jet printing is shown in Fig. 1.12. There is a propulsion element shown in the graph as piezo element. By applying a pulse electrical signal on it, ink drops can be pushed out of the nozzle one by one. The image signal will control the direction of ink

drops. By difference of the propulsion element, ink-jet printers can be divided into piezoelectric printers and thermal printers. Regarding the pulse signal and image signal, they can be categorized into continuous ink-jet printers and drop-on-demand printers. Now, most ink-jet printing equipment are piezoelectric, drop-on-demand printers. The smallest feature created by ink-jet printing can be as small as 20 μm. But the morphology is not so good. In 1997, Optomec Inc. invented aerosol-jet printing, an advanced version of ink-jet printing. The aerosol-jet printing has an ultrasonicator before the propulsion element. It can turn inks into aerosol, which is droplet suspension in air. This strategy can create features smaller than 10 μm and solve the nozzle-jam problem.

Since the versatility of ink-jet printing, almost all electronic devices have been ink-jet printed. However, as stated before, ink-jet printing has the jam issue. It's hard for it to print nanomaterials because nanomaterial-based inks, especially low-dimensional material, is easy to precipitate as to jam the nozzle. Aerosol-jet printing is used to print nanomaterials. For example, it's the most widely used method in CNT printing.[94]. So researchers have been developing various nanomaterial-based inks for ink-jet printing and got a lot of 2D-material-based, high-performance inks.[95] In recent years, ink-jet printing has been exploited in more and more different fields. For example, Japanese researchers reported ink-jet printed single-crystal films.[96]

Gravure printing

Gravure printing was born in the 19th century. But it was not long since it was introduced into flexible electronics. It's working principle is shown in Fig. 1.13. The ink was poured onto the gravure roll and filled the patterns. The doctor blade will remove residual inks. As the gravure roll rolls forward, ink drops will be transferred onto the substrate. The main advantage of gravure printing is its resolution. By careful design, gravure printing can generate features as small as 3 μm. Gravure printing can also produce thick patterns with thickness of 5 μm. But the gravure printing equipment is expensive. The patterned gravure roll is also costly.

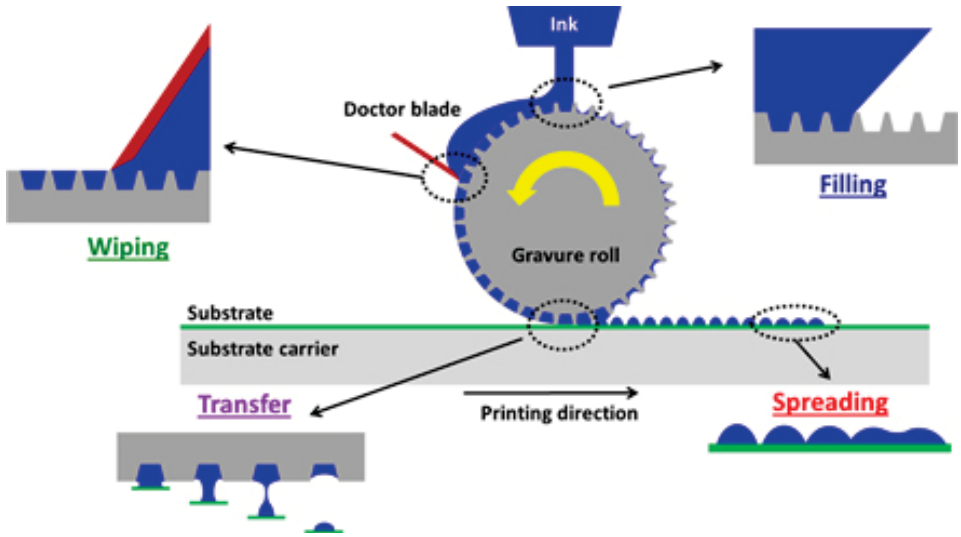

Figure 1.13: Schematic of gravure printing process. **Reprinted from [97] with permission from IOP publishing Ltd.**

Leave aside the cost issue, gravure printing has competitive performance. Many devices are fabricated based on gravure printing, like TFTs[98], [99], antenna[100] and LEDs[101].

Letterpress printing

Unlike gravure printing, letterpress printing transfers the inks on the bulge to the substrate. It is a time-honored printing technique which was invented in the 15th century by Johannes Gutenberg. By being introduced into flexible electronics, letterpress printing has drawn a lot of attentions because of its privileged advantages: low-cost and high-resolution. It has several varieties in flexible electronics in which the most widely used is **flexographic printing** and **micro-contact printing**.

Flexographic printing involves a flexible patterned plate (rubber or epoxy) on a cylinder as shown in Fig. 1.14. It doesn't require inks with specific viscosity and the patterns produced by it are usually thin and sharp. It has been reported that researchers have made 3 μm structures by flexographic printing.[103] Various prototype devices have been fabricated by flexographic

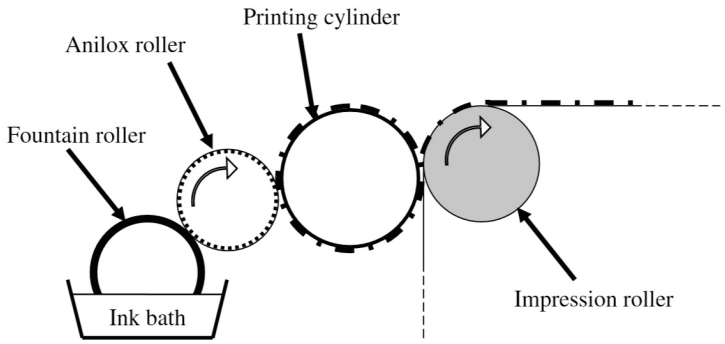

Figure 1.14: Schematic of flexographic printing process. **Reprinted from [102] with permission from Elsevier.**

printing.[104], [105]

Micro-contact printing was first introduced by Dr. George Whitesides at Harvard University. The working principle is shown in Fig. 1.15. A high-resolution mold should be made in advance and then a polymer master (usually PDMS or polyurethane (PU)) is made from the rigid mold. After the inking step, the master can be pressed onto the substrate to release the inks. The micro-contact printing is a super cost-effective method which makes it a proper method for lab-stage development. Its resolution is the highest among all printing techniques. There has been reports about sub-100 nm structure (as small as 40 nm).[107] With nanomaterial-assisted molding, the micro-contact printing has a potential to reach 2 nm in the future.[108] However, the polymer master is easy to be deformed. So the releasing speed and force need to be precisely controlled which is a hard problem in micro-contact printing.

3D printing

3D printing is a popular additive manufacturing technique in a lot of fields. This technique was born 40 years ago. And has been implemented decade by decade. It lights a way to fabricate 3D structures. With development of so many years, there has been a lot of outstanding 3D printing systems which can reach sub-micron scale resolution. However, the largest problem for application of 3D printing in flexible electronics is the limitation of materials,

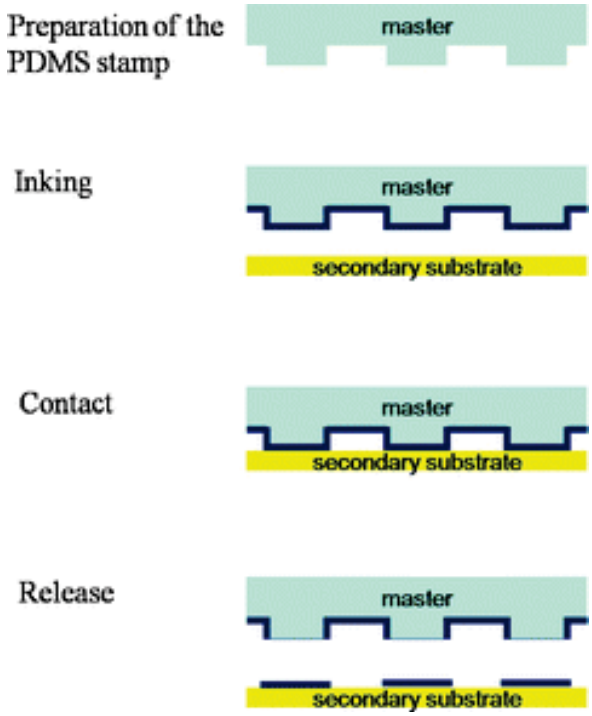

Figure 1.15: Process flow of micro-contact printing. **Reprinted from [106] with permission from Royal Society of Chemistry.**

especially for conductive materials. Researchers are fighting their way out by using liquid-metal 3D printing system, liquid conductors and composite materials.[109], [110] Most 3D-printed applications for flexible electronics are sensors.[110]–[112] With the technology advancing, more applications in other fields will come out in the future.

1.4.2 Lithography technologies

Rigid support

By applying the flexible substrate onto a rigid substrate, all conventional semiconductor manufacturing technologies are available to fabricate flexible electronic devices. The most straightforward way is the **bonding** method. However, how to debond the device without damaging is still a technical issue in this fabrication technique. The debonding process usually involves a certain type of trigger. This triggering factor may bring unwanted phenomena on the device layer. The most common debonding method is the **thermal debonding**. This method faces a problem of the CTE un-matching between

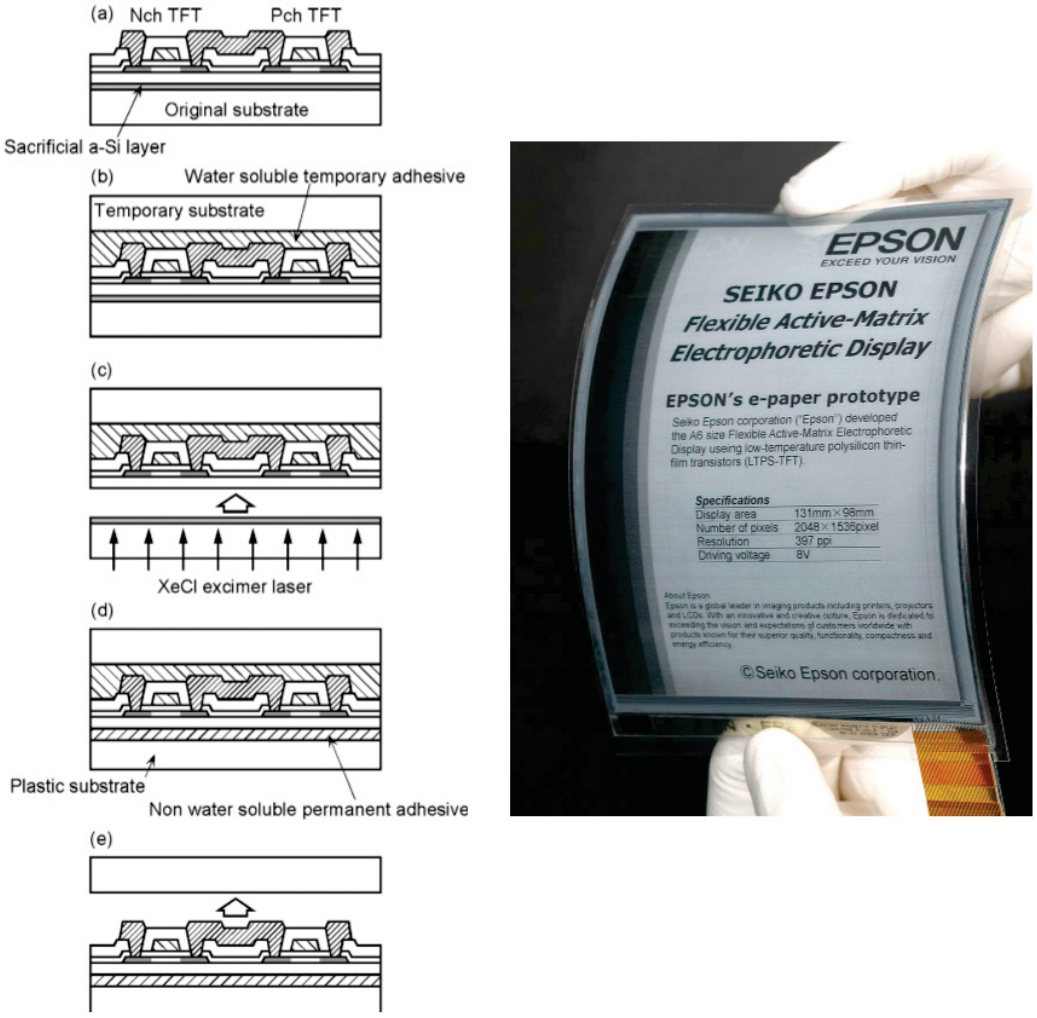

Figure 1.16: Left: process flow of SUFTLA. Right: device made by SUFTLA. **Reprinted from [113] with permission from IEEE.**

the flexible substrate and the rigid. This will lead to misalignment of devices or even device failure. In 2010, Loy et al. reported a more stable thermal debonding method by using alumina and PEN.[114] The CTEs of these two materials are similar to each other which won't cause any misalignment after baking. **Electronics on plastic by laser release (EPLaR)** is a technology developed by Philips. This process is completed by spin-coating a PI film on glass support and constructing devices on the glass support. The device layer was then debonded by UV excimer laser, which will melt the glass/PI interface. This method will also cause a certain kind of device misalignment. In 2007, Seiko-Epson developed a more complex process called **Surface-free technology by laser annealing (SUFTLA)** which also utilized UV excimer laser to ablate the device layer but limited CTE issue in quite a low level.[113] The process is shown in Fig. 1.16. All semiconductor manufacturing process is done before the device is transferred onto flexible substrate. So the heating issue is minimized. As shown in Fig. 1.16, this technique has been applied in flexible display manufacturing. Samsung has been using another debonding technique called **Joule heating induced lift-off technology (JILO)**. This technique includes a metal conductive layer as the attachment. By applying a pulsed electric field, the metal layer will melt thus debond the device layer. The heating penetration on flexible substrate is less than 1 μm according to simulation results.[115] Nowadays, a more popular flexible debonding technique, **flexible universal plane technology (FlexUP)** has emerged. This technique was developed by ITRI.[116] It introduced a weak adhensive as an attachment layer. So just mechanical debonding will detach the device layer after fabrication.

Vacuum R2R

An idealized vacuum R2R process is a perfect integration of traditional batch photolithography techniques (photolithography, vacuum deposition and etching) into R2R process line. There is no need for rigid support. So the bonding/debonding issues could be skipped. However, there still haven't been any total idealized vacuum R2R process yet. But researchers have been working

on bringing each of the conventional manufacturing process into vacuum R2R process. Like what has been stated before, the R2R ALD technique is pretty mature nowadays. The State University of New York at Binghamton developed a system of vacuum R2R process. But it consists 3 separate systems. Between the systems, it's still batch process transfer.

Nanoimprint lithography

Nanoimprint lithography is invented by Prof. Stephen Chou at Princeton in 1996. This method skips traditional photomask, which is a barrier to R2R integration. Instead, it involves a polymer mold to create patterns on flexible substrates which makes it suitable for R2R process. Nanoimprint lithography is a cost-effective method and it can reach a very high resolution (sub-10nm).[117]

1.5 Applications of flexible electronics

1.5.1 Sensing

The flexible sensing devices can be generally devided into 3 categories: **flexible photodetector, flexible physical sensor and flexible chemical/biological sensor**.

With applications in optical communication, imaging, measurement and spectroscopy, the need for **flexible photodetectors** is growing. Because of different usage scenarios, photodetectors need to work independently or simultaneously in UV, visible and IR range. Inorganic semiconducting nanomaterials are usually utilized for their mechanical flexibility. UV light detection has drawn tremendous attentions in biological analysis, space communication and environmental monitoring. Large-band-gap nanomaterials are used in UV detection, in which the most popular ones are metal oxide nanoparticles such as ZnO, TiO_2 and SnO_2 nanoparticles.[118], [119] Visible light detection has been tightly associated with our daily life. There are many types of nanomaterials used to accomplish the flexible route.[120] It should be noted that besides those nanomaterials, as another option, silicon membrane has also

been reported as a good candidate for flexible visible photodetectors.[121] IR detection is largely utilized in biological imaging, thermal imaging, and optical communication. Colloidal quantum dot and graphene are two materials widely used in IR flexible photodetectors.[122]–[124] According to device structure, flexible photodetectors can be categrized as photoconductors[122], [125], photodiodes[119], [124] and phototransistors[123]. Organic materials has also been reported to be the sensing material in flexible photodetectors. Because of their compatibility to the printing process, they mostly show up in printed flexible photodetectors.[126]

The **flexible physical sensor** is a device which can detect a physical stimulus (temperature, pressure and strain) and turn these stimuli to signals which is measurable or recordable.[127] There are many transducing mechanisms which have been already utilized on **flexible temperature sensors**. Pyroelectricity is a phenomenon which can be understood as the temperature will change the polarization of a insulator, and poly(vinylidene fluoride-trifluoroethylene) (P(VDF-TrFE)) as a pyroelectricity material has been demonstrated for flexible temperature sensors.[128] Another working mechanism usually appearing on flexible temperature sensor is resistive temperature sensing. Because of the strong relation between resistivity and temperature in metal, Pt, Ni and Cu are common materials to construct resistive temperature sensors. This type of temperature sensor is easy to fabricate and integrate into electronic systems. Thus they are widely utilized on e-skin and smart health patch.[129] Besides metals, the temperature-resistivity relation also exists in semiconductor, for example, Si has been utilized by researchers for epidermal temperature mapping.[130] **Flexible strain/pressure sensor** is another common class of physical sensors. Piezoelectric, piezoresistive and capacitive sensing are mostly employed transducing mechanisms in these physical sensors. The piezoelectric effect is a physical phenomenon which refers to reorientation of dipoles when a certain amount of strain/pressure was applied on the material. It exists in a wide range of materials, for example, P(VDF-TrFE) and ZnO.[131]–[133] The piezoresistive behavior represents the resistiv-

ity of the material will change with an applied strain/pressure. This behavior originates from a lot of mesoscopic changes, like cracks, buckling, quantum hopping/tunneling and so on.[134], [135] The capacitive sensing mechanism is mainly based on the capacitance change from the dimensional alternation brought by strain/pressure. PU, PDMS and Ecoflex are common materials as the capacitive sensing materials. A simple sandwich structure can fulfill the requirement for capacitive pressure sensing. But the low sensitivity and long response time are issues which prevent capacitive pressure sensors to large-scale applications. In order to solve these issues, researchers have integrated capacitive sensor onto FETs and largely increased the sensitivity.[136]

A **flexible chemical/biological sensor** will respond to a certain type of analyte and transform its chemical concentration into another type of signal.[137] Nowadays, flexible chemical sensors can detect a wide range of analytes, such as electrolytes (e.g. pH, Na^+, K^+, Cl^- and Ca^{2+}), heavy metal (e.g. Cu, Zn, Pb, Hg, and Cd), small substances (e.g. alcohol, caffeine and gases) and large substances (e.g. DNA and protein).[138] Based on the transducing mechanism, the flexible chemical sensors can be divided into electrical sensors, electrochemical sensors and colorimetric sensors. The electrical sensors can be as simple as a flexible conductor to sense the electrolytes and gas molecules[72], [139] or as complex as a FET structure in order to enhance the sensitivity.[140], [141] Different molecules can be absorbed onto the surface of the sensing materials thus change the carrier transport properties. If the molecules or ions are absorbed on the open gate in a FET-like device, they will induce a gate voltage in FET. In recent years, as the development of ionomers such as Nafion, the electrochemical sensors are improved dramatically. Electrochemical sensors detect the oxidation and reduction reactions on electrodes. Gao and his colleagues have done tremendous works in flexible electrochemical sensors.[142], [143] There has also been reported enhanced flexible electrochemical sensors by charge-coupling devices.[144] Colorimetric sensing devices usually appear in microfluidic devices. By different chemical reactions, the color of fluids will alter differently. Rogers et al. developed dif-

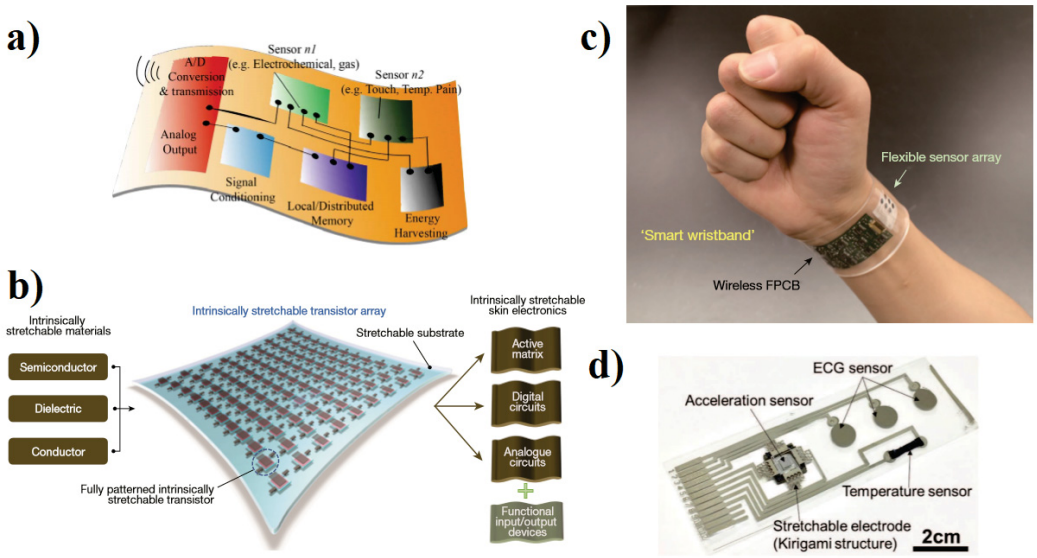

Figure 1.17: a) A conceptual schematic of a e-skin device. **Reprinted from[146] with permission from IEEE.** b) Schematic of e-skin developed by Bao et al. **Reprinted from [147] with permission from Springer Nature.** c) Healthcare patch developed by Javey et al. **Reprinted from [143] with permission from Springer Nature.** d) Healthcare patch developed by Takei et al. **Reprinted from [148] with permission from John Wiley and Sons Inc.**

ferent types of colorimetric epidermal sensing devices in detecting sweats.[145]

E-skin and **healthcare patch** are the two most important applications of flexible sensors. E-skin is a flexible or stretchable device which can mimic the functionality of skin. By proper integration of different type of sensors, as shown in Fig. 1.17a), it will acquire similarities with skins. It has advantages of low cost and scalablity. In the future, it can be applied in robotics and prosthesis devices. Dr. Zhenan Bao at Stanford has done a lot of works to advance this application.[134], [147] Healthcare patch is a multisensory patch, sometimes with needles or micropumps to deliver drugs. It can monitor various human health condition by non-invasive methods like sweats, temperature, pulse etc as shown in Fig. 1.17c) and d).

1.5.2 Energy harvesting

Energy harvesting is the process in which energy is captured from a the environment and converted into usable electric power. Flexible energy harvesters can be generally categorized into: **flexible mechanical energy harvester**, **flexible solar energy harvester**, and **thermal energy harvester**.

The mainstream of **flexible mechanical energy harvester** includes piezoelectric harvester and triboelectric harvester. The earliest piezoelectric energy harvest is developed by Zhong Lin Wang at Georgia Tech.[149] Because the ZnO nanorod itself is flexible, the ZnO-based flexible piezoelectric energy harvester on polyethersulfone (PES) substrate has been reported.[150] Since then, there has been works about different flexible, transparent electrodes on ZnO nanorods and different designs and structures. Triboelectric energy harvester utilizes a time-honored physical phenomenon of friction charging. When two materials contact each other, because of their different surface groups, there will be charge transfer happening on the interface. This particular phenomenon has been applied in energy harvesting since the 19th century.[151] In 2012, Fan et al. reported the first flexible triboelectric energy harvester by PET and Kapton^{TM} film.[151] Since then, various materials, from insulators to conductors have been utilized in flexible triboelectric energy harvester. Both piezoelectric and triboelectric energy harvesters have the advantage of being cost-effective and easy to be applied into daily use. But they cannot produce high-density energy to sustain a large, complicated system since the energy source, mechanical movement, cannot generate large electric power. These pros and cons make them a perfect candidate as the power sources in wearable systems.

As mentioned before, the first flexible electronic device is the **flexible solar energy harvester**, also known as flexible solar cell. With advancements of thin-film technology and increasing needs for cheap, sustainable energy source, flexible solar cells become popular nowadays. The most successful flexible so-

lar cell by now is the previously mentioned amorphous silicon solar cell. It has been largely utilized in building-integrated photovoltaics (BIPV) with a promising power conversion efficiency of 8.5%.[152]. Cu(In,Ga)Se_2 (CIGS) is a star material in PV industry. It has amazing capability of 99% absorption in less than 1 μm thickness which makes its PCE (20.3%) comparable to crystalline silicon solar cell's.[153] Researchers are also marching towards 20% in flexible CIGS solar cells. A research group in the Empa has reported a flexible CIGS solar cell on PI film with power-conversion efficiency (PCE) of 18.7%.[154] Companies like Global Solar Energy and Nanosolars are commercializing flexible CIGS solar cells in BIPV applications.[155] Organic semiconductor are also employed for flexible solar cells[156]–[158] in which the most efficient one can reach an impressive PCE value, 10.4%.[158] However, the stability of organic solar cell is still an issue in this field. So colloidal quantum dots emerges as another option because its better air stability. There has been report of spray-printed flexible CQD solar cell with PCE of 7.2%.[71] In recent years, since perovskite solar cell is on a highway, flexible perovskite solar cell attracts a lot of attentions. Flexible perovskite solar cell has reached a high PCE over 18%.[159] The application of flexible solar cell is not just on wearable systems, it can also be applied to large-scale BIPV.

flexible thermal energy harvester utilizes the Seebeck effect to generate electricity. Because of temperature difference, there will be carrier generation in a p-n junction. By making thermal energy harvester flexible, they can be easily adapted to human skin. Thus, it can generate power for wearable systems by body temperature. As early as 2001, there has been a report about flexible thermal energy harvester.[160] Nowadays, flexible thermal energy harvester can reach power of 3.8 mW/cm^2.[161]

1.5.3 Circuits

The flexible circuits can be categorized as **single-sided circuit**, **double-sided circuit**, **sculpted circuit**, **multilayer circuit** and **rigid-flex circuit**

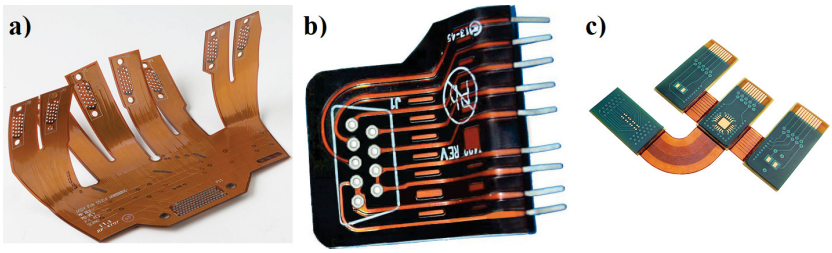

Figure 1.18: a) Multilayer flexible circuits. b) Sculpted flexible circuits. c) Rigid-flex circuits.

by architecture. The single-sided and double sided circuits are circuits with single or double side patterned. Multilayer circuit (Fig. 1.18a))usually has different functional layers connected by complex vias. There are usually different shielding and insulating layers involved. The sculpted circuit is shown Fig. 1.18b), the wiring or connections are patterned with different thickness. The rigid-flex circuit (Fig. 1.18c)) is a combination of flexible circuitry and rigid circuitry to achieve more complicated functions. Flexible circuits can be fabricated by various techniques including printing and lithography. The materials are already stated in the flexible conductor part.

1.5.4 Display

Display is now one of the most important parts in modern consumer electronics and it's more of an urgent need to produce flexible display to fit in various application scenarios. Researchers from both industry and academia have paid considerable attention in developing new-class of flexible displays. History of flexible display can date back to 1970s'. In 1973, Xerox Palo Alto Research Centre developed the first flexible e-ink display, Gyricon. This display utilizes electric field to control microscale carbon particles to produce paper-like images. In 1980s', researchers at Texas Instruments invented flexible liquid crystal display (LCD). The liquids were sealed in polymer foils.[162] Recently, since the smartphone market is booming, flexible OLED display attracts a lot of attentions. OLED has an extraordinary performance than other LED displays. The flexibility of organic semiconductors makes them easier to be made

into flexible devices. The emission of them is also stronger and the viewing angle is much larger. Samsung is the leader in advanced display technologies. Its flexible OLED displays has been massively applied in smart phones and it also developed high-performance stretchable OLED displays.[163] CQD is another candidate for future flexible displays because of its sharp emission and better air-stability. There has been reports of flexible CQD displays.[70]

1.6 Objectives and outline of the thesis

1.6.1 Challenges in flexible electronics

As I have stated before, flexible electronics has attracted plenty of attentions from both academia and industry. The market is continuously accelerating year by year. The technologies in this area are advancing fast. However, the challenges are still lying ahead. In my opinion, there are two major challenges in this area, one is the **cost** issue, the other one is the **performance** issue.

Regarding the cost issue, the first aspect is about materials. To obtain devices with better flexibility, better electrical/optical properties, new materials are developed and imported for flexible electronics, such as various organic flexible/stretchable materials. I don't think these materials are not potentially to be cost-effective. Actually, the fact is just the opposite. The new candidates in flexible electronic devices, like organic materials, are usually low-cost materials if massively produced. However, nowadays, mass production of those materials are almost impossible due to lacking of upstream industry and downstream customers. For example, organic photovoltaic devices' low-cost feature has been proved again and again, but after 20 years of development, they are still more costly than conventional silicon photovoltaic devices. Even though researchers from both academia and industry are devoting to reduction of the cost of organic photovoltaic devices, the cost of silicon photovoltaic devices is dropping faster because of complete upstream and downstream facilities. The other aspect is immature manufacturing technologies. For example, the vacuum R2R technology is immature to some degree. The transfer between

photoresist patterning process and deposition process needs to be batch processed. This will largely increase the manufacturing cost.

In my opinion, there are two routes to address this issue. One is developing a killer application. A widely used application can make the material able to be mass-produced. In the meantime, it can also facilitate both upstream and downstream industries, which will pave the way for other flexible electronic devices. The other one is making new materials which have extremely low cost or have other unique properties like being able to recycled etc. By taking this approach, one can develop a prototype device which is even cheaper than mass-produced devices.

There is a trade-off lying in the performance of flexible electronics. Usually a material with good electrical/optical properties suitable for electronic devices won't be flexible enough. Paradoxically, a material with good flexibility are usually not ideal in terms of electrical/optical properties. For example, a-Si is a flexible material because of its amorphous nature. However, its electron mobility is only $\sim 1\ cm^2 \cdot V^{-1} \cdot s^{-1}$, which largely restrains its application in electronics.

There are also two approaches to solve this problem. One is developing new materials which are tie breakers. These materials should not only be flexible, but also have extraordinary electrical/optical properties, such as 2D MoS_2, CNTs etc. The other approach is to introduce devices with new working mechanisms for new applications. By new working mechanisms and designs, one can fabricate high-performance devices with materials which have relatively worse electrical/optical properties.

1.6.2 Challenges in flexible sensors

In my research, I focused more on various sensing applications. The overview to flexible sensing applications can be found in the previous section. The same issues as in general flexible electronics also haunt the flexible sensors.

For example, in flexible sensors, the preparation of the novel active materials is always a bottleneck. The sophisticated processes involved in the fabrication of these novel materials based devices also decrease the yield which will further increase the cost. But now, the cost of various nanomaterials, like graphene and CNT, has been decreased dramatically in the past few years. In the future, this situation is expected to be improved further. Another example is about the manufacturing process. Printing technology is an important manufacturing technology in the fabrication of flexible sensors. It will enable large-scale, roll-to-roll manufacturing which will largely decrease the cost. However, in current stage, printing still has lots of limitations due to various factors like viscosity, solubility etc. which will increase the manufacturing cost.[164] Regarding the performance issue, besides the trade-off I mentioned before, there has been another problem lying there. For flexible sensors with novel working mechanisms (piezoelectric etc.), the manufacturing technologies for these devices are not mature, so one would expect large device-to-device variations for device performance compared to conventional rigid sensors.

1.6.3 Objectives of the thesis

In this thesis, I focus on the aforementioned two major issues in flexible sensors and try to address them from different approaches, novel substrates and transducers. Based on these two approaches, I developed flexible sensors for different sensing applications like strain sensing, force sensing and touch sensing.

I utilized CNC based paper to make fully recyclable strain sensing devices. Through our unique PDMS stencil technology, we were able to fabricate small features on CNC paper. By enabling recyclable devices, materials can be collected and used for new devices, which will reduce material cost of devices. In another work, by a simple surface passivation method, I obtained a surface suitable for CQD based printed electronics. With this method, one can introduce printing technology into fabrication of flexible CQD devices, which will largely reduce the production cost.

In terms of new transducers, I demonstrated two types of transducers to introduce new working mechanisms of flexible sensors in order to increase device performance. Firstly, I designed digital flexible MEM sensors, which can lead to high durable, calibration-free devices. On the other hand, because this type of device avoids expensive new materials and costly fabrication techniques, its cost is low. Secondly, I combined triboelectricity with CQD-based FET, which is an introduction of T-FET into flexible sensors. By using this transduction mechanism, the device exhibits higher performance than normal PDMS triboelectric sensors.

1.6.4 Outline of the thesis

The thesis is divided into six chapters. In chapter 1, it first introduces the topic of flexible electronics. Then, a literature survey is done to give the overview of flexible electronics, focusing on materials, manufacturing technologies, and applications. In the end, the objectives and deliverables of the thesis are described.

Chapter 2 is dedicated to utilizing a recyclable substrate, nanofibril paper based on cellulose nanocrystals. This substrate is derived from wood which makes it sustainable and cost-effective. However, for a water-soluble substrate, traditional semiconductor manufacturing techniques are not feasible anymore. A new technique, PDMS stencil lithography, is developed to precisely make patterns on water-soluble substrates. The strain sensor fabricated by PDMS stencil lithography exhibits large sensitivity and it's totally recyclable by dissolving in water.

In Chapter 3, a new strategy to create a trap-free substrate surface suitable for PbS QD ink by Cl modification is proposed. By this novel surface modification strategy, higher-performance PbS QD FET can be expected and inkjet processing of PbS QD is implemented. This strategy is also extended to halide modification for various rigid and flexible substrate surfaces and verified

by Fourier-transform infrared spectroscopy (FTIR), X-ray photoelectron spectroscopy (XPS), Energy dispersive X-Ray analysis (EDX) and contact angle measurement. The Cl-modified SiO_2 surfaces are utilized for high-performance QD FETs as a demonstration.

Digital microelectromechanical (MEM) sensor with novel transduction mechanism, microelectromechanical system (MEMS) working mechanism, is demonstrated in Chapter 4. This device consists a PDMS bridge structure and Kapton^{TM} substrate. Durability and reproducibility testing was tested. We also demonstrated gesture detection and heart rate detection applications by this device. Compared to new-materials based sensors with analog signal output, our digital MEM sensors will set much lower requirements in fabrication and do not need calibration after long time usage. With engineered sensing structures, digital MEM devices with different sensitivities can be integrated together to achieve the same function as provided by sensors with analog-signal output. Considering above advantages, digital MEM sensors can be an alternative solution for strain and pressure sensing in the fields of pressure mapping, sound wave detection and more. In this paper, we managed to control the sensitivity of the digital MEM sensor by changing the 'pier' height of the PDMS bridge.

In Chapter 5, a new transduction mechanism, triboelectricity combined with field effect transistors is introduced to flexible touch sensors. In this touch sensor, we use the PDMS film to generate triboelectric voltage in response to touching and a floating gate CQD FET to produce the source-drain current driven by the triboelectric voltage. This design makes the device responsive to different materials and possible to generate a much larger current change compared to the freestanding PDMS touch sensor, while the simple fabrication process of CQD triboelectric field-effect transistors (TFETs) enables the potential of our devices to be mass produced by printing technologies at low cost.

Chapter 2 and 3 mainly focused on novel substrates for flexible strain sen-

sors and printable electronics. Chapter 4 and 5 discussed new transduction mechanisms of flexible force, strain and touch sensing applications.

Chapter 6 concluded all the contents and looked into the future for plans of improvement, which are platform-level integration and improvement of transparency and semiconductor materials.

Chapter 2

Flexible devices on CNC paper by PDMS stencil lithography for strain sensing

2.1 Introduction

Transient electronics have drawn a lot of attention in recent years for their unique property of being soluble in water, which is not feasible in modern silicon electronics. It has been demonstrated that transient electronics can be partially or fully dissolved in a controlled period of time.[165]–[167] This will enable potential applications in biomedical implants, drug delivery, zero-waste consumer electronics and even security devices for military applications.[168] In this research area, Bettinger,[169] Bao[166] and Irimia-Vladu[170] have reported devices based on biocompatible and biodegradable organic materials. Rogers and his colleagues lead the development of transient electronics[165], [167], [171]–[174] using a silk substrate and a variety of materials,[175]–[181] such as magnesium, zinc, silicon germanium, indium-gallium-zinc oxide etc., for electrodes or conducting channels.

Wood-derived cellulose nanocrystal CNC based nanofibril paper is a good candidate for substrates in transient electronics because of its high-Young's modulus, low-density, low-thermal expansion, and non-toxicity.[182], [183] In addition, an acid hydrolysis method will enable mass production of CNC at low cost. Fig. 2.1(a) summarizes the unique properties and applications

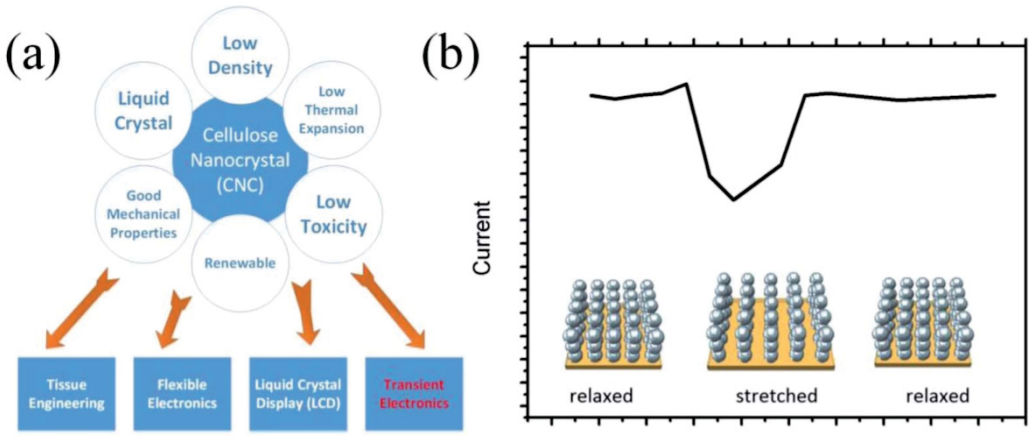

Figure 2.1: (a) The advantages and applications of CNC materials. (b) The working principle of metal nanoparticle based strain sensors. With a strain applied on it, the output current is going to drop down sharply.

of CNC materials. Many applications that use CNC films as substrates for electronics, such as organic solar cells,[183], [184] field-effect transistors,[41] nanowire-based strain sensors,[185] and organic light-emitting diodes,[186] have been demonstrated in the last two years. As an environmentally friendly nanomaterial, CNC was approved for unrestricted use in Canada and was the first nanomaterial included on Canada's Domestic Substances List (DSL). Herein, we show the fabrication and characterization of metal nanoparticle based strain sensors on CNC films. The electrical current in our devices will change when the device goes through a shape deformation, as shown in Fig. 2.1(b).

In transient electronics, one major challenge in device fabrication is the substrate. Because of the high sensitivity of CNC to water and most organic solvents, traditional photolithography process cannot be applied to pattern electrodes on CNC films. Rogers and his colleagues used transfer-printing technique to avoid direct patterning and electrode deposition on water-soluble substrates. Nogi et al. reported direct electrode deposition on wood derived green materials by printing with a metal paste or ink.[184], [187], [188] Another common solution to this problem is using stencils and shadow masks. Previously reported metal[41] and PI[165], [189] shadow masks cannot

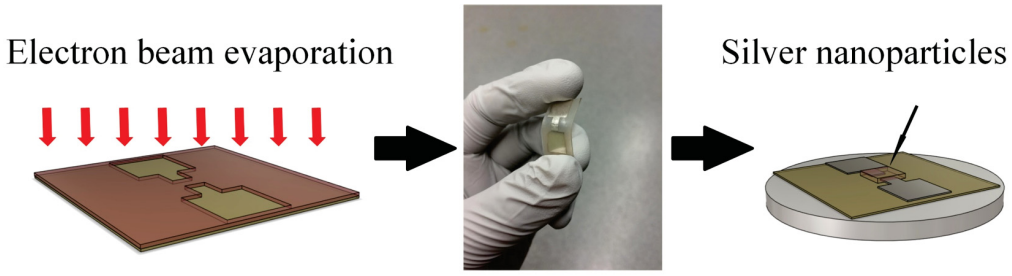

Figure 2.2: The fabrication process of strain sensors. From left to right: electron beam evaporation assisted by PDMS stencil to deposit Ag electrodes, picture of flexible CNC film with Ag electrodes, spin-coating Ag nanoparticles on the electrodes shown in the middle graph.

lead to high-resolution features because there are gaps between the mask and the substrate. All physical vapor deposition methods used in metal electrode deposition are not fully directional, thus metal atoms may diffuse to substrate surfaces under the mask and result in reduced device performance. A PDMS shadow mask can solve this problem for the large London dispersion force between the PDMS mask and flexible substrates,[190] providing good adhesion between the mask and the substrate. For example, a typical feature size by a metal and PI shadow mask is above 160 μm,[41] whereas for the PDMS shadow mask, the feature size can be as small as 5 μm.[191] Up until now, no one has achieved this in device fabrication on water-soluble substrates.

In this paper, we reported the first demonstration of applying PDMS shadow masks to deposit metal electrodes on water-soluble substrates. We also improved the fabrication of PDMS masks in the previous report.[191] We used the doctor blade method with self-drying of PDMS to replace the method using hexane to dissolve the top PDMS layer. This enables the controllable and reproducible fabrication of PDMS masks. Our strain sensors employed a thin-film of Ag nanoparticles as the sensing material, shown in Fig. 2.2, and showed a high gauge-factor of $\sim$50, which is the highest gauge-factor of strain sensors reported on water-soluble substrates. Our device can disintegrate in water within 30 minutes.

2.2 Experimental

2.2.1 Materials

CNCs were mass produced in the CNC pilot plant at Alberta Innovates Technology Futures (AITF, Edmonton, Alberta, Canada). Trichloro(1H, 1H, 2H, 2H-perfluorooctyl)silane (97%) was purchased from Sigma Aldrich. Glycerine was purchased from Fisher Scientific. Ag nanoparticles (∼20 nm in diameter) were purchased from US Research Nanomaterials Inc. The PDMS stencils were made using a Dow Corning Sylgard 184 silicone elastomer kit.

2.2.2 CNC synthesis

CNC was synthesized by acid hydrolysis. First, two Pfaudler 50 gallon (189 liter) acid-resistant glass-lined reactors with a steam-heated jacket were employed to perform the sulfuric acid hydrolysis with an acid concentration of 64% and an initial reaction temperature of 45 °C. Then, a centrifuge step was performed using a GEA Westfalia SC-35 Separator. Later, the microfiltration step was performed in a GEA Filtration-Ultrafiltration Plant. In the end, the wet CNC powder was dried in a SPX-Anhydro Model 400 Spray Dryer Plant at the conditions of a 220 °C inlet temperature and an 85 °C outlet temperature.

2.2.3 CNC film deposition

CNC films were prepared by the following steps. First, the CNC powder (5 wt%, 2 g) and deionized water (95 wt%, 37 g) were mixed together to form a CNC solution. Then 0.8 mL glycerine (Fisher Scientific Inc.), which is a non-toxic add-on, was added to the solution to avoid cracks after drying. Finally, this mixture was poured into a plastic Petri dish and dried at room temperature for 18 hours. The dried CNC film was detached from the Petri dish for use.

2.2.4 PDMS stencil fabrication

As shown in Fig. 2.3, the fabrication process of the PDMS shadow mask can be divided into 6 steps. The first two steps are commonly used in conventional

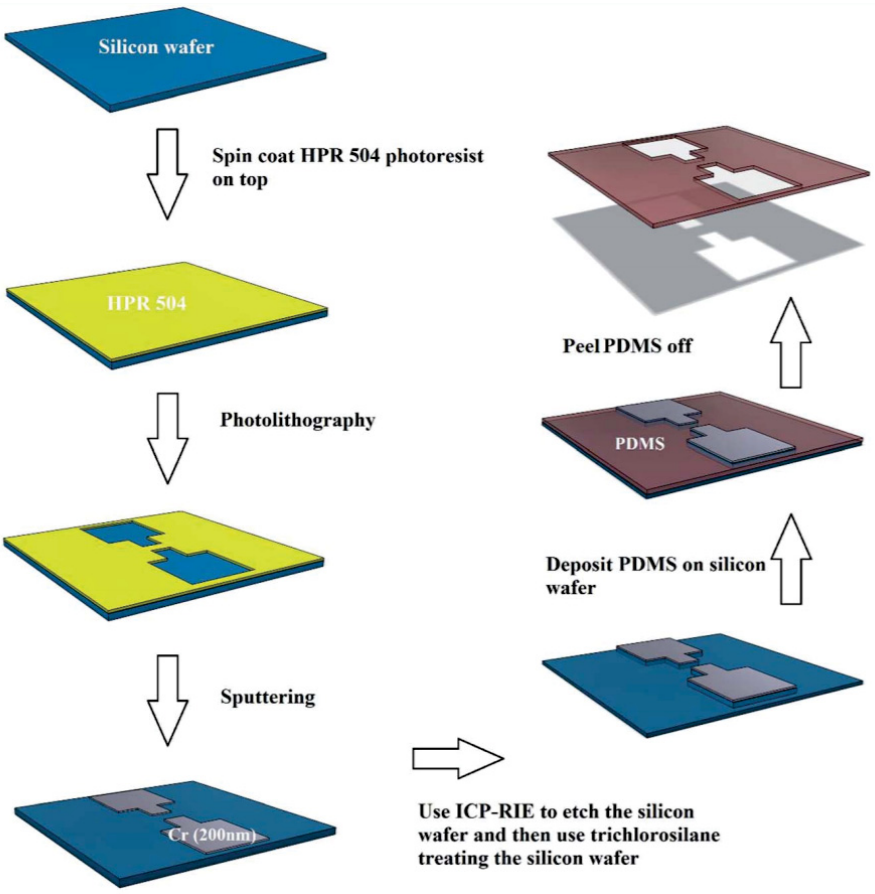

Figure 2.3: Process flow of the fabrication of the PDMS shadow mask.

photolithography. In these 2 steps, a HPR 504 photoresist was spun onto the surface of a silicon (Si) wafer, and the wafer was spun for 10 s at a spin speed of 500 rpm followed by an additional spin of 40 s using a spin speed of 4000 rpm. Before UV exposure, the wafer was put onto a hot plate baking at 115 °C for 90 s to evaporate the solvents in the photoresist so as to obtain an HPR 504 photoresist film with a thickness approximately 1 μm. The UV exposure was carried out using a mask aligner (ABM Inc. San Jose, California) for 4 s with a UV light intensity of 66.7 $mW \cdot cm^{-2}$. Finally, the wafer was rinsed in Developer 354 for 40 s to get the pattern as shown in Fig. 2.3.

In step 3, the chromium (Cr) etching mask was fabricated by depositing a 200 nm thick Cr film onto the wafer via sputtering. After the lift-off process, the Cr etching mask showed up on the surface of the silicon wafer.

In step 4, a Bosch process (SF_6 as the etching gas and C_4F_8 as the passivation gas) was applied to get the silicon mould with an etching depth of 200 μm.

In step 5, the trichloro(1H, 1H, 2H, 2H-perfluorooctyl)silane vapor was first employed to passivate the surface of the Si mould to make it hydrophobic. Then, the PDMS base was mixed with the cross-linker curing agent at a ratio of 10 : 1 (v%), and degassed in a desiccator for 30 minutes to prepare the PDMS mixture. Later, the PDMS mixture was poured onto the surface of the Si mould. Excess PDMS was removed from the top surface of the mould using a doctor blade. The PDMS mixture was then cured at 80 °C for 30 minutes on a hotplate.

In the last step, the PDMS was peeled off from the mould to form the stencil.

2.2.5 Strain sensor fabrication

As shown in Fig. 2.1(b), our strain sensor is a two-terminal device. When strain is applied on the substrate, the current across the two terminals will change under a applied voltage. The fabrication process of our devices is briefly illustrated in Fig. 2.2. At first, a PDMS stencil was attached onto the CNC film. The large London dispersion force between the PDMS stencil and CNC

substrate enabled good adhesion between them. In the second step, an Ag film was deposited on the aforementioned sample using e-beam evaporation. Then, the PDMS stencil was peeled off from the CNC substrate, and the obtained sample was the CNC substrate with patterned Ag electrodes. In the last step, an Ag nanoparticle suspension was spincoated onto the sample (CNC substrate with patterned Ag electrodes), and the sample would be ready for testing. The concentration of the Ag nanoparticle suspension is $0.5 mmol \cdot mL^{-1}$ in N,N-dimethylformamide (DMF).

2.2.6 Strain testing setup

The strain sensors were characterized using various steel blocks with different radii commonly used in strain-gauge testing. The strain sensor tightly attached to the curved surface of the steel block was stretched to certain strains. The electrical measurement was performed by a SourceMeter (Keithley 2400).

2.3 Results and discussion

Smooth, uniform CNC films are desired in high-performance transient electronics. We produced high-quality CNC films by optimizing the film-processing conditions. In this process, we used glycerin as a plasticizer and a dried CNC/plasticizer suspension to get a flexible CNC film. In the profilometer measurement, the thickness of the CNC films was determined to be approximately 200 μm. Three randomly selected locations of the CNC film surface were imaged using atomic force microscopy (AFM), and the measured roughness values were 3.51 nm, 4.75 nm and 2.77 nm, respectively. As shown in Fig. 2.4(a), the AFM image provides evidence that the smooth CNC film with a variation of less than 10 nm was produced. This is further confirmed by the scanning electron microscopy (SEM) image in Fig. 2.4(b). It can be seen there are no prominent specks or dents on the surface of the CNC film. The PDMS masks processed by Si moulds and doctor blade method show high quality under SEM imaging. In Fig. 2.5(a), the shadow mask produced by our process shows a channel length of 150 μm and width

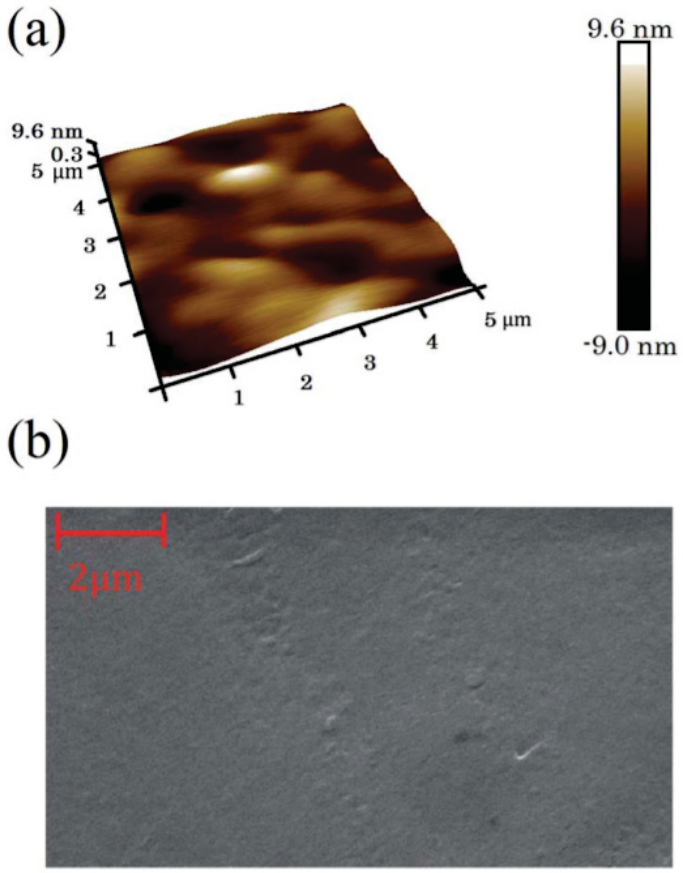

Figure 2.4: (a) AFM picture of the CNC film. (b) SEM picture of the CNC film.

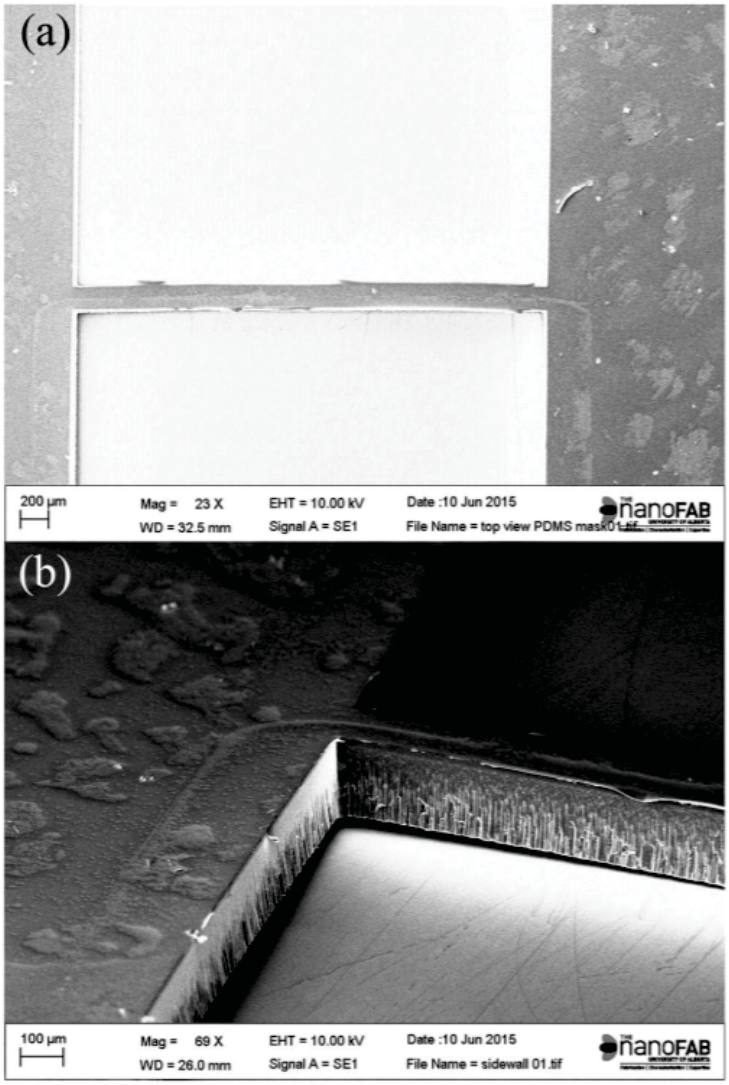

Figure 2.5: SEM images of the PDMS shadow mask (a) top-view (b) 60 ° side-view.

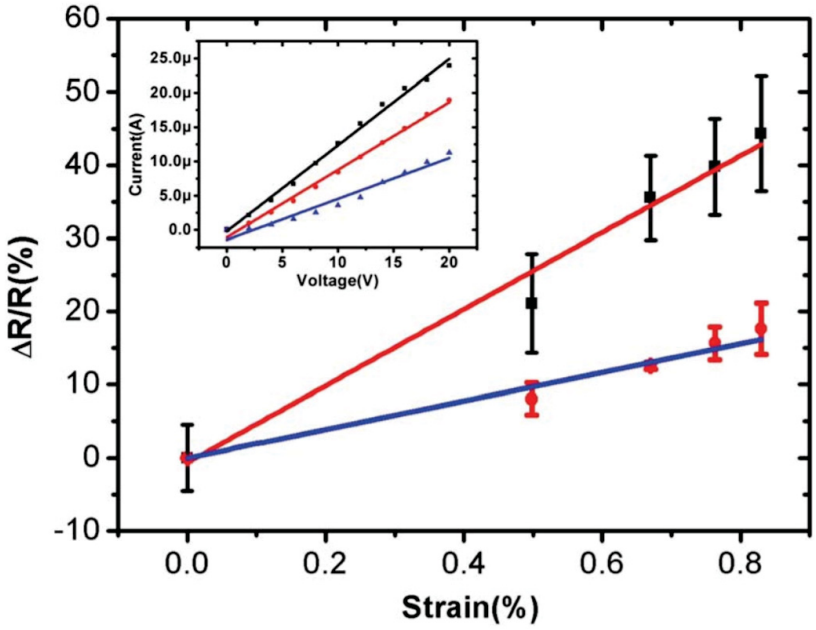

Figure 2.6: ΔR/R–strain curves of the devices, through which GF of strain sensors can be calculated. The red line represents the device made by PDMS stencil lithography which has a conducting channel of around 150 μm. The blue line refers to the device with copper tapes as electrodes and the conducting channel is about 3 mm. Inset: I–V curves of the same device under different strains. The blue, red, and black curves show I–V curves under the strain of around 0.5%, 0.7%, and 0.8%, respectively.

of 3 mm between adjacent electrodes. Sharp sidewalls of the shadow mask are clearly pictured in Fig. 2.5(b), and this can lead to good patterns on the water-soluble substrate when metal electrode is deposited using physical vapor deposition. For the large London dispersion force between the PDMS mask and CNC substrate, we can easily attach our shadow mask onto the CNC substrate without any glue or tape in the experiment.

The operational principle of the strain sensor is based on the fact that the resistance of the conducting channel changes when the device is under shape deformation. A current–voltage characteristics measurement (Fig. 2.6 inset) of the device can be used to calculate the resistance value of the strain sensor at a given strain. The sensitivity of strain sensors is characterized by the gauge-factor (GF), which is extracted by taking the ratio between the

electrical measurable response ΔR/R and the strain ϵ applied to the sensor, as expressed in eqn 2.1:

$$GF = \frac{\Delta R}{R} / \frac{\Delta L}{L} = \frac{\Delta R}{R} \times \frac{1}{\epsilon} \tag{2.1}$$

Since the relation between $\Delta R/R$ and the strain ϵ is nearly linear, as shown in Fig. 2.6, we used the slope of the linear fitting lines of the scatter points on the graph to represent GF of the devices. From the plot in Fig. 2.6, the GF for our device is 52.44 with a standard error of 3.28, which is among the highest values in previous reports.[192]–[194] We also tested the device without using our PDMS stencil lithography, where copper tapes act as electrodes to make a device with a conducting channel of approximately 3 mm. As shown in Fig. 2.6, a GF of 19.67 with a standard error of 0.96 was extracted from the curve representing the device without PDMS stencils. According to our testing, the maximum strain applied to the device without permanent damage is approximately 1.4%. It is noted that the CNC substrate can absorb water molecules because of its high solubility in water. However, the electrical property of the device is barely influenced.

We attributed the high GF to the quantum transport between Ag nanoparticles and carried out an analysis using the Arrhenius model.[195] According to the former reports, electron transport in the metal nanoparticle matrix granular metal system[196] could be described as thermally activated tunneling.[195], [197], [198] The conduction is determined by several parameters such as the particle radius, interparticle distance and so on. According to the model in former reports, the thermally activated tunneling conductivity is described as the Arrhenius equation:

$$\sigma = \sigma_0 \; exp(-\beta d) \; exp[-\frac{0.5e^2}{4\pi\epsilon\epsilon_0 RT} \; (\frac{1}{r} - \frac{1}{r+d})] \tag{2.2}$$

Where σ_0 is the intrinsic conductivity of the Ag nanoparticles defined by $\sigma_0 = ne\mu$, β is a particle size and temperature dependent electron coupling term usually varying from 1 nm^{-1} to 10 nm^{-1}, d is the interparticle distance,

ϵ is the relative dielectric constant of the interparticle medium and r is the particle radius. Under uniaxial strain, the interparticle distance will change from d_1 to d_2. So the resistance ratio for the stretched device and the relaxed device should be:

$$\frac{R_2}{R_1} = exp(-\beta(d_2 - d_1)\ exp[-\frac{0.5e^2}{4\pi\epsilon\epsilon_0 RT}\ (\frac{1}{r+d_2} - \frac{1}{r+d_1})] \tag{2.3}$$

Which can be rewritten as:

$$\frac{\Delta R}{R} = exp(-\beta\epsilon_s d_1)\ exp[-\frac{0.5e^2}{4\pi\epsilon\epsilon_0 RT}\ (\frac{1}{r+\epsilon_s d_1} - \frac{1}{r+d_1})] - 1 \tag{2.4}$$

Where ϵ_s is the strain applied to the device, and the second exponential term in this formula can be used to extract the activation energy of metal nanoparticles. In our experiments, by non-linear curve-fitting, we get that d is 36.2 nm^1 and β is 1.21 nm^{-1}.

As shown in Fig. 2.6, our device works at small strains showing a linear relation for ΔR/R and ϵ, which means that it can fit to the Arrhenius model. The decreased performance in devices made without PDMS stencils is due to more micro-cracks in long conducting channels. For a small channel length, it is expected that nanoparticles will separate in a relatively homogenous way with more or less the same distance when the strain is applied on the device. Whereas, in long channel devices patterned without PDMS stencils, more micro-cracks appear in the conducting channel and divide nanoparticles into domains. While in each domain, nanoparticles still separate with similar distances under a certain strain, where most of the applied strain is shared by the opening of these micro-cracks. Thus, the actual strain within the nanoparticle domain may be much smaller than the applied strain.

To verify the reproducibility and reliability of our technique, we produced more than 25 stencils from the same Si mould. The recorded SEM images of PDMS stencils made after 15, 20 and 25 times using the same Si mould are provided in Fig. 2.7, and strain sensors made by these PDMS stencils were

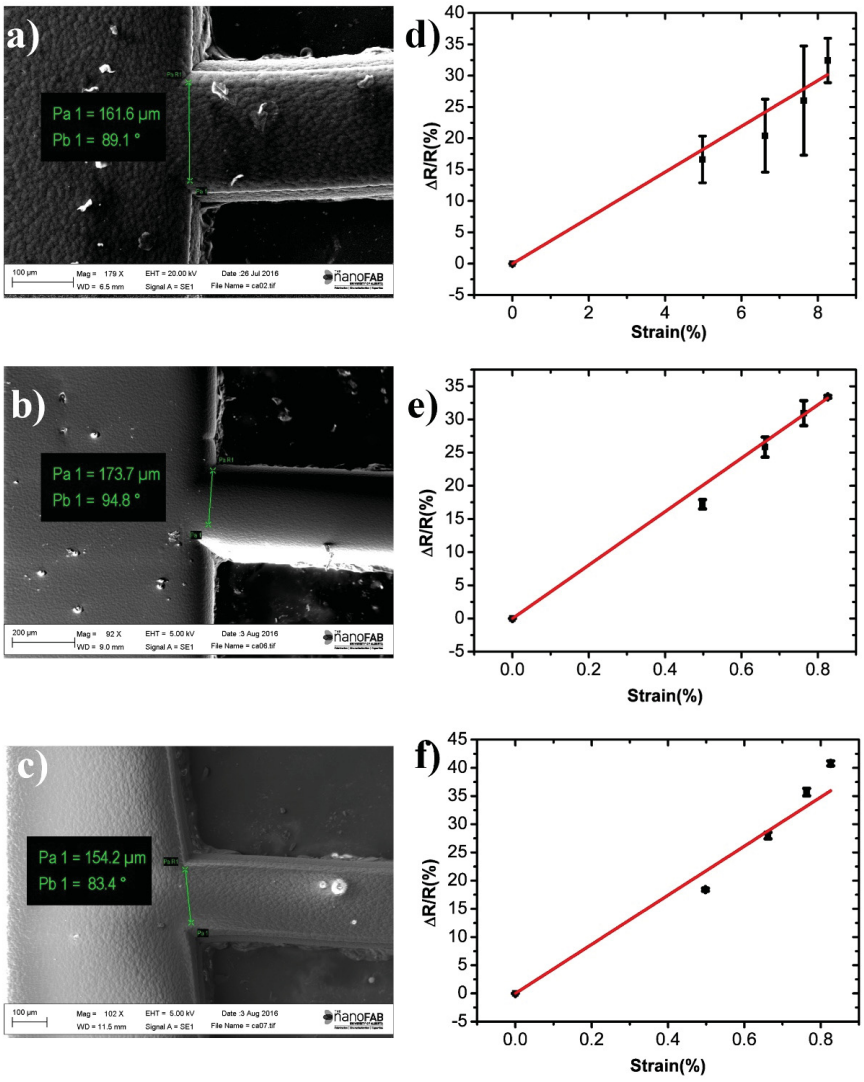

Figure 2.7: a)-c) SEM picture of the PDMS stencil made by mould which has been used for 15, 20 and 25 times. d)-f) Resistance change vs. strain curves of devices made by the stencils shown in their left.

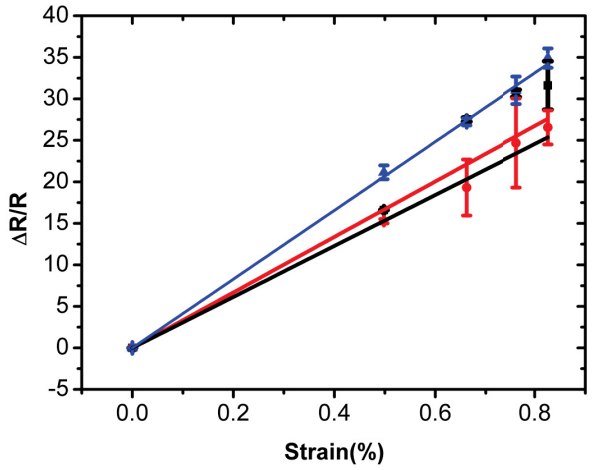

Figure 2.8: Resistance change–strain characteristics of a device after 0, 10 and 40 times' bending. The red curve represents device after 0 times' bending while the black and blue ones are 10 times and 40 times.

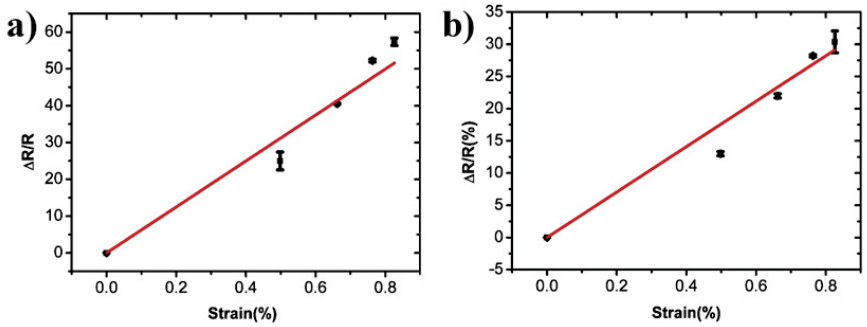

Figure 2.9: Extra resistance change-strain curves for different devices.

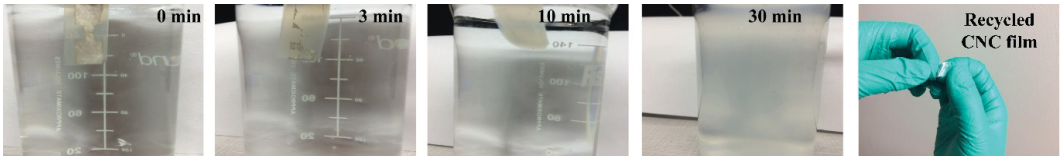

Figure 2.10: The dissolving process of CNC film with Ag electrodes in water and recycled CNC film.

also tested. According to the experimental data, the PDMS stencils and strain sensors can be reproduced within a reasonable variance. We also fabricated several devices from the same PDMS stencil, and a similar performance was achieved in these devices (Fig. 2.8). After repeatable bending of 40 times, our sensors still show a high GF of about 42 (Fig. 2.9).

In order to know how this device deforms and partially dissolves in water, we put the substrate with Ag electrodes into a beaker with deionized (DI) water. As shown in Fig. 2.10, after 3 minutes, the Ag electrodes began to dissociate. At 10 minutes, there is no Ag on the substrate which has a strong deformation. In 30 minutes, the entire substrate dissolved in water. After the substrate was fully dissolved, we collected the supernatant of the solution only for recycling CNC materials. Finally, a new CNC film was produced as shown in the last graph in Fig. 2.10 when the solution was fully dried.

In reality, after the whole device dissolves in water, Ag electrodes can be filtered out by a normal filter, and Ag nanoparticles can be isolated by a hyperfiltration membrane or ultracentrifuge. The metals can be filtered out and recycled by some chemical process. Our strain sensors only contain Ag and materials. Ag is a biocompatible material, and has been used in surgical implants. As mentioned before, CNC is an environmentally friendly material. Therefore, our strain sensors have a minimal environmental impact from the perspective of materials. Inhaled nanoparticles are still huge concerns for human safety, and the medical use of our devices should be carefully investigated before real applications.

2.4 Conclusions

2.4.1 Summary of Chapter 2

In conclusion, we reported on the fabrication and characterization of a strain sensor employing Ag nanoparticles and water-soluble CNC substrates, which is the first demonstration of using PDMS stencils to pattern metal electrodes on water-soluble substrates. The stencil was fabricated using a silicon mould and PDMS stencils, and has the potential to be widely used in the field of transient electronics and produce high-resolution features with further optimization. Our strain sensors show a high gauge-factor of 52.44 as can be seen from the comparison in Table 2.1, which is higher than any other strain sensors on water-soluble substrates and comparable with the best metal nanoparticle based strain sensors on other types of substrates.

Table 2.1: Comparison of different strain sensors in terms of GF

Type	substrate	GF	Reference
Ag NP piezoresistive (device in this chapter)	CNC paper (flexible&soluble)	52.44	
CNT piezoresistive	PDMS (flexible)	0.06-0.82	[193]
CNT piezoresistive	PDMS (flexible)	∼4	[134]
Metal foil piezoresistive (metal strain gauge)	Plastic (flexible)	2	[193]
Pentacene piezoresistive	PEN (flexible)	11.5	[199]
PEDOT:PSS piezoresistive	PEN (flexible)	11.5	[200]
Platinum NP piezoresistive	Silicon (rigid)	75	[201]
Chromium NP piezoresistive	PET (flexible)	20	[192]
Gold NP piezoresistive	PET (flexible)	20-180	[202]
Gold NP piezoresistive	Inkjet transparency film (flexible)	99	[196]
Ag NP piezoresistive	PDMS (flexible)	0.06-2.05	[203]
Silicon nano-membrane piezoresistive	Silk (flexible&soluble)	∼40	[165]

2.4.2 Contribution to the thesis

In this chapter, I discussed our work about a strain sensor assembled on a recyclable and renewable substrate, CNC paper. With the recycling ability

enabled, the production cost of device can be lowered.

Chapter 3

Surface-modified substrates for quantum dot inks in printed electronics

3.1 Introduction

Printed electronics enables electronic and photonic devices to be fabricated by printing-based technologies such as screen printing, inkjet printing, roll-to-roll printing, and so on.[5], [204] As an additive manufacturing technique, the printing technique can effectively reduce costs by high volume manufacturing and less utilization of complicated semiconductor manufacturing instruments (e.g., metal organic chemical vapor deposition). Thanks to these advantages, the market of printed electronics is fastly growing and it is predicted to reach 330 billion USD by 2027. Consequently, researchers from both industry and academia are making efforts in developing high-performance functional devices, from simple circuits[205] to complex transistors[98] and light-emitting devices,[206] by the printing technique. However, there are still challenges in this field, which need to be conquered, such as seeking of high-performance electronic inks and higher-resolution printing technologies,[85], [207] while the substrate is another major consideration in printed electronics and one needs to match the properties of the electronic ink with the surface properties of the substrate. One of the most important properties of the substrate surface is its hydrophobicity or the surface energy. If the surface is more hydrophilic, the water-based ink tends to adhere better to the surface. Plasma treatment is a

popular method to create a hydrophilic surface, which is brought about by dangling bonds and hydroxyl groups. Other than hydrophobicity, the interface trap is another important issue on the substrate surface in printing functional electronic devices.[208] Dangling bonds and hydroxyls on the surface will form interface trap sites that will affect the performance of printed electronic devices. Therefore, an extra passivation strategy is needed to eliminate these trap sites.[209] The use of self-assembled monolayers is a common route to surface passivation. Usually, self-assembled monolayers are long-chain, complex organic molecules, such as bis(trimethylsilyl)-amine,[210] octadecyltrichlorosilane (OTS), divinyltetramethyldisiloxane-bis(benzocyclobutene), and polystyrene.[211] However, these molecules will create an extremely hydrophobic surface, which is a problem in printing manufacturing.

CQDs are gradually attracting the attention of researchers, not only because of their extraordinary features such as tunable absorption spectrum and narrow emission spectrum that make them widely used in solar energy harvesting,[212], [213] light-emitting devices,[70] and light sensing[214] but also due to their solution processability and amorphous nature that enable a lot of flexible electronic devices, such as flexible touch sensors,[215] flexible gas sensors,[72] and flexible logic circuits.[216] The solution-processed CQD-based devices also have the potential to be mass-produced by printing methods. To fit in this trend, solution-phased in-situ ligand exchange is developed to acquire CQDs with short ligands.[217] Among different types of CQDs, PbS CQDs are one of the most promising candidates because of their unique properties and multi-exciton generation, which makes PbS CQDs gain a lot of attention in photonic applications, such as photovoltaic devices[218] and photodetectors.[219], [220] Previously, because of the existence of long ligands, layer-by-layer deposition was demonstrated to be an effective way to create high-quality, device-level PbS CQD films.[221] However, this deposition method heavily restricts the application of printing PbS CQD devices because it does not allow the CQD films to be deposited in one cast. Recently, phase-transfer ligand exchange was introduced into fabricating PbS CQD

inks.[222]–[224] Phase-transfer ligand exchange allows PbS CQDs to obtain extremely short ligands, such as halide atoms, in suspension conditions. Thus, the ligand-exchanged CQD suspension is able to form a high-quality film in one cast. It is the CQD ink that has the potential to be used in printing instruments. However, the PbS CQD ink is usually made using a polar carrying solvent like DMF which does not allow the PbS CQD ink to be printed on well-passivated hydrophobic substrates. However, researchers only developed ways to suppress the substrate trap sites by using self-assembled monolayers with nonpolar head groups;[225] the electronic device-friendly, trap-free passivated hydrophilic surface is still an obstacle for the PbS CQD ink to be fully printed.

Here, we propose a new strategy to create a trap-free substrate surface suitable for PbS CQD ink by Cl modification. Iodine atoms were previously utilized to eliminate trap states at the heterojunction interface to fabricate high-performance photonic devices.[226] We extend it to halide modification for various rigid and flexible substrate surfaces and apply Cl-modified SiO_2 surfaces for high-performance CQD FETs. In this study, we first verified the successful passivation of Cl on the SiO_2 surface using XPS. The contact angle measurement further showed the reduced contact angle between a droplet of DMF and the SiO_2 substrate. Then, this modification method was extended to other rigid and flexible substrates, such as Si and PI (Kapton^{TM} films from DuPont). Finally, PbS CQD ink was utilized to make an FET with a Cl-modified interface, which shows an obvious higher mobility than the unmodified control device due to suppressed surface trap sites by Cl-modification. The whole solution process shows the potential of PbS CQD inks to be introduced into printing manufacturing, which will foster the development of CQD materials for future printed electronics.

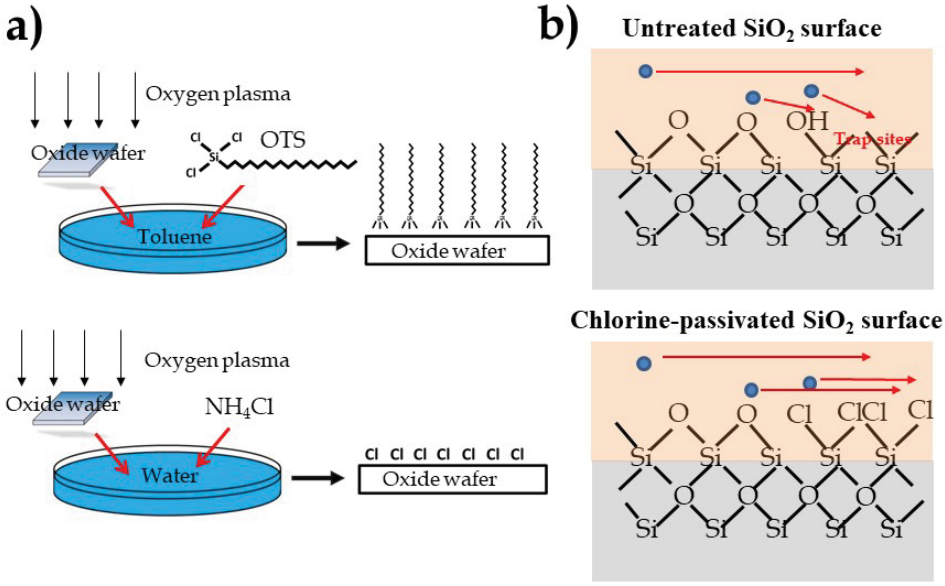

Figure 3.1: (a) Illustration of the surface passivation process. (b) Schematic of the interface trap mechanism.

3.2 Results and discussion

The surface modification process is shown in Fig. 3.1(a). The substrates were treated by oxygen plasma to acquire a surface that contains a lot of silicon dangling bonds. Then, the substrate would be placed in a Petri dish that contains OTS/toluene solution or NH_4Cl/water solution for 30 min. The detailed experimental procedures are described in the Experimental Section in this Chapter. By this simple solution surface modification, passivated surfaces can be obtained. Normally, SiO_2 surfaces have a large number of hydroxyls and Si dangling bonds as shown in the top panel of Fig. 3.1(b). These surface groups can act as trap sites that will trap charge carriers. Thus, the dangling bonds and hydroxyls will affect carrier transport as indicated as trap states. So, the passivated surface is an essential part in making a high-performance electronic device. Either the modification molecule of OTS or the Cl as we proposed can eliminate hydroxyls and dangling bonds as shown in the bottom panel in Fig. 3.1(b), which will make carrier transport more efficient.

To verify that the chemical reactions in modification did occur on the surfaces, we carried out FTIR and XPS on substrates with different modifications. From Fig. 3.2(a), it can be easily seen that the bare SiO_2 and Cl-modified substrate show no abnormal absorption in the wavenumber range 2700-3200 cm^{-1}. However, there are two absorption peaks observed at 2849 and 2917 cm^{-1}, which coincide with the results of previously reported OTS absorption on the SiO_2/Si substrate.[227] Because the characteristic peaks of Cl cannot be observed in the infrared range, XPS was utilized to confirm Cl on the SiO_2 substrate. It is shown in Fig. 3.2(b) that the Cl 2p peak, which has a similar binding-energy value to that in a previous report,[228] can be seen in the right panel (the fitted red dashed line), which represents the Cl-modified interface, whereas the OTS-modified interface only shows noise. EDX measurement (Fig. 3.3) was also performed on a bare SiO_2 substrate, which shows no Cl characteristic peaks.

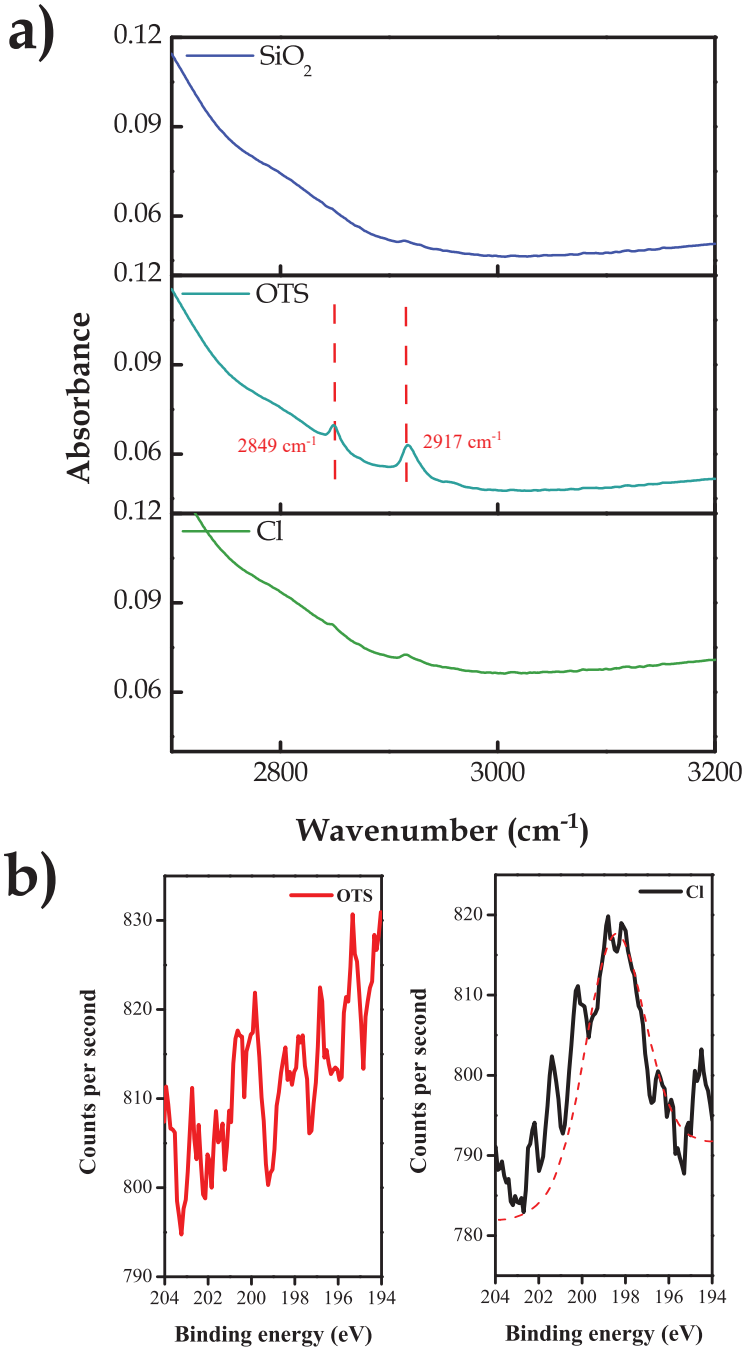

Figure 3.2: . (a) FTIR results of substrates with different modifications. (b) XPS results of the OTS-passivated surface and the Cl-passivated surface. The red dashed line is fitted with the Cl 2p peak.

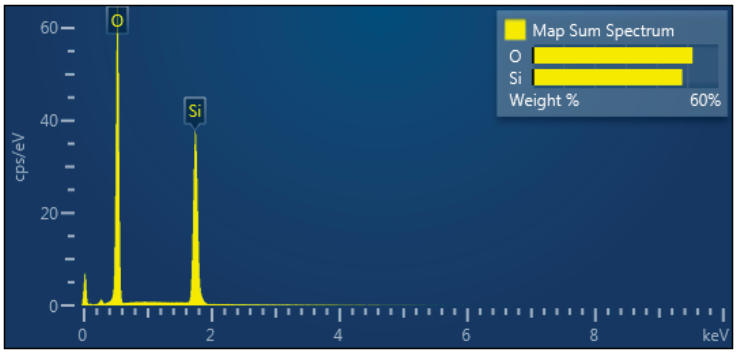

Figure 3.3: (a) FTIR results of substrates with different modifications. (b) XPS results of the OTS-passivated surface and the Cl-passivated surface. The red dashed line is fitted with the Cl 2p peak.

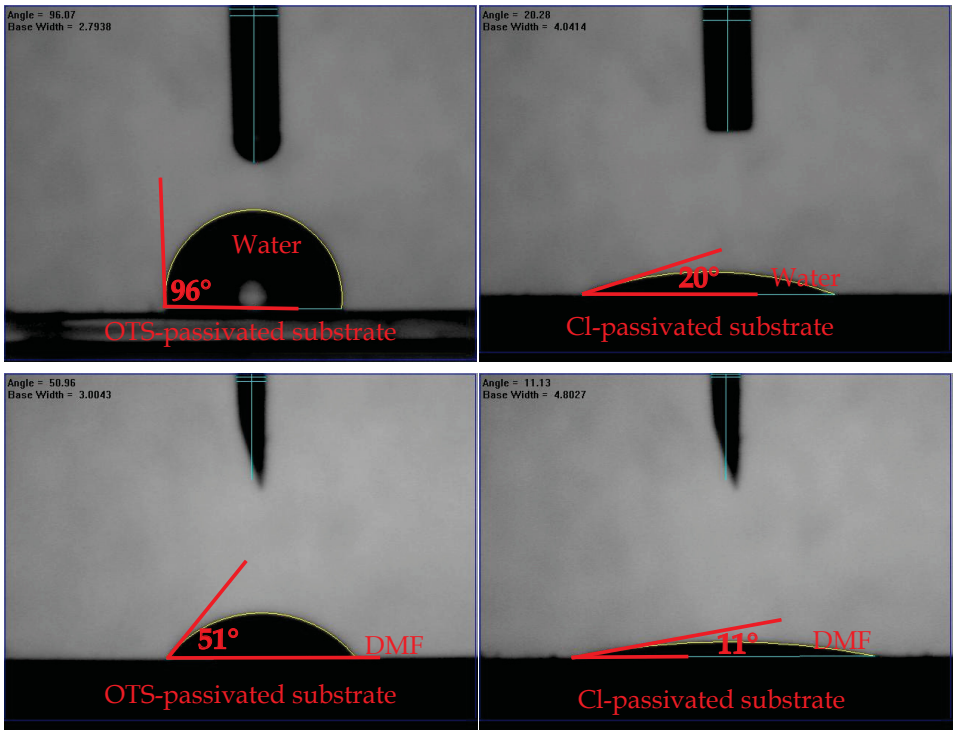

Figure 3.4: Contact angle measurement of water and DMF on OTS-passivated and Cl-passivated surfaces.

Figure 3.5: Contact angles between Cl-modified SiO_2 substrate and water/DMF after 1, 4 and 8 days.

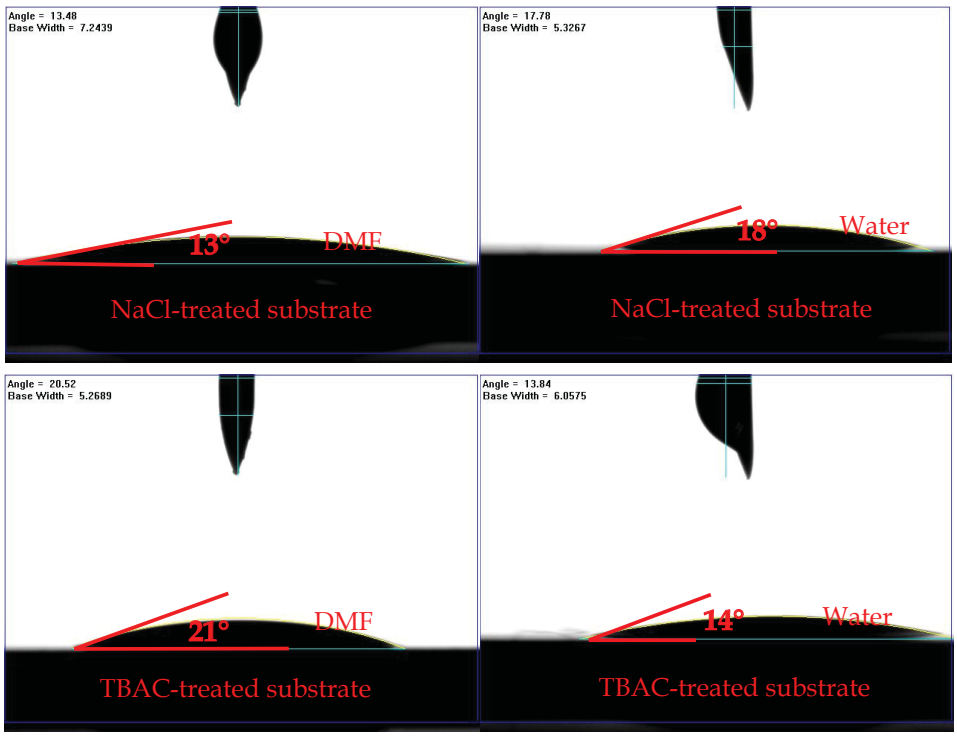

Figure 3.6: Contact angles between NaCl/TBAC-treated substrates and water/DMF.

To investigate the processing compatibility of Cl-modified surfaces for PbS CQD inks, we made contact angle measurement of water and DMF (carrying solvent of PbS CQD inks) on glass substrates. The OTS-modified SiO_2 substrate, a previously reported[225] substrate for mobility measurement of PbS CQD films, is used as the control sample here. From the left panel of Fig. 3.4, it can be seen that the contact angles of water and DMF on OTS-modified substrates are 96 and 51°, which may induce some problems in the printing process due to the large contact angles. However, the Cl-modified surface can significantly reduce these contact angles to 20 and 11°, respectively. The small contact angles are in favor of printing PbS CQDs in water and DMF. We also performed experiments to investigate the stability of the Cl-passivated substrates in ambient conditions. As shown in Fig. 3.5, it can be clearly seen that after 1, 4, and 8 days, the water contact angles remain in a relatively similar value, whereas the value of the DMF contact angle with the substrate is slightly increasing. We attributed it to a small amount of desorption of Cl atoms and this indicates that it is preferred to fabricate devices on the substrate before 4 days after Cl treatment. The Cl-modification strategy includes NH_4Cl treatment but not limited to it. Other chloride ionic compounds (NaCl, 3 mg/mL; tetrabutylammonium chloride (TBAC), 15 mg/mL) are also tested by the same treatment process. As shown in Fig. 3.6, NaCl and TBAC treatments can achieve similar results to NH_4Cl treatment. It can be concluded that other chloride ion compounds can also achieve effective substrate modification.

We further applied this surface modification strategy to PI (Kapton^{TM}) and silicon substrates. The results of contact angle measurement are shown in Fig. 3.7. It is seen in the first row that Cl-modification will largely decrease the water contact angle on the Kapton^{TM} substrate, which makes it suitable for aqueous inks. Because both Kapton^{TM} and DMF have a similar structure, the contact angle of DMF on the orginal Kapton^{TM} substrate is already small. Cl-modification will not make a big difference on it. The difference between the values of modified and unmodified surfaces should be a result of system

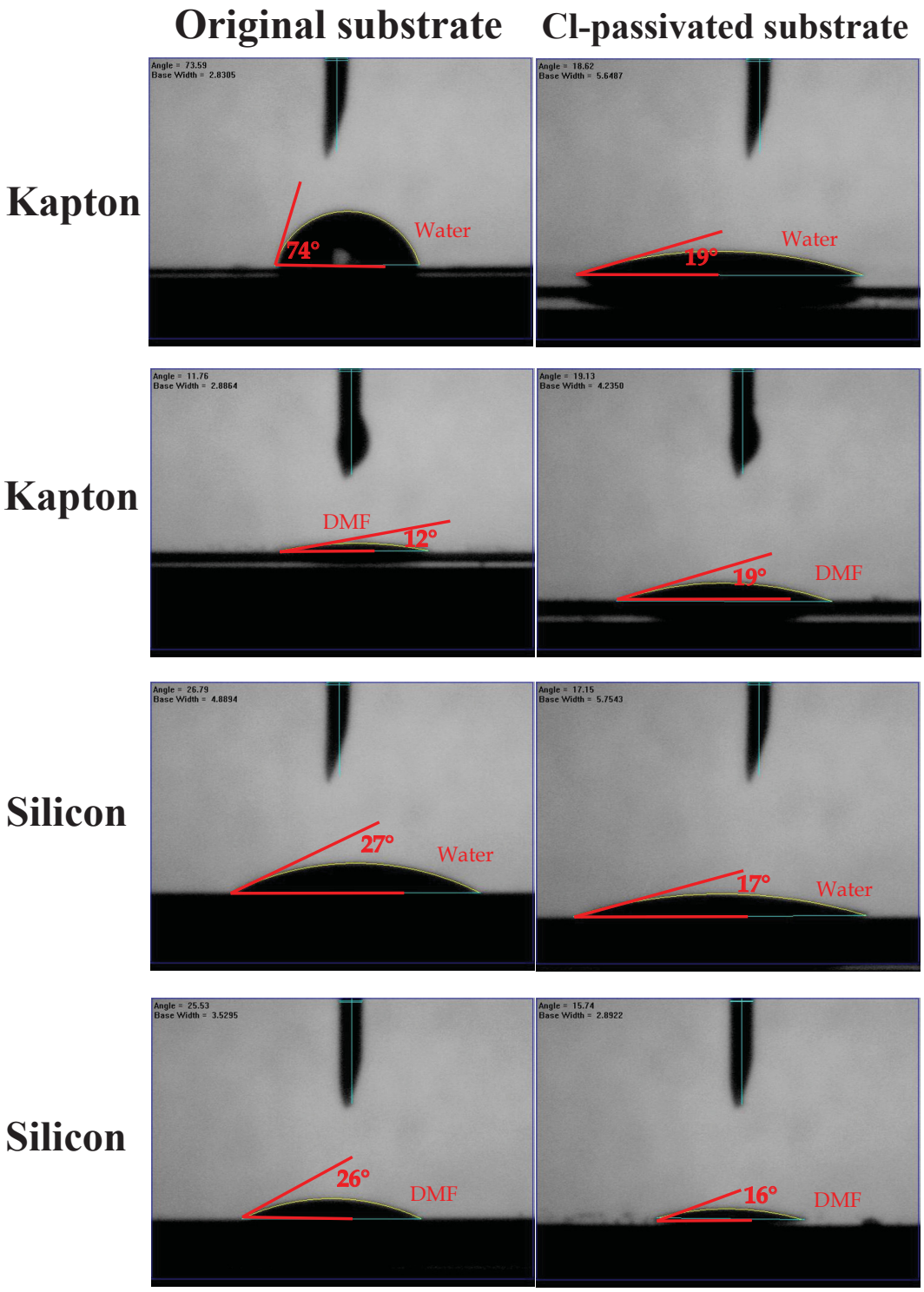

Figure 3.7: Contact angle measurement of solvents on Cl-passivated Kapton™ and silicon substrates.

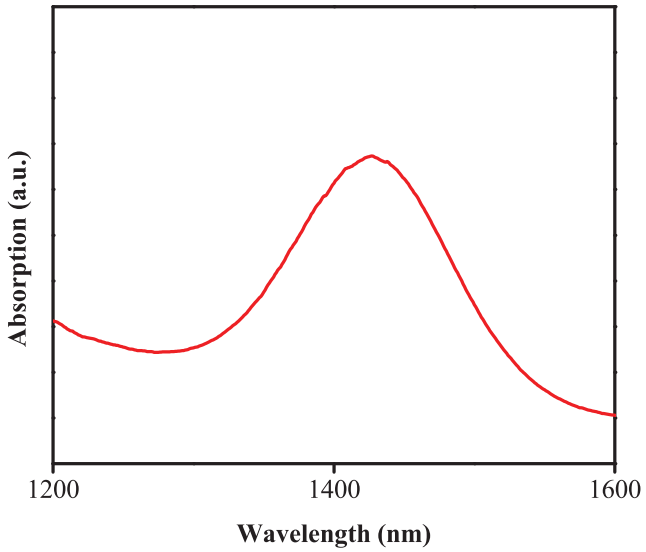

Figure 3.8: PbS CQD absorption spectrum.

error.

The contact angles on the silicon substrate is also shown in Fig. 3.7. Due to the native oxide (low-quality silicon oxide grown in ambient environment) on top of the silicon substrate, the contact angles between water/DMF and the silicon substrate are small. However, after Cl-modification, the contact angles become smaller, which proved that the proposed substrate modification strategy is more effective than the use of a bare silicon substrate. More importantly, the proposed strategy can effectively passivate silicon substrates using Cl-modification, which is confirmed in the demonstration below. Considering that the Cl-modification strategy is effective on the polymer substrate and other silicon-based materials, we conclude that this strategy has potential to act as a universal method to passivate various substrates in printed electronics.

To characterize the interface traps, we performed experiments to examine the carrier decay dynamics. PbS CQD films were deposited between gold electrodes by the traditional layer-by-layer strategy.[221] The detailed procedure of PbS CQD synthesis is in the Experimental Section in this Chapter. As shown in Fig. 3.8, the first excitonic peak is observed at

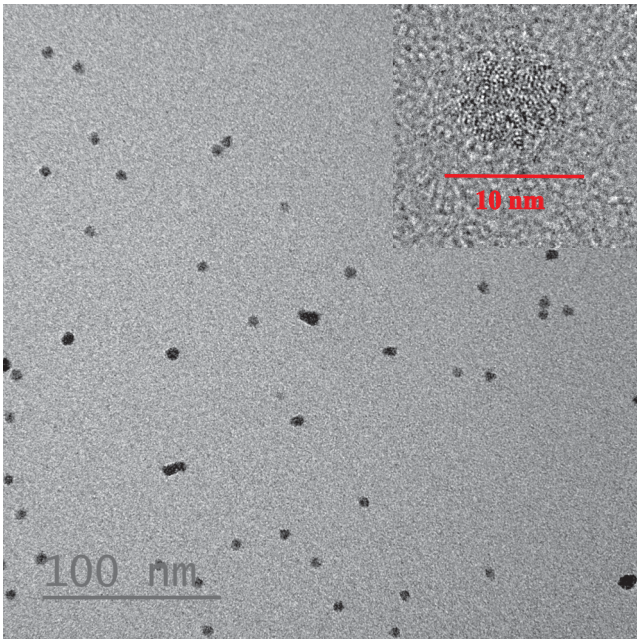

Figure 3.9: TEM image of PbS CQDs.

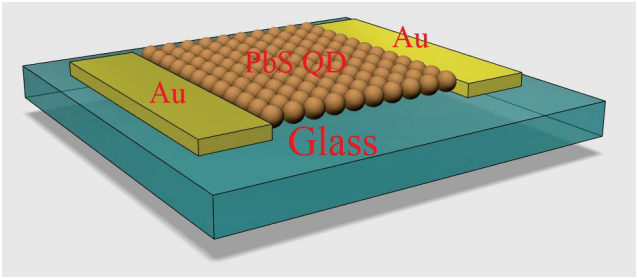

Figure 3.10: Schematic of device for carrier decay dynamic analysis.

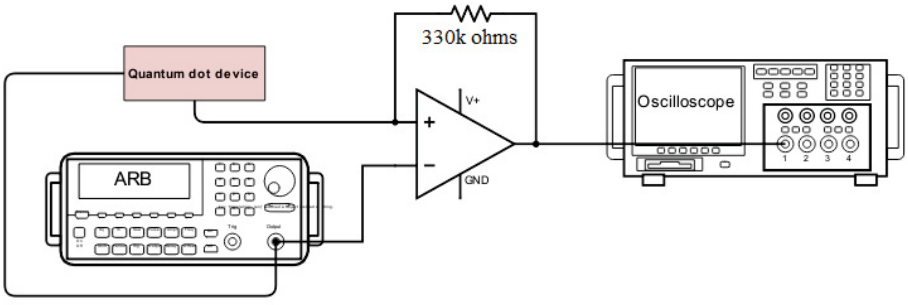

Figure 3.11: Carrier decay testing set-up.

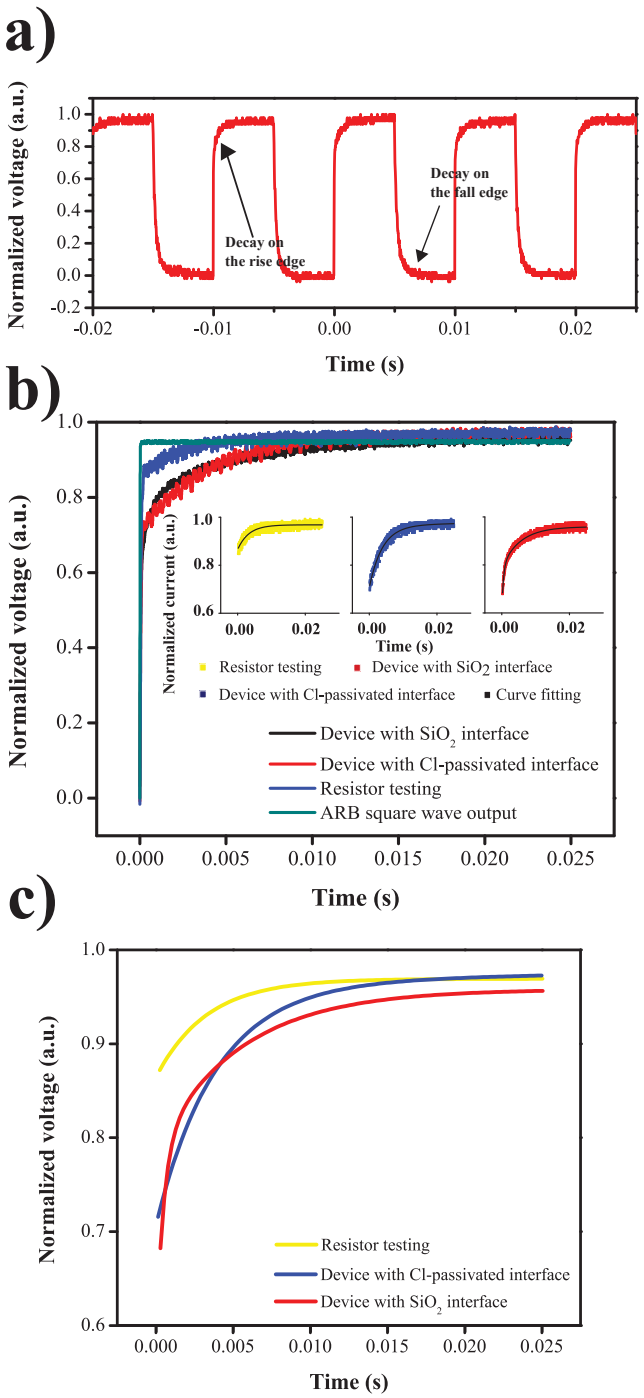

Figure 3.12: (a) Voltage response of a quantum dot device to a 100 Hz square wave. (b) Zoom-in graphs of decay on the rise edge. Inset: curve-fitting of different devices. (c) Fitting curves which show different decay times.

1430 nm. The size of the quantum dots is around 6 nm as shown in the transmission electron microscopy (TEM) image in Fig. 3.9. The device we used in this testing has two terminals as shown in Fig. 3.10. The detailed device fabrication procedure is shown in the Experimental Section in this Chapter. The testing set-up is shown in Fig. 3.11. In the measurement, the device is driven by a function generator. The current response of the quantum dot device is linearly converted to a voltage signal by an LM741 operational amplifier with a feedback loop. The output voltage signals are collected by an oscilloscope. The function generator has the output voltage of the square waveform and the device should respond in current signals of the square waveform. However, the rising and falling edges are not as sharp as the original signal from the function generator, as shown in Fig. 3.12a.

Table 3.1: Decay time of different devices

	Pure resistor	Device with Cl-passivated interface	Device with SiO_2 interface
τ_1	3.28 ms	3.40 ms	3.28ms
τ_2	—	5.29 ms	5.40ms
τ_3	—	—	0.49ms

According to previous reports, the rising and falling edges of measured currents can be explained from the trapping and detrapping of charges in PbS CQD films and SiO_2 interfaces.[229], [230] Therefore, the I-t curves (transient responses) of devices can be expressed as multiple exponential decays considering trapping dynamics:

$$V_{amp} \propto I = I_0 \pm \sum_i I_i exp(-\frac{t}{\tau_i}) \tag{3.1}$$

In eq 3.1, V_{amp} is the voltage generated from the operational amplifier, which is linearly proportional to the current (I_{ds}) flowing through the device, whereas τ_i is related to the lifetimes of different types of carrier traps. If the decay curve is on the rising edge, the operator between I_0 and Σ should be minus because it is a trapping process; Otherwise, the operator should be plus

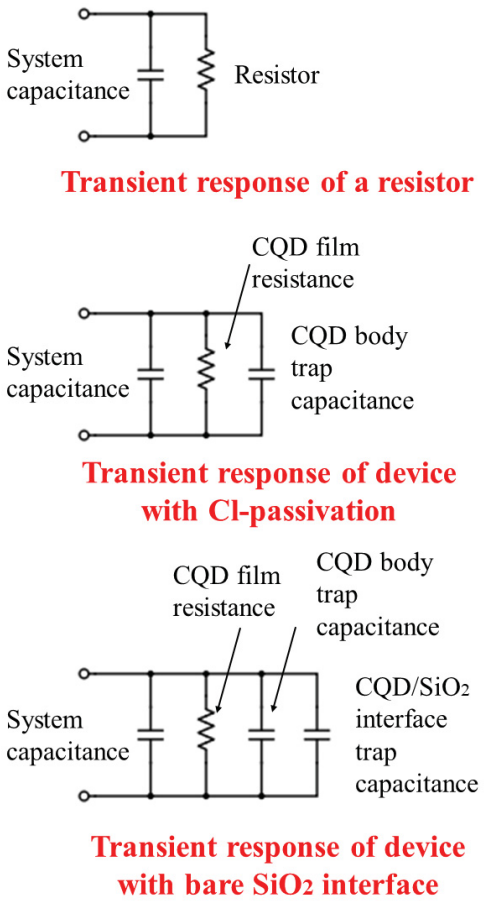

Figure 3.13: From top to bottom: equivalent circuits to a pure resistor, PbS CQD conductor on Cl-passivated surface and PbS CQD conductor on bare SiO_2 surface.

because it is a detrapping process. Here, as shown in Fig. 3.12b, the rising edge is taken for analysis. We first used a 1 MΩ resistor (similar resistance to the CQD devices) to extract the RC charge time (τ_1) of the measurement circuit. Then, the I-t curves of the 1 MΩ resistor, PbS CQD device with the Cl-passivated interface and PbS CQD device with the SiO_2 interface were fitted to eq 3.1, as shown in Fig. 3.12c. The equivalent circuits are shown in Fig. 3.13 and the various decay times (τ_i) of different samples are shown in Table 3.1. In addition to τ_1, the device with the Cl-passivated interface shows another exponential component with a decay time of 5.29 ms and the device with the SiO_2 interface shows two more exponential components with decay times of 5.40 and 0.49 ms. Since 5.29 and 5.40 ms are very close, we attributed them to the trapping time inside PbS CQD films and it may originate from charging the electronic states on CQD surfaces. Another decay time of 0.49 ms is only shown in the device with the SiO_2 interface, and we attributed it to charging the interface traps on SiO_2 substrates. Therefore, we conclude that the Cl-passivation strategy can eliminate SiO_2 interface trap states.

To verify the potential of Cl-passivation as an effective way towards hydrophilic, trap-free substrates, we fabricated PbS CQD FETs with different interfaces. The original PbS CQDs are capped with long oleic acid suspending in octane. To acquire PbS CQD ink, the phase-transfer ligand exchange procedure is followed. As shown in Fig. 3.14a, before ligand exchange, the PbS CQDs were in nonpolar octane solvent. After agitation, the PbS CQDs were covered by iodide. Thus, they were transferred to the bottom polar DMF solvent. The XPS spectrum in Fig. 3.15 indicated the successful ligand exchange by observing the I3d peaks in CQDs. Finally, the CQD FETs were fabricated as the steps described in the Experimental Section. The device schematic is shown in Fig. 3.14b. In the FET device, bottom highly doped silicon can act as a gate, whereas the source and drain gold electrodes are made by sputtering. The channel width between the source and drain electrodes is 5 μm. The PbS CQD film is deposited on the substrate by an one-time spin-

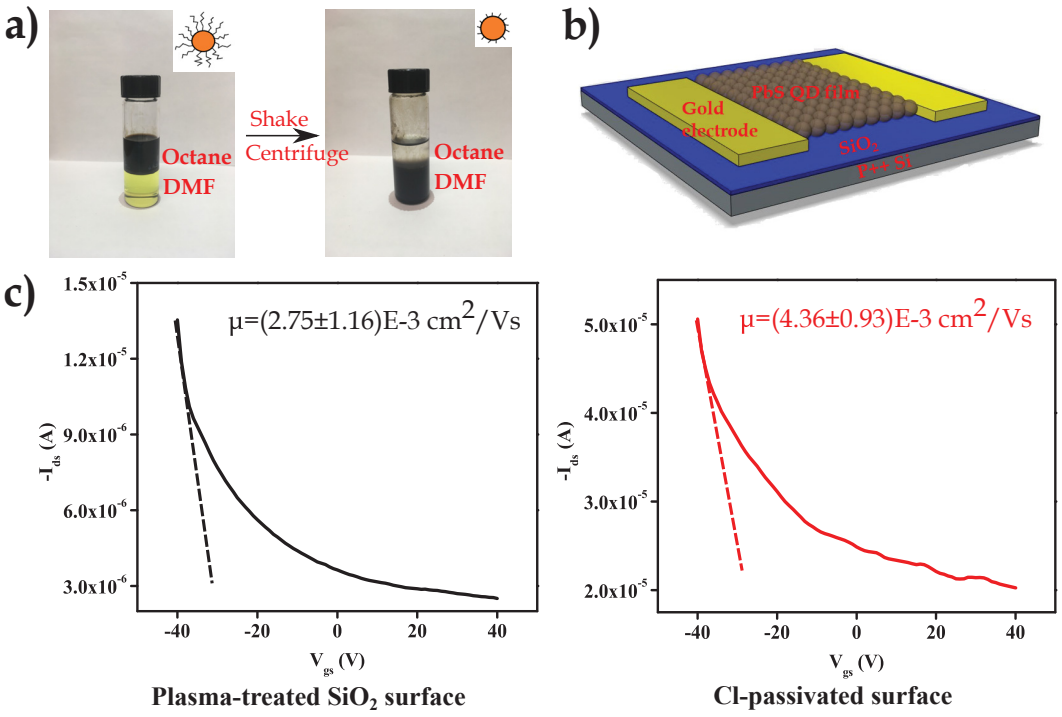

Figure 3.14: (a) Pictures of phase-transfer ligand exchange. (b) Schematic of a CQD ink field-effect transistor. (c) Transfer curves of the CQD ink FET with a plasma-treated SiO2 surface, OTS-passivated surface, and Cl-passivated surface.

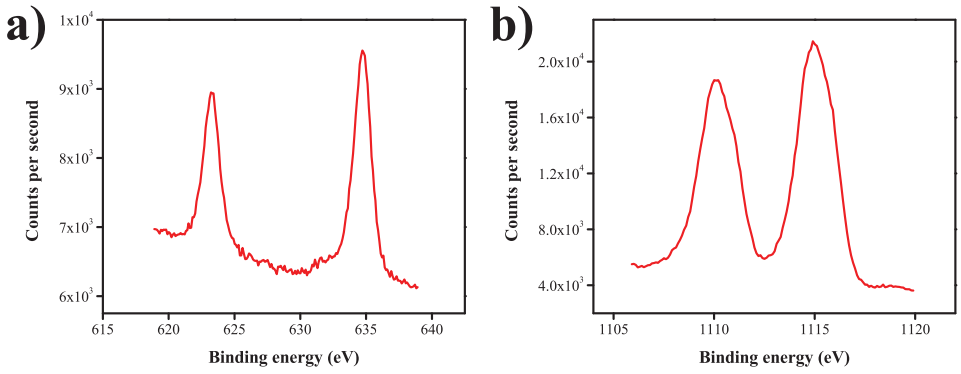

Figure 3.15: a) I3d XPS spectrum of a CQD ink thin film. b) Pb4f XPS spectrum of a CQD ink thin film.

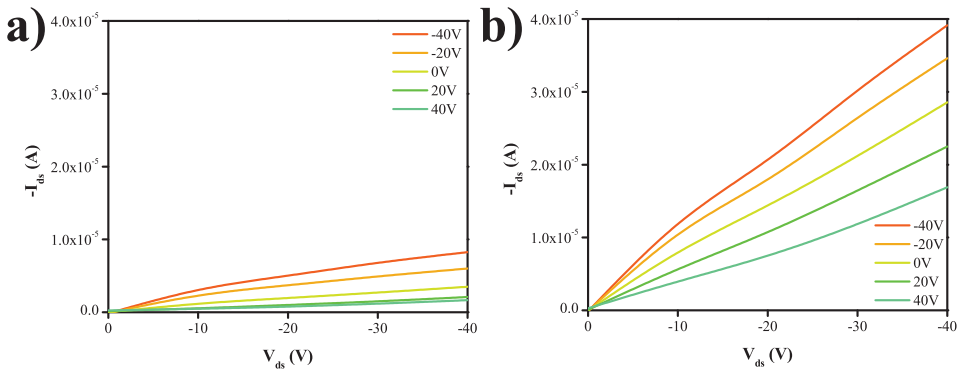

Figure 3.16: a) $I_{ds} - V_{ds}$ curves of device with SiO_2 interface under different gate voltages. b) $I_{ds} - V_{ds}$ curves of device with Cl-passivated interface under different gate voltages.

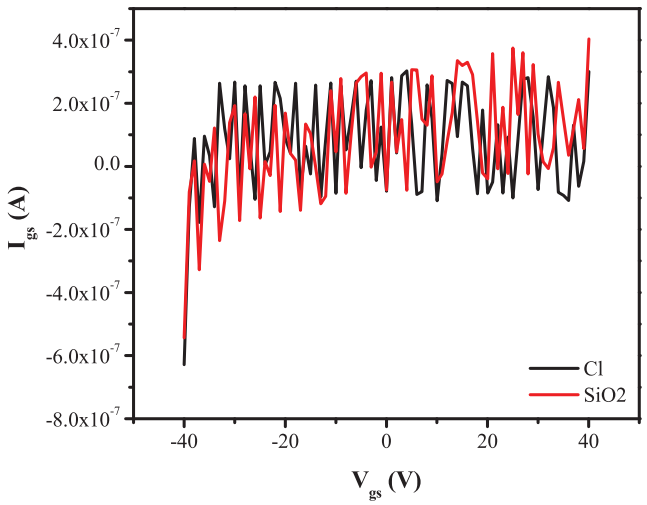

Figure 3.17: Gate currents in transfer curve testing. The red line is from device with SiO_2 interface while the black line is from device with Cl-passivated interface.

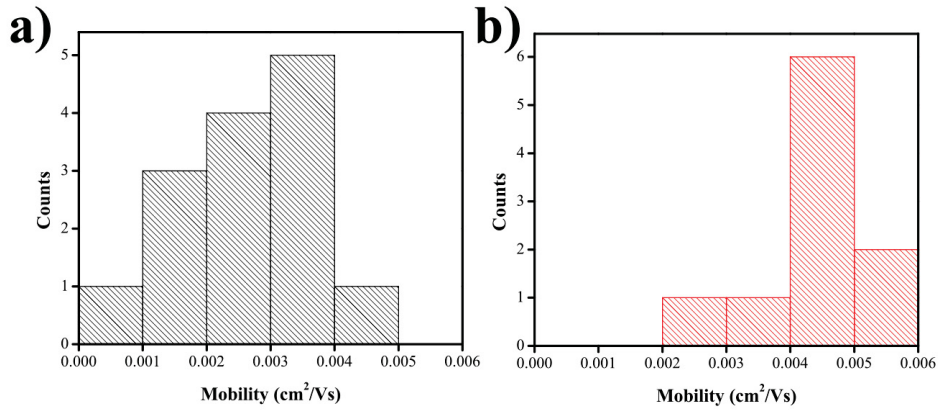

Figure 3.18: Device mobility statistics: a) histogram of mobilities of CQD FETs with SiO_2 interfaces. b) histogram of mobilities of CQD FETs with Cl-passivated interfaces.

coating of CQD inks. The $I_{ds} - V_{ds}$ curves are shown in Fig. 3.16, whereas the transfer curves of these FETs are shown in Fig. 3.14c. The gate currents were also monitored to rule out the gate leakage in FET devices. As shown in Fig. 3.17, the gate current is within noises floating around zero and is several orders of magnitude smaller than the channel current (I_{ds}) at any given voltage (V_{gs}).

The hole mobilities of CQD films are retrieved from the transfer curves. According to previous reports[210], [231], [232], one can assume the CQD FET works in the linear regime. Thus, the expression for I_{ds} would be[208]:

$$I_{ds} = \frac{WC_i\mu}{L}(V_{gs} - V_T - \frac{V_{ds}}{2})V_{ds}. \tag{3.2}$$

The transconductance should be:

$$g_m = \frac{\partial I_{ds}}{\partial V_{gs}}\bigg|_{V_{ds}=const} = \frac{WC_iV_{ds}}{L}\mu. \tag{3.3}$$

In our device, the channel length L is 5 μm, the channel width W is 3 mm and the drain voltage is $V_{ds} = -40\ V$. According to $C_i = \epsilon_{SiO_2}/d$, where $\epsilon_{SiO_2} = 3.9\epsilon_0$ and $d = 500\ nm$, the insulation layer capacitance C_i can be easily calculated. The transfer curves are shown in Fig. 3.14. We can retrieve the mobility of CQD films from these curves using equation 3.3. The transconductance is calculated from the dashed tangent lines. By testing

multiple devices, the mobilities of plasma treated FET and Cl-modified FET can be averaged as 2.75 ± 1.16 $\times 10^{-3}$ and 4.36 ± 0.93 $\times 10^{-3}$ $cm^2/V \cdot s$, respectively. The histograms are shown as Fig. 3.18. We attributed the low mobility of the plasma-treated FET to trap sites on the plasma-treated SiO_2 surface. The Cl-modified FET showed a large mobility, 60% larger than the plasma-treated one, because Cl can effectively passivate the surface trap sites. We also tried to fabricate a PbS CQD ink FET on an OTS-modified substrate. However, we cannot retrieve any reliable data out of it, due to the poor film quality on the OTS-modified surface. This agrees with the large contact angle between CQD ink and the OTS-modified surface.

3.3 Experimental

3.3.1 Materials

Lead acetate (PbAc), n-octane, ammonium acetate (NH_4Ac), and DMF were purchased from Fisher Scientific Inc. Ammonium chloride (NH_4Cl), 1-octadecene (ODE), oleic acid, hexamethyldisilathiane (TMS2-S), tetrabutylammonium iodide, and lead iodide (PbI_2) are all acquired from Sigma-Aldrich Inc. The PI (Kapton^{TM}, 5 mil) films we used in contact angle testing were purchased from DuPont Inc. (Delaware). All of the silicon and oxide wafers utilized in the experiments were from University Wafer Inc. (Boston, MA).

3.3.2 Cl modification

All substrate surfaces were activated by oxygen plasma (ICP-RIE, Alcatel) first. After surface activation, the substrates were immediately transferred into an NH_4Cl solution with a concentration of 3 mg/mL. After 30 min, the substrates were taken out and washed with water and ethanol.

3.3.3 Characterization

The absorption spectrum of CQDs was acquired on a Perkin Elmer NIR-UV spectrophotometer. A Nicolet 8700 FTIR spectrometer was utilized to obtain

the infrared absorption spectra, whereas XPS was performed on a Kratos AXIS 165 system. The contact angle measurement was performed on an FTA-200 system and the field-effect transistor measurement was done by using a Wentworth probe station and Keithley 2400 sourcemeter.

3.3.4 Quantum dot synthesis

The synthesis process can be referred to in our previous publication.[215] The colloidal lead sulfide quantum dots were synthesized by using a classic two-step hot-injection method. For this, 570 mg of PbAc and 1.05 mL of oleic acid were dissolved in 15 mL of ODE at 100°C in a three-neck flask with a vacuum environment. After 8 h of heating and stirring, the lead oleate precursor would be formed. The vacuum environment was then switched to a nitrogen environment quickly by a Schlenk line. The flask was then heated up to 160°C. After the above steps, another reactant, TMS2-S (160 μL), was prepared by mixing with 7.5 mL of ODE. The reactant solvent was injected quickly to the reaction flask by a syringe. Then, the flask was immediately removed out of the heating mantle to cool down while continuously stirring. When the temperature of the product cooled down to room temperature, it was transferred to centrifuge tubes and washed with acetone two times. Finally, the product was dried in a vacuum and redispersed in octane at a concentration of 50 mg/mL.

3.3.5 TEM and EDX characterization

TEM images were taken using a JEOL JEM-ARM200CF S/TEM system. To prepare the samples, we diluted the PbS CQD suspension in octane to approximately 2 mg/mL and ultrasonicated for 10 min. The diluted suspension was then added dropwise onto a copper grid. After being dried overnight at ambient conditions, the samples were ready for imaging.

The EDX data were acquired by an Oxford EDX on a Zeiss EVO M10 SEM. The samples used were surface-modified quartz glass.

3.3.6 Fabrication of samples for carrier decay dynamic analysis

The two-terminal device was fabricated on a borosilicate glass. A conventional lift-off photolithography process was utilized to create electrodes on top. At first, an HMDS hydrophobic monolayer was assembled on top of the SiO_2 layer by an YES HMDS oven. A HPR-504 photoresist layer was then created by spin-coating. The spread step was performed at 500 rpm for 10 s, whereas the spin step was conducted at 4000 rpm, which will last for 40 s. After spin-coating, the wafer was then transferred onto a hotplate for softbaking (90 s @ 115°C) to evaporate all solvents. The exposure step was conducted on a mask aligner from ABM Inc. (San Jose, CA). The exposure time was 3 s with an intensity of 66.7 mW/cm^2 at 365/405 nm. Developer 354 was then applied to develop photoresist patterns for 45 s with agitation. The electrode deposition (5 nm of chromium as the adhesion layer and 65 nm of gold) was performed on a home-made sputtering system. Finally, the wafer was soaked in acetone to lift off extra gold.

Before deposition of the CQD film, the substrate was treated by oxygen plasma to remove all HDMS molecules. It was then modified by Cl as shown in the previous step. The control device was fabricated on an OTS-modified substrate. The substrate was treated in 1% (v/v) OTS solution for 2 h.

The CQD film deposition was done by a traditional layer-by-layer strategy as described in a previous report.[221] The original CQD suspension (50 mg/mL) was diluted to 16.7 mg/mL in octane. Each layer iteration included three substeps: (1) three drops of lead sulfide CQD suspension was applied on the surface and spun (2500 rpm) for 10 s; (2) 0.25 mL of ammonium chloride (NH_4Cl, Sigma-Aldrich Inc.) solution in methanol was added dropwise on the CQD film and remained there for 5 s and then spun for 10 s to flush the solution away; (3) methanol was employed to wash the CQD film finally. We let the methanol remain on the film for 10 s and then spun it away. This washing

step should be repeated two times.

3.3.7 Phase-transfer ligand exchange

To enable biphasic ligand exchange, 0.235 g of PbI_2 and 0.015 g of NH_4Ac were dissolved in 5 mL of DMF. Then, 5 mL of PbS CQD suspension (10 mg/mL, in octane) was added. After 1 min shaking by hand and centrifuging, the PbS CQDs were transferred from the octane phase to the DMF phase. The octane should be removed by a pipette. New octane was added and mixed by a vortex mixer to wash out the residual oleic acid. After that, the product was centrifuged to separate the octane. This washing iteration should be repeated three times. After these steps, 5 mL of toluene was added to precipitate the PbS CQDs. The supernatant was then poured out and the CQDs were dried in vacuum for 20 min. Finally, the CQDs were redispersed in DMF.

3.3.8 Field-effect transistor fabrication

The FET devices were based on a SiO_2 wafer with highly doped degenerated silicon, which can act as a back gate. At first, backside SiO_2 was etched off by inductively coupled plasma plasma etching. The fabrication process is exactly the same as in the fabrication of samples for carrier decay dynamic analysis.

The substrate was then treated by oxygen plasma to remove all HDMS molecules. It was then modified by Cl as shown in the previous step. Since the CQD ink can form a highly coupled film by a single cast, the traditional layer-by-layer deposition can be abandoned. Three drops of CQD ink were casted on the top of the substrate. Then, it was spun for 1 min at 2500 rpm. Finally, the device is baked at 150°C for 30 min to evaporate all residual solvents and accomplish a highly coupled thin film.

3.4 Conclusions

3.4.1 Summary of Chapter 3

In this work, we showed a Cl-modification strategy to passivate rigid and flexible substrates for printed electronics. This method can create polar-solvent friendly surfaces on various polymer and inorganic substrates. FTIR and XPS were utilized to verify the passivation. Surface hydrophobicity was characterized by contact angle measurement. Then, carrier dynamic analysis was performed to verify the elimination of surface traps. Finally, we fabricated PbS CQD ink-based FETs on Cl-modified substrates. They showed much higher mobilities in PbS CQD films on Cl-modified substrates than the values extracted from CQD films on plasma-treated substrates and OTS-modified substrates due to effective suppression of surface trap sites by Cl-modification. It can be concluded that Cl-modification can suppress the surface trap sites while creating a hydrophilic surface, showing its potential to be applied in printing techniques.

3.4.2 Contribution to the thesis

In this chapter, I introduced our work about an easy route towards hydrophilic, trap-free surfaces, which can be potentially applied in printed CQD electronic devices. On one hand, the trap-free surface will reduce interface traps to realize high-performance devices. On the other hand, this strategy makes printing technology more practical for flexible CQD devices, which can lower the cost of flexible CQD devices potentially.

Chapter 4

Flexible digital microelectromechanical devices with an engineered PDMS bridge structure for force and strain sensing

4.1 Introduction

Flexible electronics involves the assembly of electronic devices and circuits on flexible substrates. In recent years, functional electronic devices on flexible substrates with sensing and actuating capabilities have been prolifically demonstrated in applications where bending and stretching of devices are required or preferred,[72], [134], [193], [199], [201], [205], [233]–[235] such as in wearable electronics,[143] health-monitoring devices,[236] optical diffusers,[237] e-skin products[134] and flexible radio-frequency identification (RFID) tags.[238] With a booming market in flexible electronics, research on flexible sensors is of great interest in academic settings and for industrial applications.

Strain and pressure sensing are two fundamental sensing functions. Traditional strain sensors use metal foils for good air-stability and reusability. However, a GF of only 1-2 can be obtained by metal foil strain gauges, depending on the conductor's geometry.[239] In recent years, various flexible

and high-GF strain sensors were demonstrated using new-class-of materials, including metal nanoparticles,[201], [203], [205] CNTs,[193] PDMS/metal nanoparticle composites,[240] fabric based materials[241] and polymers.[199] These materials were also employed to develop flexible pressure sensors in recent years.[242]–[244] For example, Bao et al. applied CNTs on a PDMS substrate to form e-skin with both pressure and strain sensing capabilities[134]. However, the analog-signal output of these sensors requires high standards in device fabrication for mass-production. On the other side, sensors with digital-signal output could provide high tolerance for easy fabrication, and are of interest if these sensors can be engineered to achieve various sensitivities. In 2016, Lai et al. reported an e-skin sensor with digital signal output, which was based on the electrical insulating-to-conducting transition.[242] In the same year, Jiang et al. demonstrated another type of strain sensors with digital signal output using triboelectric effect.[245]

Here we presented a new design of flexible strain/pressure sensors, which can switch from insulation to conduction in a tiny amount of time. To our best acknowledgment, this work is the first report of flexible digital sensors with both strain and pressure sensing abilities. Compared to new-material based sensors with analog signal output, our digital MEM sensors will set much lower requirements in fabrication and do not need calibration after long time usage. With engineered sensing structures, digital MEM devices with different sensitivities can be integrated together to achieve the same function as provided by sensors with analog-signal output. Considering the above advantages, digital MEM sensors can be an alternative solution for strain and pressure sensing in the fields of pressure mapping, sound wave detection and more. In this paper, we managed to control the sensitivity of the digital MEM sensor by changing the 'pier' height of the PDMS bridge.

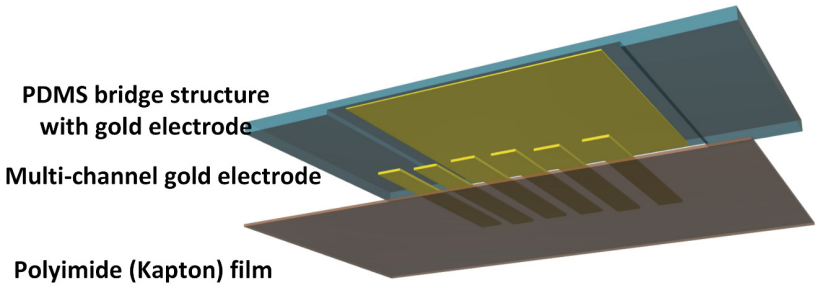

Figure 4.1: Structure of the digital MEM sensors.

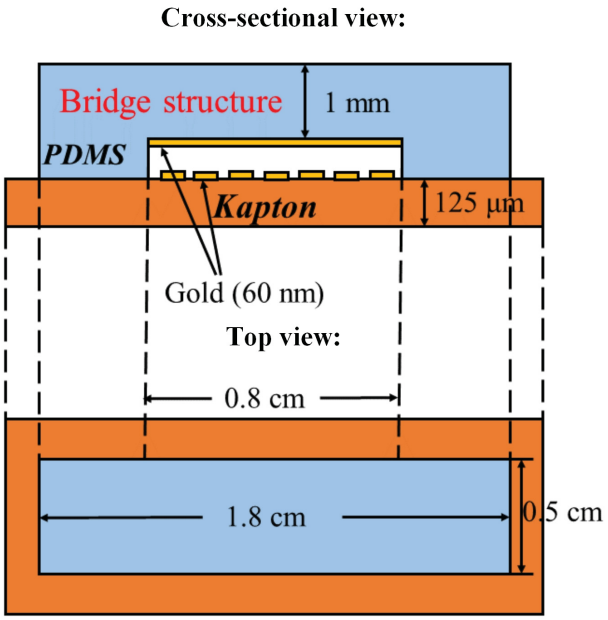

Figure 4.2: Dimension of the digital MEM sensor.

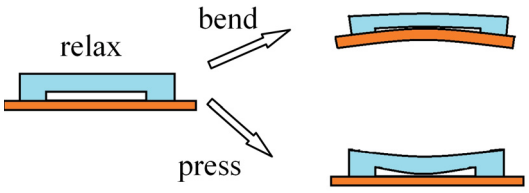

Figure 4.3: Working principle of the digital MEM sensors in two different working modes.

4.2 Device structure and working principle

As illustrated in Fig. 4.1, we chose PI film (DuPont, Kapton^{TM}) as the substrate for bottom electrodes, and used PDMS as the material for the bridge structure. The electrodes on the downside of the bridge structure and on the Kapton^{TM} substrate are all made of gold with thickness of 60 nm. The distance between the top electrode and bottom electrodes can be controlled by adjusting the height of the 'piers' of the bridge structure. The details of the dimension for this digital MEM sensor is shown in Fig. 4.2.

Our digital MEM sensors only provide digital signal output. The '0' state means there is no electrical signal between bottom electrodes. When bottom electrodes on the Kapton^{TM} substrate contact the top electrode on the PDMS bridge, electrical current will be observed under applied voltage. This is referred as '1' state, in which the conducting channel is formed between bottom electrodes. As shown in Fig. 4.3, the digital MEM sensor has two working modes. The first mode is the strain sensing mode. In bending test, the PDMS bridge is more likely to be stretched from tangential direction by the bridge piers while the Kapton^{TM} substrate is bent in a fixed radius. This will make bottom electrodes contact the top electrode on PDMS to form the conducting channel. The other mode is the pressure sensing mode. Since the young's modulus of PDMS is much smaller than the Kapton^{TM} film, the bridge will touch the Kapton^{TM} substrate when we apply certain pressures on the PDMS bridge. Thus, the conducting channel is formed between bottom electrodes.

4.3 Experimental

4.3.1 Preparation of PDMS bridge structures

Table 4.1: SU-8 photolithography parameters

	Spin speed (rpm)	Soft bake 1 (min)	Soft bake 2 (min)	Exposure dose (mJ/cm^2)	PEB 1 (min)	PEB 2 (min)	Development time
58 μm	3000	3	10	230	1	7	5
90 μm	2000	3	10	275	2	8	7
124 μm	1200	7	45	375	1	12	10

As shown in the left part in Fig. 4.4, the PDMS bridge structures were prepared by soft lithography. At first, SU-8 cuboids of which the thickness can be controlled by the speed of spin-coating were patterned on a piranha-cleaned 4-inch silicon wafer by photolithography. Detailed SU-8 lithography parameters can be found in Table 4.1. In our experiment, we used three different speed, 1200 rpm, 2000 rpm and 3000 rpm, to produce SU-8 films with the thickness of 124 μm, 90 μm and 58 μm (measured by profilometer), respectively. By controlling the height, we managed to control the sensing ability of our digital MEM sensors. We bent our digital MEM devices using aluminum blocks with different radii. The strain applied to each device was calculated using the method described in the Appendix. A Keithley 2400 source meter was employed to apply 0.1 V across two electrodes on the Kapton^{TM} substrate, and the current passing through these two electrodes was probed by the same instrument. The details of the experimental setup was shown in Fig. 4.5.

Then the wafer was passivated with the vapors of OTS (Sigma Aldrich Inc.) in a vacuum desiccator for over 8 hours. PDMS was prepared from Dow Corning Sylgard 184 kit with a base-to-crosslinker ratio of 10:1. The mixture of base and crosslinker was then degassed, syringed out for 6 ml and poured onto the SU-8 patterned silicon wafer. After being cured at 80°C for 30 min, the PDMS will be solidified. Because of the OTS monolayer on the silicon wafer, the PDMS membrane was easy to be peeled off and cut into

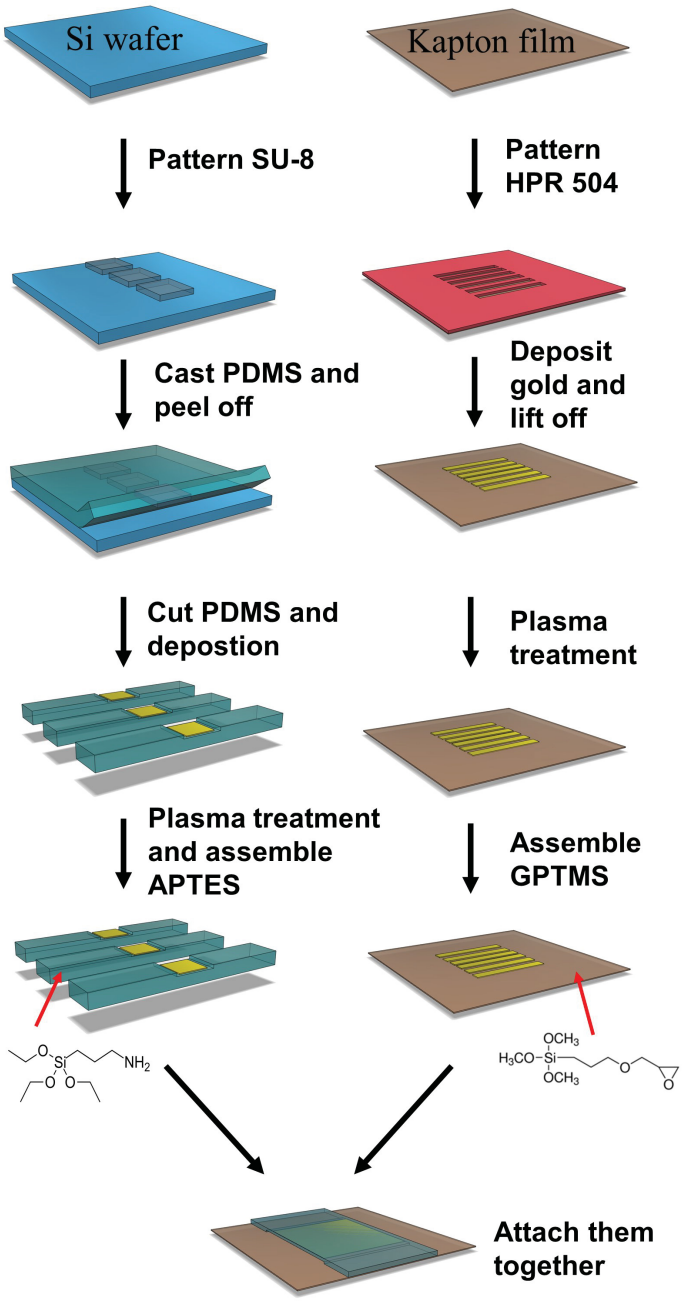

Figure 4.4: Process flow of the fabrication of digital MEM sensors.

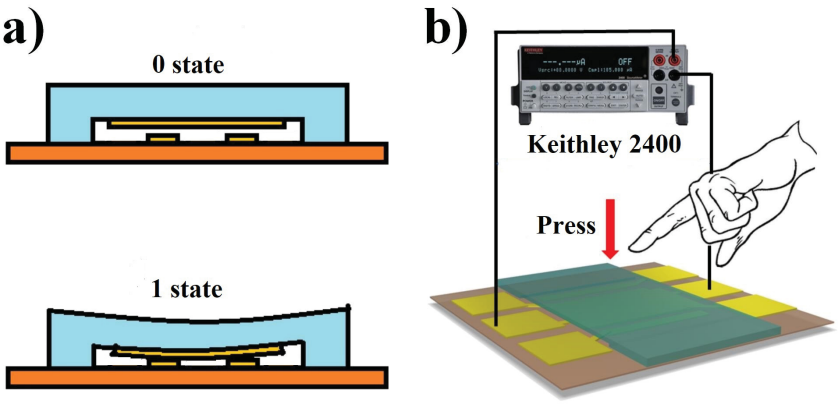

Figure 4.5: a) Schematics of the digital MEM sensor at '0' and '1' states. b) Measurement testing setup illustration.

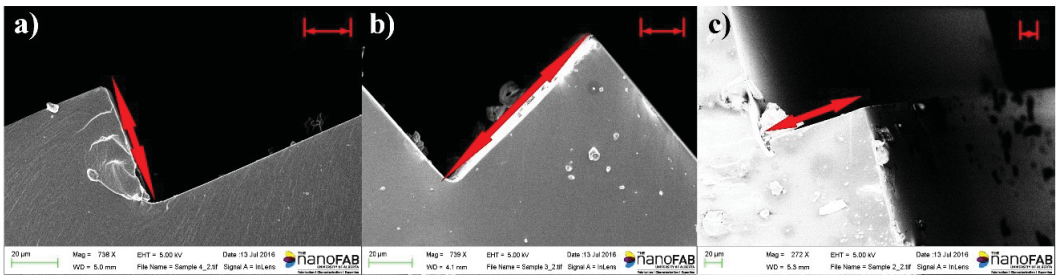

Figure 4.6: SEM images for bridges with different heights. a), b) and c) show 54 μm, 90 μm and 128 μm bridges, respectively. (Red arrows are showing heights for bridges while red legend represents 20 μm.)

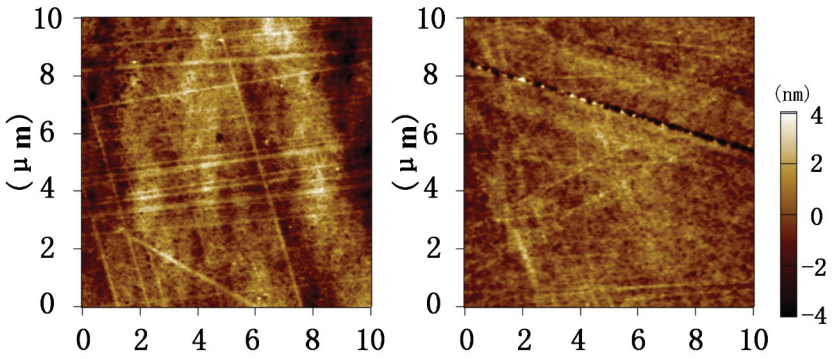

Figure 4.7: AFM images of PDMS bridge surfaces: the left one is the area which contacts silicon wafer while the right one is the area contacting SU-8 patterns.

bridge structures we want. SEM images in Fig. 4.6 show that the shape of SU-8 moulds was successfully transferred onto PDMS structures. The height of each bridge structure is almost the same as the SU-8 mould. At last, 60 nm gold layer with a Cr layer of 10 nm as adhesion layer was sputtered on the bottom of the bridge structure assisted by a PDMS shadow mask.[42] We did AFM measurement to check the smoothness of PDMS surfaces. As shown in Fig. 4.7, both the surfaces contacting SU-8 and silicon wafer are very smooth, with the roughness standard deviation of 0.893 nm and 1.283 nm, respectively.

4.3.2 Preparation of bottom electrodes on PI substrate

Gold electrode on PI film was produced by a lift-off lithography process. HPR 504 photoresist was patterned on Kapton^{TM} film by photolithography and 60 nm gold layer with 10 nm chromium adhesion layer was sputtered on the Kapton^{TM} film. A lift-off process by soaking the Kapton^{TM} film in acetone for 2 hours was then followed.

4.3.3 Bonding of the bridge structure and Kapton^{TM} film

PDMS bridge structures and Kapton^{TM} film with gold electrodes were ultrasonically cleaned and activated with oxygen plasma (60W, 700 mTorr, 60s). According to the previous report,[246] we immediately immerse the PDMS and Kapton^{TM} structures into (3-Aminopropyl) triethoxysilane (APTES, Sigma Aldrich Inc.) and (3-Glycidoxypropyl) methyldiethoxysilane (GPTMS, Sigma Aldrich Inc.) water solutions (10%, v/v) for 2 hours. Two water baths were followed to clean them. Then both structures should be well dried and bonded together as shown in the last graph in Fig. 4.4. Gentle pressure should be applied on the piers of the bridge structure to make them attached tightly. At last, after 16h's reaction time, these two structures will be bonded together permanently and irreversibly.

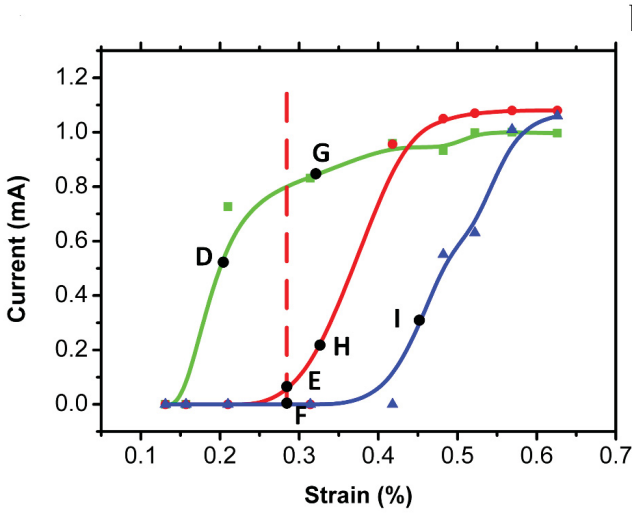

Figure 4.8: Currents flowing through the device when different strain applied on Kapton^{TM} substrate. In this graph, the green, blue and red curves represent sensors with 58 μm, 90 μm and 124 μm pier height, respectively.

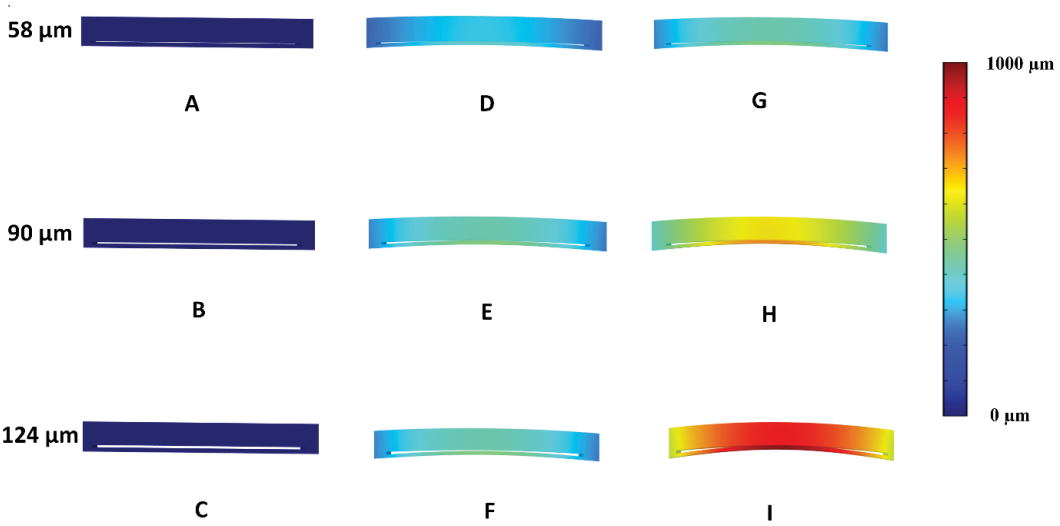

Figure 4.9: Simulated displacement distribution of devices with different pier height in relax and bending conditions.

4.4 Results and discussions

Sensors with digital signal output may set high tolerance in device fabrication, but it won't be broadly adopted until the sensor can be engineered to achieve desired sensitivity. In this demonstration, we show various digital MEM sensors with different detection limits by engineering the PDMS bridge structures. Fig. 4.8 is the electrical current vs. strain curves of three MEM sensors with different pier heights of the PDMS bridge. The curves were smoothed by B-spline in OriginLab. In the bending test, when we tightened our devices on steel blocks with different radii, these devices were stretched to certain strains. When the radius got smaller, the strain became bigger and the Kapton^{TM} substrate tended to touch the PDMS bridge. We observed small current when the Kapton^{TM} substrate gently touched the PDMS bridge, and this current was saturated when two films were firmly touched. Depending on the geometry of the structure, we can design the MEM sensor to achieve different detection limits for strains. As shown in Fig. 4.9, the green, blue and red curves represent devices with 58, 90 and 124 μm, respectively. We can clearly see that the threshold strain becomes larger with increasing the pier heights of the bridge.

Simulation results on cross-sections of devices at different bending radii are shown in Fig. 4.9 and they fit well with the experimental results. The simulation was carried out by finite element analysis using COMSOL Multiphysics. In this figure, A, B and C show devices with different pier heights when no strain was applied to the Kapton^{TM} substrates. G, E and F are the three states that 0.280% strain was applied to the Kapton^{TM} substrates. At this strain value, the PDMS bridge with 58 μm height was in total contact with the substrate, the PDMS bridge with a pier height of 90 μm showed part contact to the bottom substrate, and the one with 124 μm pier height was not in any contact. From Fig. 4.8, we find that D, H and I states are the three critical transition points for devices changing from the insulation state to the conduction state. The strain values of Kapton^{TM}

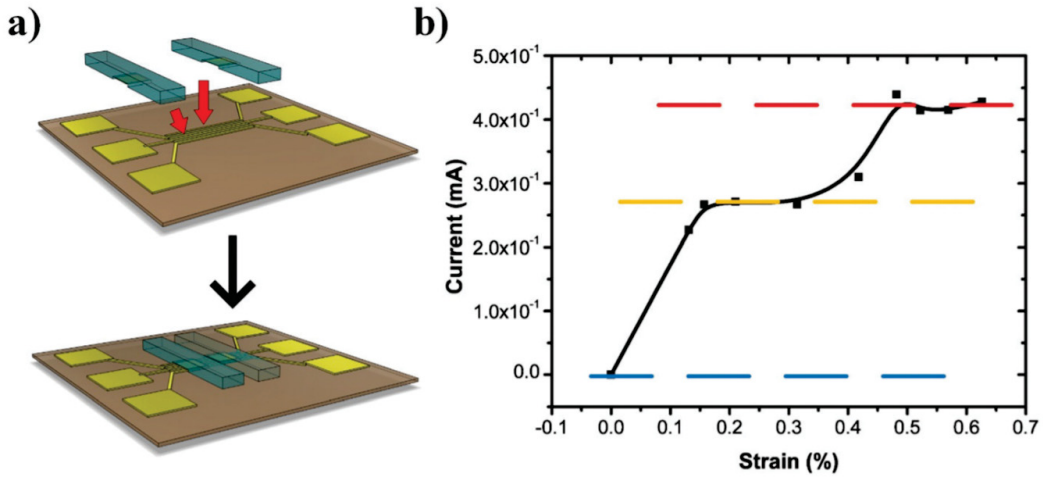

Figure 4.10: Integration of two PDMS bridges with different pier heights into a single MEM sensor. (a) The method used to fabricate the integrated devices. (b) Current vs. strain response of one integrated MEM sensor. The red line indicates both the 58-μm- and 90-μm-high bridges being in contact with the bottom electrodes on the Kapton^{TM} substrate. The yellow line indicates only the 58-μm-high bridge being in contact with the Kapton^{TM} substrate. The blue line indicates neither bridge being in contact with the Kapton^{TM} substrate.

substrates are 0.174%, 0.310% and 0.441% for these transition points.

Generally speaking, our digital MEM sensors only output two states – '0' and '1' for zero current and saturated current. One approach to simulate the function of a regular sensor with analog-output will be integrating several PDMS bridges into one MEM sensor, as shown in Fig. 4.10a. Since each PDMS bridge has its own detection limit, the integrated sensor shows a step curve for the current vs. strain response (Fig. 4.10b).

Our digital MEM sensors show good reliability in life cycle measurement. The results of the device with 58 μm pier height are shown in Fig. 4.11. We have clearly seen that even after 10,000 times' bending, this device can still work stably in both working modes (pressure sensing and strain sensing). The good stability of our MEM sensors relies on the simple structure design and simple readout mechanism of the device. The results relevant to the device reproducibility is shown in Fig. 4.12.

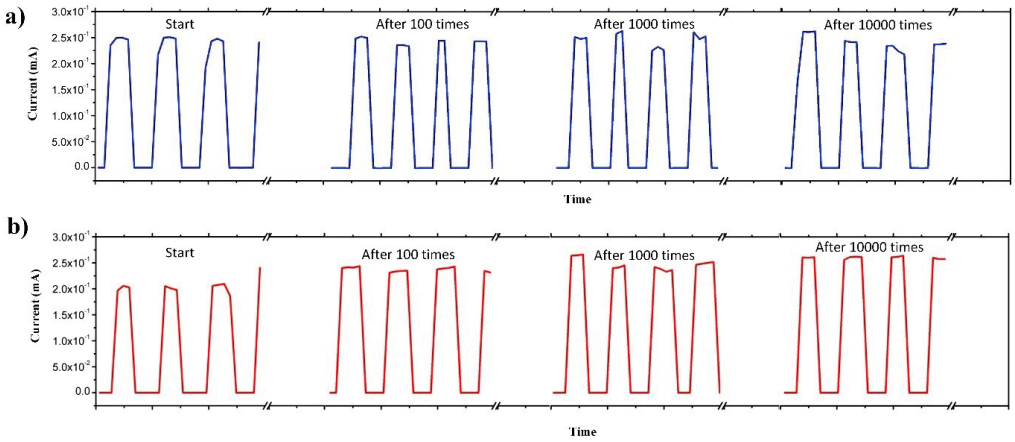

Figure 4.11: a) Durability testing by bending. b) Durability testing by pressing.

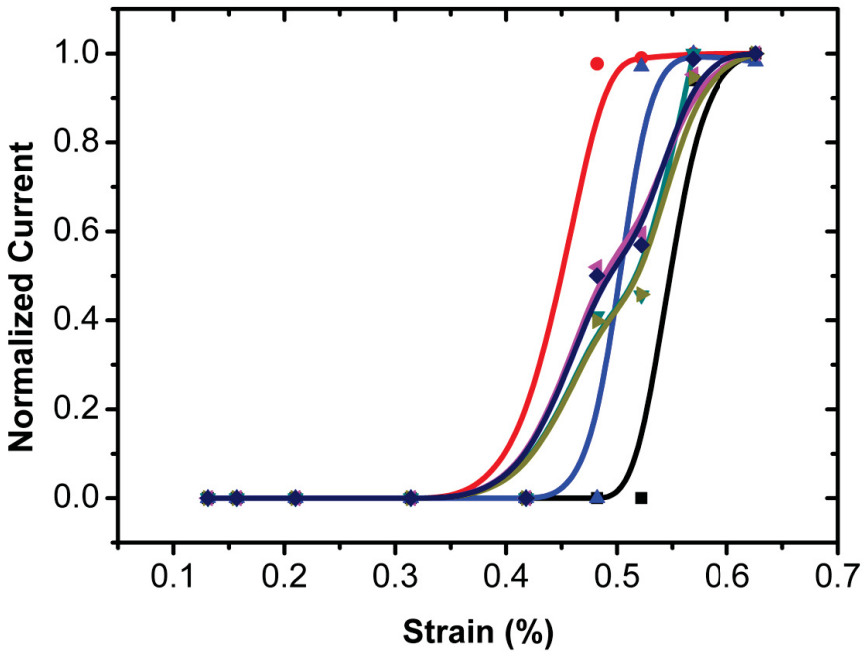

Figure 4.12: Normalized current vs. strain curves of 7 digital MEM sensors that all have 124 μm pier height. Curves of different colors represent different devices with the same design and fabrication method.

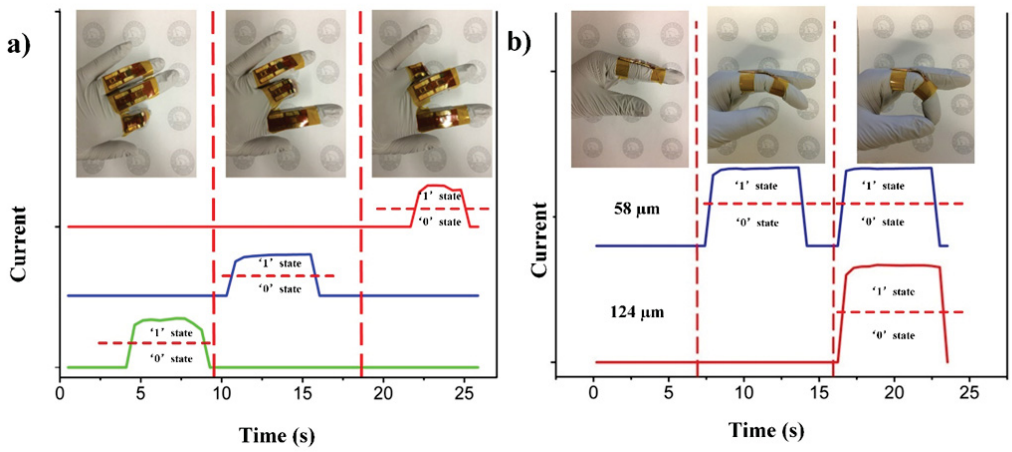

Figure 4.13: a) Response to different fingers' bending with digital MEM sensors. b) Digital MEM sensors with different bridge pier heights respond to different bending radii.

For proof of concept, we demonstrated the potential applications of our MEM sensors in each working mode. The readout of our digital MEM sensors only has two states – '1' state for conduction and '0' state for insulation. As shown in Fig. 4.13a), we attached devices with 58 μm pier height onto joints of three fingers, index, middle, and ring fingers. When different fingers bent, different MEM sensors responded. The output from the device on the index finger is the green curve, the output from the device on middle finger is the blue curve, and the red curve represents the output from the device on the ring finger. This demonstration enables the potential of digital MEM sensors for gesture detection. Furthermore, we integrated two MEM sensors with 58 μm and 124 μm pier heights onto the same finger, as seen from Fig. 4.13b). According to previous experiments, the smaller value in pier height leads to better detection limit. When the finger slightly bent, only the device with 58 μm pier height showed '1' state in signal output. Further bending made both devices show '1' state in signal output. The extension of this work to more digital MEM sensors integrate on one finger will be able to simulate the function of sensors with analog signal output.

We also demonstrated an application of digital MEM sensors for heart rate

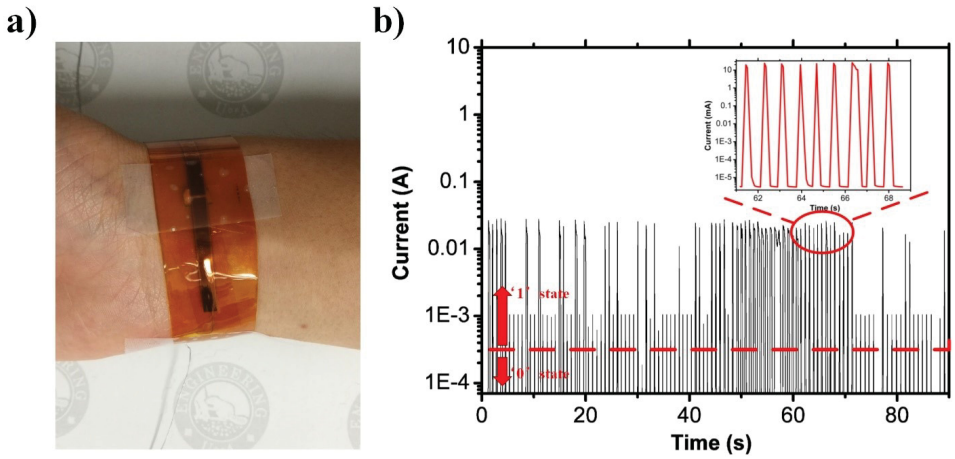

Figure 4.14: (a) Experimental set-up on a human wrist. (b) Heart rate pulses detected using the device on the wrist. Inset: Pulse signals over a course of six seconds.

monitoring using the pressure sensing mode. This was achieved by detecting pressures of wrist pulses on the PDMS bridge. Here we used a digital MEM sensor with 58 μm pier height as the wristband as shown in Fig. 4.14a) to detect wrist pulses. This demonstration involved a healthy, 24-year-old male. No allergic reactions, redness or damage to the skin were observed in any of our studies. From Fig. 4.14b), we observed the visible spikes which should represent the incident waves of blood pressure. Because of the wrist movement or some other unknown factors, some spikes are much lower than normal spikes. However, digital output can still be retrieved from the graph as shown in Fig. 4.14b). If we set a low current as the threshold between '1' and '0' states, it is easily to get these two states separated. In a 5 second time zoom-in window (inset figure of Fig. 4.14b), we found that the heart rate of our experimental subject is around 72/min. To verify the reliability of our test results, we also used a commercial sphygmomanometer (Nissei DS-114 computer digital blood pressure pulse monitor) to test the heart rate of the experimental subject at different time of a day and got the result of 71$\pm$3/min. This demonstration shows the potential of our devices for small signal detection in the medical field.

4.5 Conclusions

4.5.1 Summary of Chapter 4

In summary, our concept of using digital MEM sensors has been shown to open a new way to detect strain and force, one with higher device durability than previously available as can be seen from the comparison in Table 4.2. We also demonstrated the ability of our devices to detect gestures and monitor heart rates. With appropriate designs, we expect integrated digital MEM sensors to be used for more complex functions in various applications.

Table 4.2: Comparison of different strain sensors in terms of device durability

Type	Durability	Reference
Digital MEM sensor (device in this chapter)	No significant change observed after 10000 times' bending	
CNT piezoresistive sensor	Around 10% resistance change after 10000 times' bending	[193]
CNT piezoresistive sensor	Around 15% resistance change after 1500 cycles	[134]
Metal foil piezoresistive (metal strain gauge)	Needs calibration	

4.5.2 Contribution to the thesis

In this chapter, I discussed our work about a new design of sensors, digital MEM sensor, which utilized easy fabrication technology to output digital signals. From this unique design, the device will obtain higher durability. In the mean time, the cost of it will still maintain in a rather low level.

Chapter 5

Flexible triboelectric field-effect transistor for touch sensing

5.1 Introduction

With growing demands for flexible and stretchable features in industrial applications, flexible electronics, which integrate functional electronic devices on paper and plastic substrates, are drawing more and more attentions recently.[134], [238], [247]–[251] Consequently, there are a lot of active research works on developing new-class materials, which can fit to flexible sensors, to fulfill this urgent need. Over the past two decades, various materials have been applied on flexible sensing systems, such as a-Si,[252], [253] indium zinc oxide (IZO),[254] CNTs,[255] and metal nanowires.[256] In the process of seeking low-cost, printing-compatible materials for flexible systems, semiconductor CQDs are gradually appearing for being able to be solution-processed. Other attractive features of CQDs include the tunable absorption spectrum and narrow emission linewidth brought by sizes. Besides the above-mentioned properties, the polycrystalline nature of CQD thin-films enables them to be mass-produced on lightweight, flexible plastic substrates using reel-to-reel printing, spray painting, and inkjet printing.[257] Till now, CQDs have been widely used in solar energy harvesting,[221] logic devices,[258] and displays.[259], [260] There are also plenty of flexible electronic and photonic systems fulfilling various functions by CQDs, such as flexible full-color displays,[70] flexible gas sensors,[72] flexible LEDs,[261] and flexible integrated

circuits.[262] However, CQDs have not been widely used on strain and pressure sensing systems due to the fact that CQDs lack proper transduction mechanisms (i.e., piezoelectric, piezoresistive) to respond to strain or pressure.

The triboelectric effect is a phenomenon that researchers are taking advantage of to develop high-performance touch sensors.[245], [263] Triboelectric devices output current and voltage utilizing contact electrification. Basically, when two different materials come into contact with each other, there will be electrical and chemical interactions occurring at the contacting surfaces. To balance the electrochemical potential between two materials, a charge distribution will emerge at the interface. The triboelectric effect was first used to build up a Wimshurst machine and a Van de Graaff generator for energy harvesting in the 19th century. In 2012, Wang et al. made triboelectric nanogenerators by taking advantage of the triboelectric effect.[151] Then, researchers broadened the applications of it in sensing devices, for the touch-induced charges make it a perfect solution for touch sensors. In order to enhance the performance of triboelectric touch sensors, scientists and engineers designed various binary material systems with gaps between two materials to create friction while touching.[245], [263], [264] Such systems will produce a large current or voltage. However, the fabrication processes of these devices usually involve complex semiconductor manufacturing technologies and expensive instrument like reactive ion etching (RIE).

Here, we reported a CQD T-FET combining the triboelectric effect and CQD FET to create high-performance touch sensors for flexible systems. In our touch sensor, we use a simple PDMS film to generate triboelectric voltage in response to touching and a floating gate CQD FET to produce the source-drain current driven by the triboelectric voltage. This design makes it possible to generate a much larger current change compared to the freestanding PDMS touch sensor, while the simple fabrication process of CQD T-FET enables the potential of our devices to be mass-produced by printing technologies at low cost.

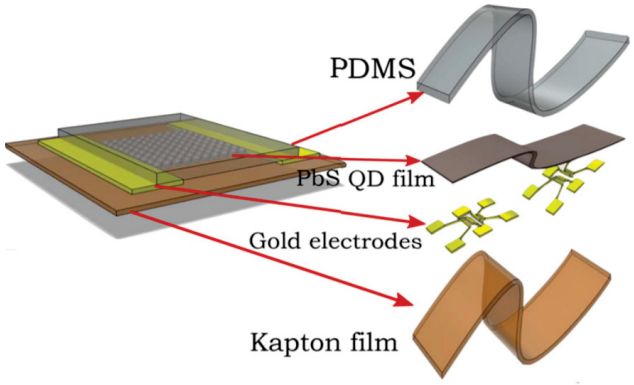

Figure 5.1: A schematic of detailed structure of the T-FET device

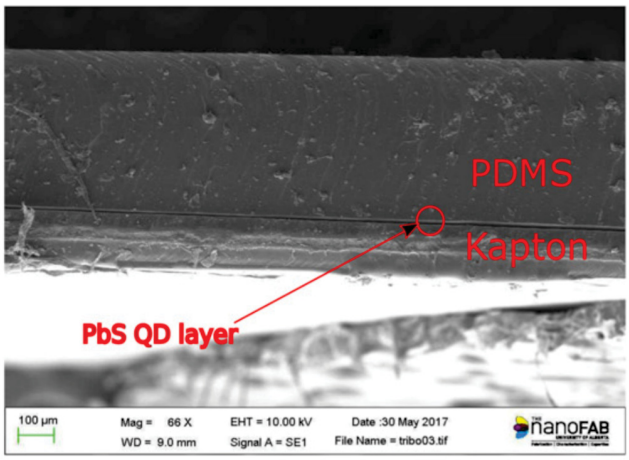

Figure 5.2: Cross-sectional SEM image of the T-FET device.

5.2 Device structure and working principle

As shown in Fig. 5.1, the device architecture is similar to that of a floating-gate FET. Gold electrodes are fabricated on a flexible PI film (Kapton^{TM}, DuPont). The semiconductor channel material is PbS CQDs with halide ligands. Fig. 5.2 shows that the CQD thin film is between PDMS and the PI film. The thickness of the film is about 50 nm. On top of the CQD thin film, there is a PDMS floating gate named the triboelectric gate.

When human finger or other objects are placed on the triboelectric gate, contact electrification will happen on the surface of PDMS, leading to charge

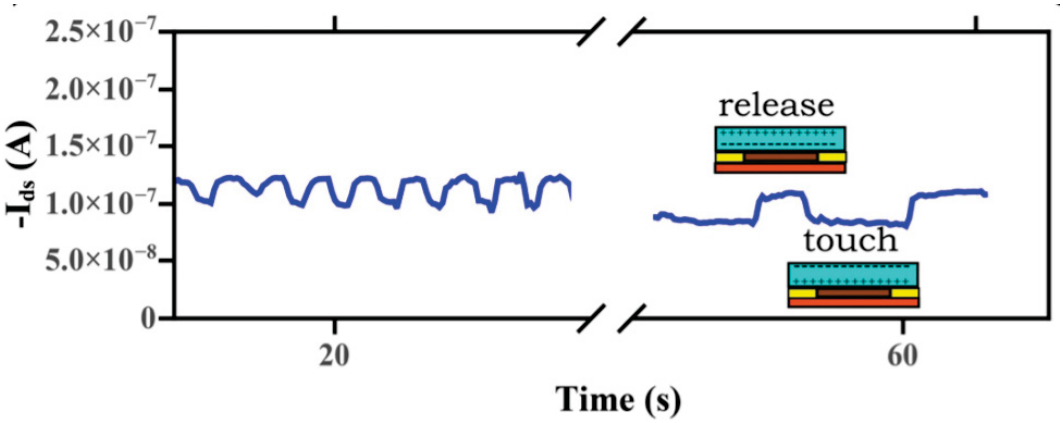

Figure 5.3: The drain current change with finger touching and releasing.

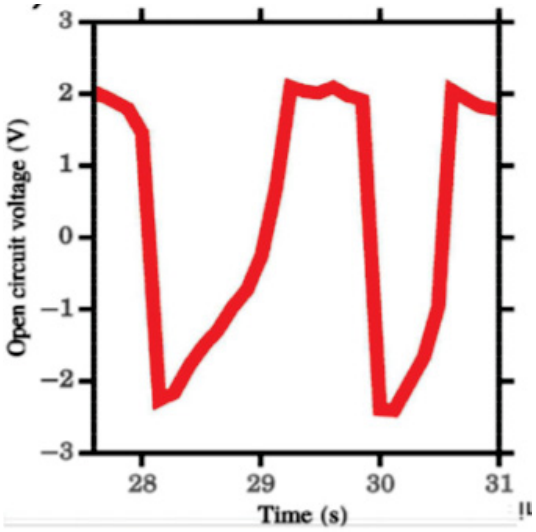

Figure 5.4: The open circuit voltage of a free-standing PDMS thin film with a thickness of 300 μm.

induction to PDMS. This induced charge in PDMS will generate an electric field inside the PDMS film, equivalent to a gate voltage. At the same time, this gate voltage will change carrier density in the CQD thin film and generate a large current change between source and drain electrodes. With this amplification from the field effect, the current change in the CQD thin film can be easily detected. This process is demonstrated in Fig. 5.3. A Keithley 2400 sourcemeter was employed to measure the open circuit voltage of a free-standing PDMS thin film with finger touching on it, as shown in Fig. 5.4.

5.3 Experimental

The PbS CQDs were prepared by a two-step hot-injection method. In this method, lead acetate (PbAc, Fisher Scientific Inc., 570 mg) was dissolved in 15 ml ODE (Sigma Aldrich Inc.) with 1.05 ml oleic acid (OA, Sigma Aldrich Inc.) and heated to 100°C for 10 h in a vacuum environment to synthesize a lead oleate precursor in a three-neck flask. After the above step, the lead oleate precursor was further heated up to 167°C in nitrogen. Then, another reactant, 160 μL TMS2-S (Sigma Aldrich Inc.), was mixed with 7.5 mL ODE and quickly injected into the three-neck flask. The flask was then immediately removed out of the heating jacket to cool down to room temperature while keeping stirred. At last, the products were centrifuged and washed with acetone and methanol. After being dried and weighed, they were redispersed in octane. The absorption spectrum of the suspension shows that the first excitonic peak is 1500 nm.

The device was fabricated on a PI (Kapton^{TM}, DuPont, Delaware, USA, 125 μm) film. The gold electrodes on the Kapton^{TM} film were made by using conventional photolithography. At first, an HPR 504 photoresist layer with a thickness of 1.2 μm was formed on the surface by spin-coating and soft-baking (90°C, 90 s). Consecutively, the exposure step was carried out using a mask aligner (ABM Inc. San Jose, California) for 3 s under UV light with a 365/405 nm wavelength light intensity of 66.7 mW/cm^2. Developer

354 was applied to develop the photoresist patterns. At last, a standard sputtering deposition process was used to deposit a gold layer of 65 nm with 5 nm Cr as an adhesion layer.

The CQD film deposition was done by a layer-by-layer strategy. We diluted PbS CQD suspension in octane to 16.7 mg/mL. After cleaning the surface of the electrodes, we spin-coated 3 layers of CQDs on the surface. All the spin-coating process was performed at 2500 rpm, and the tetrabutylammonium iodide (TBAI, Sigma Aldrich Inc.) ligand solution with a concentration of 10 mg/mL in methanol was prepared at the beginning. Each layer iteration included three sub-steps: (1) three drops of lead sulfide CQD suspension was applied on the surface and spun for 10 s; (2) 0.25 mL TBAI solution was dropped on the CQD film and remained there for 30 s and then spun for 10 s to flush the solution away; (3) methanol was employed to wash the CQD film at last. We let the methanol remain on the film for 10 s and then spun it away. This wash step should be repeated 2 times. After the CQD deposition, the device is annealed at 150°C for half an hour.

The PDMS triboelectric gate was made from Sygard 184 PDMS kit (Dowcorning Inc., Michigan, USA). The base and crosslinker were mixed together in a ratio of 10:1. After being stirred to a homogeneous condition, the mixture was placed into a vacuum desiccator to degas for 3 times, each time 10 min. Then, 5 drops of PDMS uncrosslinked mixture were drop-coated on top of the PbS CQD thin film. The liquid PDMS was then heated on a hotplate at 80°C for half an hour before being fully crosslinked.

5.4 Results and discussion

To retrieve the performance of our devices, we used different materials to touch the device. As shown in the left panel of Fig. 5.5, a plastic ball pen, steel tweezers, and a finger with a rubber glove were brought to contact with the device consecutively. The corresponding drain current changes with

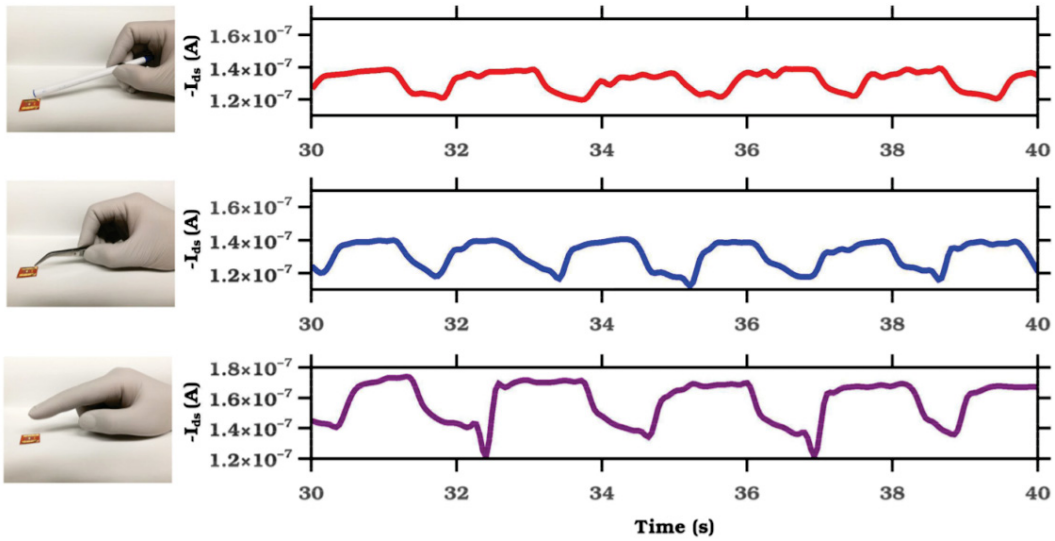

Figure 5.5: Drain current change of different materials touching on T-FET.

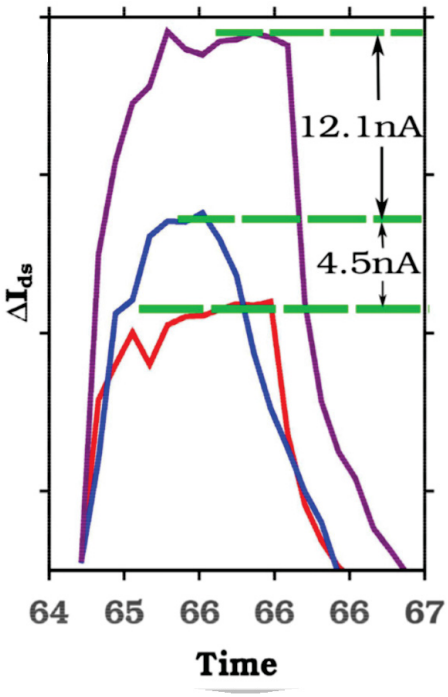

Figure 5.6: Comparisons of peaks in each curve.

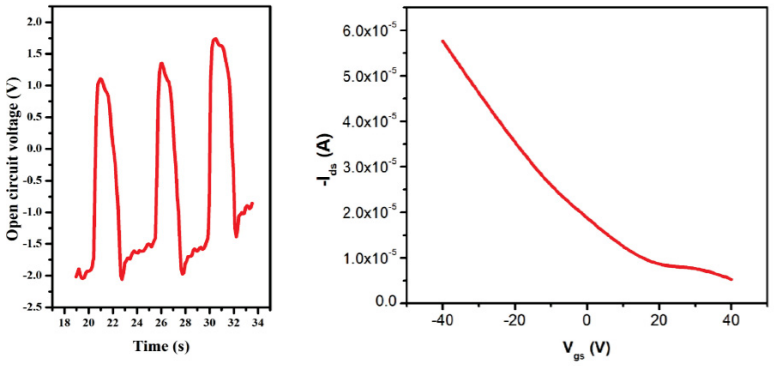

Figure 5.7: a) Open circuit voltage measurement of a free-standing PDMS film with a tweezing touching on it repeatitively. b) $-I_{ds}$ *vs* V_{gs} curve of a bottom-gated CQD FET device.

time are shown in the right panel. It is seen that the drain current changes are different for each material. The rubber glove gives the largest change, while the plastic pen leads to the smallest change. This comparison is clearly shown in Fig. 5.6, in which signals for one touch event from various materials are put together. The differences in drain current change can be attributed to different surface properties which will lead to different surface charge densities. According to previous reports, the charge transfer mechanism in a system without semiconductors can be attributed to ion transfer between surfaces having mobile ions.[265] Therefore, the amount of triboelectric charges is highly dependent on material surface functional groups.[266] In our experiments, the rubber glove, tweezers, and plastic pen have different surface groups, so the devices have different responses even if the touching forces may be similar in each touch event. This theory has also been employed to enhance triboelectric energy harvesting devices.[267] We can retrieve the hole mobility of the CQD thin film using the open-circuit voltage and the tweezer touching response curve. The detailed calculations which refer to previous reports[208], [210], [232] are shown in Chapter 3. Comparing this mobility value with a transfer-curve-retrieved mobility on a FET device, it is concluded that the touching response is mostly induced by the field effect.

From comparison of the three peak values in Fig. 5.6, the difference in peak current is easy to be noticed. According to equations in Chapter 3, the voltage induced by touching will change with the peak current. From $Q = CV$, we can derive $Q = \epsilon SV/d$. It is easy to obtain the surface tribo-charge density by the transfer curve in Fig. 5.7 for finger-touch, which is 0.29 $\mu C/m^2$; the tweezer one and pen one are 0.18 $\mu C/m^2$ and 0.13 $\mu C/m^2$.

Our T-FET sensor also shows a consistent performance under different bending radii. As shown in Fig. 5.8(a), from to top to bottom, the curves represent drain current changes upon finger touching when the device is bent from the relaxed (unbended) state to the radii of 2 cm, 1.5 cm, 1.3 cm, and 1.2 cm, respectively. We can clearly see that the current changes of the device are almost the same when the device is being bent. However, we do observe a reduced electrical response of the device in the bending state, compared to the relaxed state. We attribute this deterioration to the formation of microcracks inside the CQD thin film in bending. When microcracks are formed, the carrier transport will be blocked through these microcracks, leading to reduced electrical performance. While the numbers and locations of these microcracks are likely to be unchanged at different bending curvatures, the electrical response of these devices can be consistent when in 'bent' conditions. The averaged results of current changes upon finger touch at various bending radii (strains) are illustrated in Fig. 5.8(b). We performed measurements after three extra bending cycles (large bending condition with a small bending radius down to 1.1 cm) to check whether the micro-cracks will heal themselves. The results are shown in Fig. 5.9. It is observed that the micro-cracks brought permanent damage after three cycles, and the device shows smaller current change at the zero-strain condition. However, the device performance is relatively stable at other strain conditions. The x-axis in this graph indicates the surface strain applied to the CQD thin-film by bending, which is calculated using a method in the Appendix.[42]

At last, we compared our T-FET sensor with a PDMS triboelectric sensor.

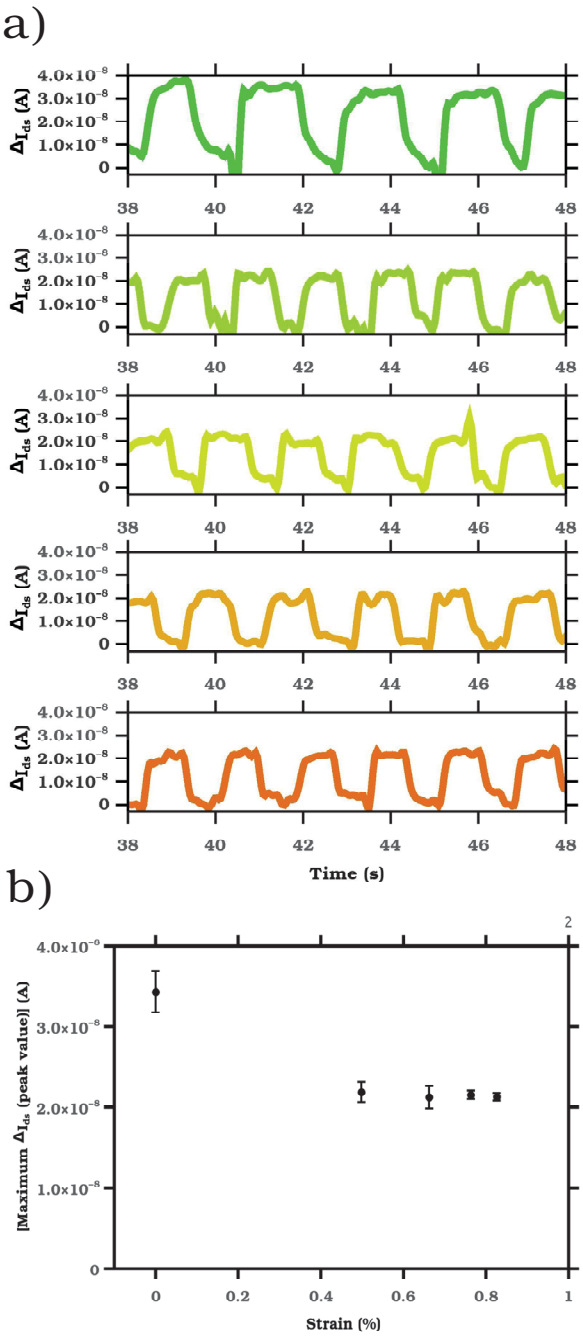

Figure 5.8: (a) Finger touching response of T-FET when being bent to different curvatures. From top to bottom are flat condition, bending radii=2 cm, 1.5 cm, 1.3 cm, and 1.2 cm. (b) Peak value comparison of every condition. The x axis represents surface strain on top of the Kapton^{TM} substrates which are derived from bending radii.

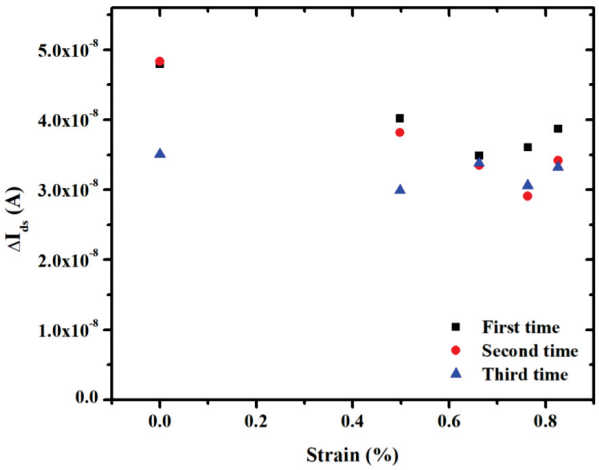

Figure 5.9: Device performance in different bending radii with multiple bending cycles.

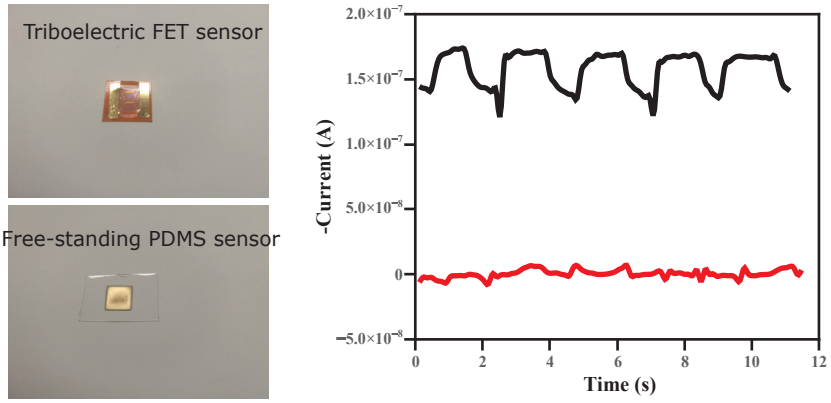

Figure 5.10: The negative current response from finger touching of a T-FET sensor and a PDMS sensor. The black curve is the response of T-FET sensor while the red curve is from the PDMS sensor. The left panel shows pictures of the two devices.

We applied the same finger touch on these two devices; however, the responses are very different. We measured the short circuit current on the PDMS triboelectric sensor upon finger touching and plotted it as the red curve in Fig. 5.10 which is almost buried in the electric noise. According to the previous report of devices with the similar structure, the short circuit current density would be 30–40 nA/cm^2.[268] While the T-FET sensor, with its unique structure, can enhance the output current density by the field effect, in our case, the output current density of the T-FET sensor is improved by several orders of magnitude to 1.9×10^7 nA/cm^2.

5.5 Improvement of the T-FET sensor

Unfortunately, PbS quantum dots have low mobility that would limit the performance of the T-FET sensor. To address this issue, single-walled carbon nanotubes (SWCNTs), a high-mobility polycrystalline semiconducting material,[98] were introduced as a replacement for quantum dots. According to our preliminary results,[269] the SWCNT T-FET touch sensor exhibits a response to a given touch event that is almost 5 times' greater than that of the quantum dot sensors. We have demonstrated a flexible touch panel consisting of arrays of our FET touch sensors with this high performance which shows potential to function as a commercial touch panel.

To investigate the carrier transportation behaviors in SWCNTs, SWCNT FETs were fabricated as the procedures stated in the previous section. The SWCNT FET was also characterized by Keithley 2400 sourcemeters and a Wentworth probe station. From the transfer curve shown in Fig. 5.11, it can be concluded that the SWCNT behaves as a p-type semiconductor. The comparison is listed as the table below:

We further constructed a four-channel touch panel with our SWCNT T-FET. Four SWCNT T-FET touch sensors were integrated onto one device. The same fabrication procedures were applied as in the single touch sensor process. Keithley 2400 sourcemeters were used to probe the current change

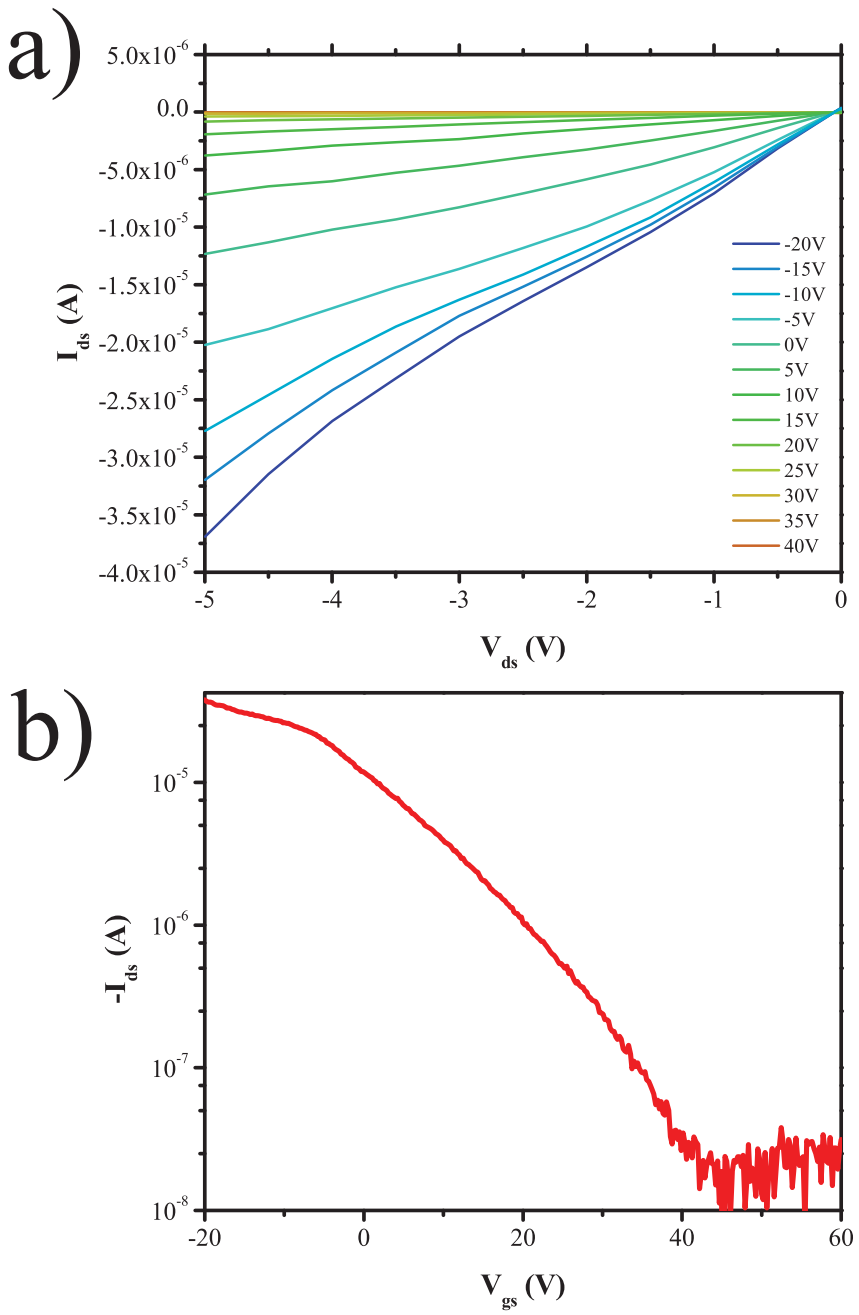

Figure 5.11: (a) $I_{ds} - V_{ds}$ curves of an SWCNT bottom-gate FET under different gate voltages. (b) Transfer curve of an SWCNT bottom-gate FET.

Table 5.1: Comparison of CQD triboelectric sensor and SWCNT triboelectric sensor

	Current output to a hand-touch event (A)	Mobility ($cm^2/V \cdot s$)
CQD T-FET sensor	3.0×10^{-8} [215]	1.2×10^{-2} [215]
SWCNT T-FET sensor	1.7×10^{-7}	5.9×10^{-2}

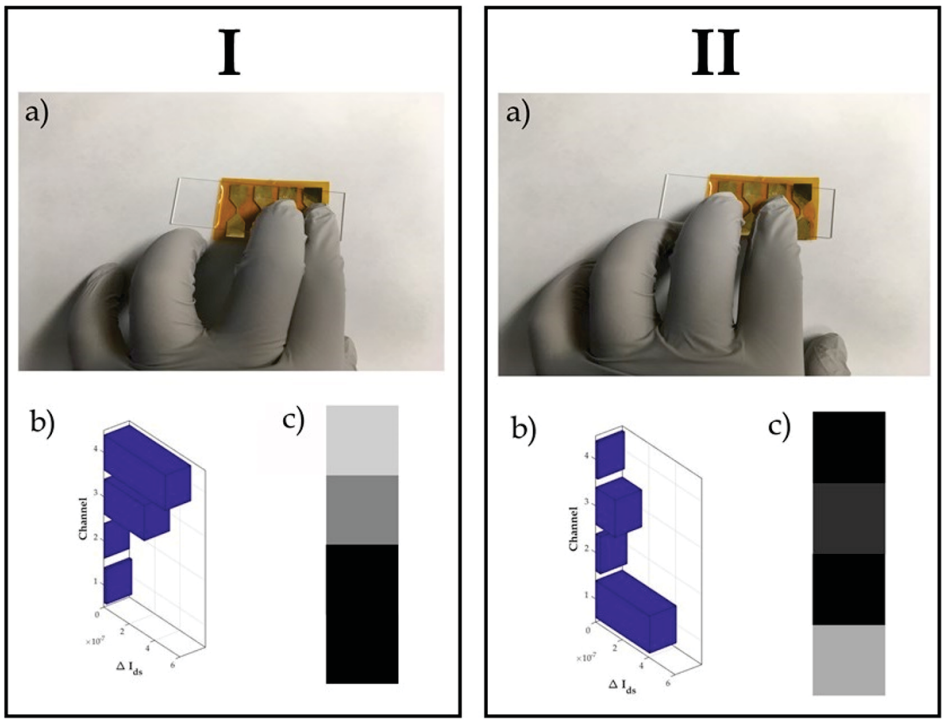

Figure 5.12: I: (a) Illustration of test with touching #3 and #4 channels. (b) Channel current changes when touched. (c) Current change in gray scale. II: (a) Picture of test with touching #1 and #3 channels. (b) Channel current changes when touched. (c) Current change in gray scale.

on all four channels. The four channels were defined as #1 to #4, from left to right, as shown in Fig. 5.12Ia). As discussed before, it can be expected that the channels with finger touch will have a large change. Fig. 5.12I demonstrates the results when fingers touch channels #3 and #4. Fig. 5.12Ib) shows that the touched channels exhibit a response 2-3 orders larger than that of untouched channels. All the current change can be normalized and converted to 256-bit grey scale as shown in Fig. 5.12Ic), which demonstrates that analog current signals can be converted well to digital signals with visible changes. This indicates the potential of SWCNT T-FET touch sensors to be applied in commercial devices. Non-adjacent channels were also tested, as shown in Fig. 5.12II, which shows that there was a small interference in the channel between two touched channels. We attribute this to issues regarding sensor size issue finger touch area. However, the difference can still be observed in the grey scale chart, which means this interference is out of consideration for the application.

5.6 Conclusions

5.6.1 Summary of Chapter 5

In conclusion, we combined triboelectric and FET techniques to develop a class of touch sensors—T-FET sensor. With the T-FET design, we are able to produce flexible touch sensors with solution-processed CQDs. The polycrystalline nature of CQD thin-films enables our T-FET touch sensors to be fabricated on flexible substrates, and the performance of this CQD touch sensor remains the same in various bending conditions. At last, the T-FET touch sensor also shows a much higher output current density than the PDMS triboelectric touch sensor.

As an improvement to T-FET sensors, SWCNT with high mobility was employed as the FET channel. Further, with this device, we constructed a touch panel and showed its potentials to practical application.

5.6.2 Contribution to the thesis

In this chapter, I introduced our work of a new type of sensors, T-FET sensors. We combined triboelectricity and CQD FET to realize them. This sensor can gain better performance than a normal triboelectric touch sensor by this new mechanism.

Chapter 6

Conclusion and future works

6.1 Summary of accomplishments and contributions

In this thesis, I focus on novel substrates and novel working mechanism of transducers to address the current problems in flexible electronics.

Chapter 2 and 3 discussed a novel recyclable substrate and a substrate surface modification strategy towards better-performance in printed electronics. CNC paper is utilized as a water-soluble, recyclable substrate to fabricate a strain sensor on it. By the unique PDMS stencil technique, I'm able to pattern electrodes with critical feature as small as 150 μm. Thank to the small features, the GF of the strain sensor can be as large as 52.44. What's more, the device is totally recyclable by dissolving the substrate in water. CNC is a material derived from wood and its unique water-soluble property makes it have a potential to be applied on cost-effective devices. The Cl-modification strategy is to passivate surfaces of rigid and flexible substrates for printed electronics. This method can create polar-solvent friendly surfaces on various polymer and inorganic substrates. FTIR, XPS, contact angle measurement and carrier dynamic analysis were were performed to verify the passivated surface. The PbS CQD ink FET made on Cl-modified surface exhibits high field-effect mobility than bare SiO_2 surface. It can be concluded that Cl-modification can suppress the surface trap sites while creating a hydrophilic surface, showing its potential to be applied in printing techniques.

Chapter 4 and 5 introduced novel transducers into flexible electronics. MEMS device is fabricated to be used as highly reliable sensors. Unlike conventional physical sensors, this sensor outputs digital signal other than analog signal, which renders higher reproduciblity and stability possible. We also demonstrated the ability of our devices to detect gestures and monitor heart rates. With appropriate designs, we expect integrated digital MEM sensors to be used for more complex functions in various applications. I also combined triboelectric and FET techniques to develop a new class of touch sensors–T-FET sensor. With the T-FET design, we are able to produce flexible touch sensors with solution-processed CQDs. The amorphous nature of CQD thin-films enables our T-FET touch sensors to be fabricated on flexible substrates, and the performance of this CQD touch sensor remains the same in various bending conditions. The T-FET touch sensor also shows a much higher output current density than the PDMS triboelectric touch sensor.

6.2 Future outlook

6.2.1 Platform-level integration

With years of development, there have been so many flexible electronic device emerging. However, most of them are just isolated islands. To bring them further into more demonstrations or even commercialization, high-level integration is needed. With a platform, one can really test the real feasibility of every component of the system. For example, as to the aforementioned digital MEM sensor, it holds a large odd to be integrated on a flexible platform, thus its full potential will be released. Recently, researchers have been working on the platform-level integration.[143] Gao et al. reported a wearable platform which will analyze real-time sweat data and transmit to smartphone simultaneously.

As shown in the Fig. 6.1, to integrate our flexible sensors a system with energy harvesting, transceiver, microcontroller and amplifier needs to be care-

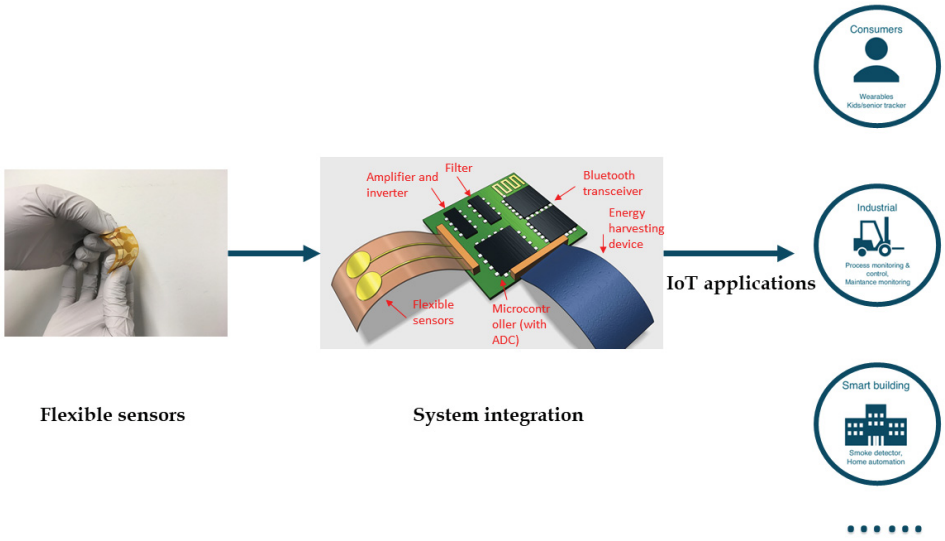

Figure 6.1: A schematic of the system integration.

fully designed. With these designs, the system can be fit into various IoT applications.

6.2.2 Improvement of device transparency

In flexible electronics, device transparency is always an important issue. In many applications involving wearable and display technologies, transparency is a necessity. The T-FET touch sensor stated before is a device which has the potential to be integrated on displays or future wearable devices. However, the substrate and electrodes are not transparent in visible light range. Some transparent substrates, like PET, can be used to replace the Kapton^{TM} film. In the Introduction Section, there are also some transparent conductive materials stated, like PEDOT:PSS or metal meshes, which can be good alternatives to the gold electrodes. With these improvements, the device can definitely increase its transparency.

6.2.3 Improvement of semiconductor materials

The performance of flexible electronic devices are largely restrained by carrier mobility. The colloidal quantum dots we utilized in our device is low in carrier

mobility. The SWCNT also didn't exhibit so high mobility as it should do. Many researchers are working on increase the mobility of quantum dots by surface chemistry and morphology reconstruction.[221], [270] The same strategy can also be applied to our sensors. The method to process SWCNT maybe not so proper, high temperature annealing and aerosol printing can be introduced to increase the device performance.

References

[1] R. I. Scace, *Electronics*. Encyclopædia Britannica, 2016. 1

[2] M. A. Alam and S. Kumar, "Flexible electronics," in *Encyclopedia of Nanotechnology*, B. Bhushan, Ed. Dordrecht: Springer Netherlands, 2012, pp. 860–865, ISBN: 978-90-481-9751-4. DOI: 10.1007/978-90-481-9751-4_147. [Online]. Available: https://doi.org/10.1007/978-90-481-9751-4_147. 1

[3] J. A. Rogers, T. Someya, and Y. Huang, "Materials and mechanics for stretchable electronics," *Science*, vol. 327, no. 5973, pp. 1603–1607, 2010. 1

[4] D. Ha, Z. Fang, and N. B. Zhitenev, "Paper-based electronics: Paper in electronic and optoelectronic devices," *Advanced Electronic Materials*, vol. 4, no. 5, p. 1 870 025, 2018. 2

[5] Z. Cui, *Printed electronics: materials, technologies and applications*. John Wiley & Sons, 2016. 2, 19, 21, 60

[6] K. A. Ray, "Flexible solar cell arrays for increased space power," *IEEE Transactions on Aerospace and Electronic Systems*, no. 1, pp. 107–115, 1967. 2, 3

[7] E. Burt, "On space manoeuvres with continuous thrust," *Planetary and Space Science*, vol. 15, no. 1, pp. 103–122, 1967. 2

[8] R. Crabb and F. Treble, "Thin silicon solar cells for large flexible arrays," *Nature*, vol. 213, no. 5082, p. 1223, 1967. 3

[9] T. P. Brody, "The birth and early childhood of active matrix—a personal memoir," *Journal of the society for information display*, vol. 4, no. 3, pp. 113–127, 1996. 3

[10] ——, "The thin film transistor—a late flowering bloom," *IEEE Transactions on Electron Devices*, vol. 31, no. 11, pp. 1614–1628, 1984. 3

[11] E. Ma and S. Wagner, "A-si: H thin-film transistors on rollable 25-μ; m thick steel foil," *MRS Online Proceedings Library Archive*, vol. 508, 1998. 4

[12] Y. Hamakawa, "Recent advances in amorphous silicon solar cells," *Solar Energy Materials*, vol. 8, no. 1-3, pp. 101–121, 1982. 4

[13] W. S. Wong and A. Salleo, *Flexible electronics: materials and applications*. Springer Science & Business Media, 2009, vol. 11. 4, 9

[14] H. Okaniwa, K. Nakatani, M. Yano, M. Asano, and K. Suzuki, "Preparation and properties of a-si: H solar cells on organic polymer film substrate," *Japanese Journal of Applied Physics*, vol. 21, no. S2, p. 239, 1982. 4

[15] V. Zardetto, T. M. Brown, A. Reale, and A. Di Carlo, "Substrates for flexible electronics: A practical investigation on the electrical, film flexibility, optical, temperature, and solvent resistance properties," *Journal of Polymer Science Part B: Polymer Physics*, vol. 49, no. 9, pp. 638–648, 2011. 6

[16] H. Le and M. Sutcliffe, "Analysis of surface roughness of cold-rolled aluminium foil," *Wear*, vol. 244, no. 1-2, pp. 71–78, 2000. 7

[17] P.-C. Kuo, V. G. Chouvardas, J. A. Spirko, K. M. Hatalis, and M. K. Hatalis, "Mechanical limitations of materials for steel foil based flexible electronics," *MRS Proceedings*, vol. 1030, 1030–G03-14, 2007. 7

[18] S. Theiss and S. Wagner, "Amorphous silicon thin-film transistors on steel foil substrates," *IEEE Electron Device Letters*, vol. 17, no. 12, pp. 578–580, 1996. 7

[19] L. Kranz, C. Gretener, J. Perrenoud, R. Schmitt, F. Pianezzi, F. La Mattina, P. Blösch, E. Cheah, A. Chirilă, C. M. Fella, *et al.*, "Doping of polycrystalline cdte for high-efficiency solar cells on flexible metal foil," *Nature communications*, vol. 4, p. 2306, 2013. 7

[20] C. Wu, S. Theiuss, G. Gu, M. Lu, J. C. Sturm, S. Wagner, and S. Forrest, "Integration of organic leds and amorphous si tfts onto flexible and lightweight metal foil substrates," *IEEE Electron Device Letters*, vol. 18, no. 12, pp. 609–612, 1997. 7

[21] D.-U. Jin, J.-K. Jeong, T.-W. Kim, J.-S. Lee, T.-K. Ahn, Y.-K. Mo, and H.-K. Chung, "Flexible amoled displays on stainless-steel foil," *Journal of the Society for Information Display*, vol. 14, no. 12, pp. 1083–1090, 2006. 7

[22] D.-U. Jin, J.-S. Lee, T.-W. Kim, S.-G. An, D. Straykhilev, Y.-S. Pyo, H.-S. Kim, D.-B. Lee, Y.-G. Mo, H.-D. Kim, *et al.*, "65.2: Distinguished paper: World-largest (6.5") flexible full color top emission amoled display on plastic film and its bending properties," in *SID Symposium Digest of Technical Papers*, Wiley Online Library, vol. 40, 2009, pp. 983–985. 7

[23] K. Beernink, S. Guha, J. Yang, A. Banerjee, K. Lord, G. DeMaggio, F. Liu, G. Pietka, T. Johnson, M. Reinhout, *et al.*, "Lightweight, flexible solar cells on stainless steel foil and polymer for space and stratospheric applications," 2007. 7

[24] K. R. Sarma, "Flexible displays: Substrate and tft technology options and processing strategies," *Handbook of Visual Display Technology*, pp. 1389–1429, 2016. 7

[25] S. Ito, G. Rothenberger, P. Liska, P. Comte, S. M. Zakeeruddin, P. Péchy, M. K. Nazeeruddin, M. Grätzel, *et al.*, "High-efficiency (7.2%) flexible dye-sensitized solar cells with ti-metal substrate for nanocrystalline-tio 2 photoanode," *Chemical Communications*, no. 38, pp. 4004–4006, 2006. 7

[26] J. Troughton, D. Bryant, K. Wojciechowski, M. J. Carnie, H. Snaith, D. A. Worsley, and T. M. Watson, "Highly efficient, flexible, indium-free perovskite solar cells employing metallic substrates," *Journal of Materials Chemistry A*, vol. 3, no. 17, pp. 9141–9145, 2015. 7

[27] W. Andrew, "Permeability and other film properties of plastics and elastomers," *Plastics Design Library. New York: Norwich*, pp. 58–60, 1995. 8

[28] Y. Leterrier, "Durability of nanosized oxygen-barrier coatings on polymers," *Progress in Materials Science*, vol. 48, no. 1, pp. 1–55, 2003. 8

[29] E. Lueder, "Passive and active matrix liquid crystal displays with plastic substrates," *Proc. Electrochem. Soc*, vol. 98, pp. 336–354, 1999. 8

[30] E. Jamieson and A. Windle, "Structure and oxygen-barrier properties of metallized polymer film," *Journal of Materials Science*, vol. 18, no. 1, pp. 64–80, 1983. 8

[31] J. S. Lewis and M. S. Weaver, "Thin-film permeation-barrier technology for flexible organic light-emitting devices," *IEEE Journal of selected topics in quantum electronics*, vol. 10, no. 1, pp. 45–57, 2004. 8

[32] J. Wang, T. Pan, J. Zhang, X. Xu, Q. Yin, J. Han, and M. Wei, "Hybrid films with excellent oxygen and water vapor barrier properties as efficient anticorrosive coatings," *RSC Advances*, vol. 8, no. 38, pp. 21 651–21 657, 2018. 8

[33] A. Pietrikova, P. Lukacs, D. Jakubeczyova, B. Ballokova, J. Potencki, G. Tomaszewski, J. Pekarek, K. Prikrylova, and M. Fides, "Surface analysis of polymeric substrates used for inkjet printing technology," *Circuit World*, vol. 42, no. 1, pp. 9–16, 2016. 9

[34] C. Foucher, B. Guilhabert, A. Kanibolotsky, P. Skabara, N. Laurand, and M. Dawson, "Rgb and white-emitting organic lasers on flexible glass," *Optics express*, vol. 24, no. 3, pp. 2273–2280, 2016. 9

[35] B. Dou, E. M. Miller, J. A. Christians, E. M. Sanehira, T. R. Klein, F. S. Barnes, S. E. Shaheen, S. M. Garner, S. Ghosh, A. Mallick, *et al.*, "High-performance flexible perovskite solar cells on ultrathin glass: Implications of the tco," *The journal of physical chemistry letters*, vol. 8, no. 19, pp. 4960–4966, 2017. 9

[36] H. Mahabaduge, W. Rance, J. Burst, M. Reese, D. Meysing, C. Wolden, J. Li, J. Beach, T. Gessert, W. Metzger, *et al.*, "High-efficiency, flexible cdte solar cells on ultra-thin glass substrates," *Applied Physics Letters*, vol. 106, no. 13, p. 133 501, 2015. 9

[37] S. Park, S. H. Shin, M. N. Yogeesh, A. L. Lee, S. Rahimi, and D. Akinwande, "Extremely high-frequency flexible graphene thin-film transistors," *IEEE Electron Device Letters*, vol. 37, no. 4, pp. 512–515, 2016. 9

[38] J. M. Grochocinski, R. Murakami, and T. Kuo, "The environmental benefits of thin glass for display substrates," *Journal of the Society for Information Display*, vol. 19, no. 11, pp. 821–824, 2011. 9

[39] R. Bollström, A. Määttänen, D. Tobjörk, P. Ihalainen, N. Kaihovirta, R. Österbacka, J. Peltonen, and M. Toivakka, "A multilayer coated fiber-based substrate suitable for printed functionality," *Organic Electronics*, vol. 10, no. 5, pp. 1020–1023, 2009. 10

[40] M. Zhu, Y. Wang, S. Zhu, L. Xu, C. Jia, J. Dai, J. Song, Y. Yao, Y. Wang, Y. Li, *et al.*, "Anisotropic, transparent films with aligned cellulose nanofibers," *Advanced Materials*, vol. 29, no. 21, p. 1 606 284, 2017. 10

[41] C.-Y. Wang, C. Fuentes-Hernandez, J.-C. Liu, A. Dindar, S. Choi, J. P. Youngblood, R. J. Moon, and B. Kippelen, "Stable low-voltage operation top-gate organic field-effect transistors on cellulose nanocrystal substrates," *ACS applied materials & interfaces*, vol. 7, no. 8, pp. 4804–4808, 2015. 10, 44, 45

[42] L. Meng, S. M. Mahpeykar, Q. Xiong, B. Ahvazi, and X. Wang, "Strain sensors on water-soluble cellulose nanofibril paper by polydimethylsiloxane (pdms) stencil lithography," *RSC Advances*, vol. 6, no. 88, pp. 85 427–85 433, 2016. 10, 91, 107

[43] L. M. Castano and A. B. Flatau, "Smart fabric sensors and e-textile technologies: A review," *Smart Materials and Structures*, vol. 23, no. 5, p. 053 001, 2014. 10, 11

[44] E. Bonderover and S. Wagner, "A woven inverter circuit for e-textile applications," *IEEE Electron Device Letters*, vol. 25, no. 5, pp. 295–297, 2004. 10, 11

[45] D.-H. Kim, Y.-S. Kim, J. Wu, Z. Liu, J. Song, H.-S. Kim, Y. Y. Huang, K.-C. Hwang, and J. A. Rogers, "Ultrathin silicon circuits with strain-isolation layers and mesh layouts for high-performance electronics on fabric, vinyl, leather, and paper," *Advanced Materials*, vol. 21, no. 36, pp. 3703–3707, 2009. 10

[46] D.-J. Kim, H.-J. Kim, K.-W. Seo, K.-H. Kim, T.-W. Kim, and H.-K. Kim, "Indium-free, highly transparent, flexible cu 2 o/cu/cu 2 o mesh electrodes for flexible touch screen panels," *Scientific reports*, vol. 5, p. 16 838, 2015. 12

[47] M.-G. Kang and L. J. Guo, "Nanoimprinted semitransparent metal electrodes and their application in organic light-emitting diodes," *Advanced Materials*, vol. 19, no. 10, pp. 1391–1396, 2007. 12

[48] B. Z. Jang and W. C. Huang, *Nano-scaled graphene plates*, US Patent 7,071,258, Jul. 2006. 13

[49] Y. H. Kim, C. Sachse, M. L. Machala, C. May, L. Müller-Meskamp, and K. Leo, "Highly conductive pedot: Pss electrode with optimized solvent and thermal post-treatment for ito-free organic solar cells," *Advanced Functional Materials*, vol. 21, no. 6, pp. 1076–1081, 2011. 13

[50] D. Alemu, H.-Y. Wei, K.-C. Ho, and C.-W. Chu, "Highly conductive pedot: Pss electrode by simple film treatment with methanol for ito-free polymer solar cells," *Energy & environmental science*, vol. 5, no. 11, pp. 9662–9671, 2012. 13

[51] M. Vosgueritchian, D. J. Lipomi, and Z. Bao, "Highly conductive and transparent pedot: Pss films with a fluorosurfactant for stretchable and flexible transparent electrodes," *Advanced functional materials*, vol. 22, no. 2, pp. 421–428, 2012. 13

[52] K. P. Goetz, D. Vermeulen, M. E. Payne, C. Kloc, L. E. McNeil, and O. D. Jurchescu, "Charge-transfer complexes: New perspectives on an old class of compounds," *Journal of Materials Chemistry C*, vol. 2, no. 17, pp. 3065–3076, 2014. 14

[53] R. D. Woodson, *Conductive rubber electrode*, US Patent 3,606,881, Sep. 1971. 14

[54] H. Cong and T. Pan, "Photopatternable conductive pdms materials for microfabrication," *Advanced Functional Materials*, vol. 18, no. 13, pp. 1912–1921, 2008. 14

[55] M. Sasaki, B. C. Karikkineth, K. Nagamine, H. Kaji, K. Torimitsu, and M. Nishizawa, "Highly conductive stretchable and biocompatible electrode–hydrogel hybrids for advanced tissue engineering," *Advanced healthcare materials*, vol. 3, no. 11, pp. 1919–1927, 2014. 14

[56] L. Pan, G. Yu, D. Zhai, H. R. Lee, W. Zhao, N. Liu, H. Wang, B. C.-K. Tee, Y. Shi, Y. Cui, *et al.*, "Hierarchical nanostructured conducting polymer hydrogel with high electrochemical activity," *Proceedings of the National Academy of Sciences*, vol. 109, no. 24, pp. 9287–9292, 2012. 14

[57] Y. Liu, J. Liu, S. Chen, T. Lei, Y. Kim, S. Niu, H. Wang, X. Wang, A. M. Foudeh, J. B.-H. Tok, *et al.*, "Soft and elastic hydrogel-based microelectronics for localized low-voltage neuromodulation," *Nature Biomedical Engineering*, vol. 3, no. 1, p. 58, 2019. 14

[58] M. E. El-Khouly, "Comparative study of the bimolecular electron transfer of fullerenes (c 60/c 70) and 9, 9-disubstituted fluorenes by laser flash photolysis," *Photochemical & Photobiological Sciences*, vol. 6, no. 5, pp. 539–544, 2007. 15

[59] Q. Cao, J. Tersoff, D. B. Farmer, Y. Zhu, and S.-J. Han, "Carbon nanotube transistors scaled to a 40-nanometer footprint," *Science*, vol. 356, no. 6345, pp. 1369–1372, 2017. 15

[60] S.-J. Han, J. Tang, B. Kumar, A. Falk, D. Farmer, G. Tulevski, K. Jenkins, A. Afzali, S. Oida, J. Ott, *et al.*, "High-speed logic integrated circuits with solution-processed self-assembled carbon nanotubes," *Nature nanotechnology*, vol. 12, no. 9, p. 861, 2017. 15

[61] Q. Cao, H.-s. Kim, N. Pimparkar, J. P. Kulkarni, C. Wang, M. Shim, K. Roy, M. A. Alam, and J. A. Rogers, "Medium-scale carbon nanotube thin-film integrated circuits on flexible plastic substrates," *Nature*, vol. 454, no. 7203, p. 495, 2008. 15

[62] D.-m. Sun, M. Y. Timmermans, Y. Tian, A. G. Nasibulin, E. I. Kauppinen, S. Kishimoto, T. Mizutani, and Y. Ohno, "Flexible high-performance carbon nanotube integrated circuits," *Nature nanotechnology*, vol. 6, no. 3, p. 156, 2011. 15

[63] J. Zhang, Y. Fu, C. Wang, P.-C. Chen, Z. Liu, W. Wei, C. Wu, M. E. Thompson, and C. Zhou, "Separated carbon nanotube macroelectronics for active matrix organic light-emitting diode displays," *Nano letters*, vol. 11, no. 11, pp. 4852–4858, 2011. 15

[64] L. Jiao, L. Zhang, X. Wang, G. Diankov, and H. Dai, "Narrow graphene nanoribbons from carbon nanotubes," *Nature*, vol. 458, no. 7240, p. 877, 2009. 15

[65] S. Lee, O. D. Iyore, S. Park, Y. G. Lee, S. Jandhyala, C. G. Kang, G. Mordi, Y. Kim, M. Quevedo-Lopez, B. E. Gnade, *et al.*, "Rigid substrate process to achieve high mobility in graphene field-effect transistors on a flexible substrate," *Carbon*, vol. 68, pp. 791–797, 2014. 15

[66] S.-L. Li, H. Miyazaki, A. Kumatani, A. Kanda, and K. Tsukagoshi, "Low operating bias and matched input- output characteristics in graphene logic inverters," *Nano letters*, vol. 10, no. 7, pp. 2357–2362, 2010. 15

[67] C.-F. Sung, D. Kekuda, L. F. Chu, Y.-Z. Lee, F.-C. Chen, M.-C. Wu, and C.-W. Chu, "Flexible fullerene field-effect transistors fabricated through solution processing," *Advanced materials*, vol. 21, no. 47, pp. 4845–4849, 2009. 16

[68] Y. Bai, Q. Dong, Y. Shao, Y. Deng, Q. Wang, L. Shen, D. Wang, W. Wei, and J. Huang, "Enhancing stability and efficiency of perovskite solar cells with crosslinkable silane-functionalized and doped fullerene," *Nature communications*, vol. 7, p. 12 806, 2016. 16

[69] Y.-C. Wang, X. Li, L. Zhu, X. Liu, W. Zhang, and J. Fang, "Efficient and hysteresis-free perovskite solar cells based on a solution processable polar fullerene electron transport layer," *Advanced Energy Materials*, vol. 7, no. 21, p. 1 701 144, 2017. 16

[70] T.-H. Kim, K.-S. Cho, E. K. Lee, S. J. Lee, J. Chae, J. W. Kim, D. H. Kim, J.-Y. Kwon, G. Amaratunga, S. Y. Lee, *et al.*, "Full-colour quantum dot displays fabricated by transfer printing," *Nature photonics*, vol. 5, no. 3, p. 176, 2011. 16, 37, 61, 99

[71] I. J. Kramer, G. Moreno-Bautista, J. C. Minor, D. Kopilovic, and E. H. Sargent, "Colloidal quantum dot solar cells on curved and flexible substrates," *Applied Physics Letters*, vol. 105, no. 16, p. 163 902, 2014. 16, 35

[72] H. Liu, M. Li, O. Voznyy, L. Hu, Q. Fu, D. Zhou, Z. Xia, E. H. Sargent, and J. Tang, "Physically flexible, rapid-response gas sensor based on colloidal quantum dot solids," *Advanced Materials*, vol. 26, no. 17, pp. 2718–2724, 2014. 16, 32, 61, 84, 99

[73] Z. Jin, X. Li, J. T. Mullen, and K. W. Kim, "Intrinsic transport properties of electrons and holes in monolayer transition-metal dichalcogenides," *Physical Review B*, vol. 90, no. 4, p. 045 422, 2014. 16

[74] M. Choi, Y. J. Park, B. K. Sharma, S.-R. Bae, S. Y. Kim, and J.-H. Ahn, "Flexible active-matrix organic light-emitting diode display enabled by mos2 thin-film transistor," *Science advances*, vol. 4, no. 4, eaas8721, 2018. 16

[75] W. Zhu, S. Park, M. N. Yogeesh, and D. Akinwande, "Advancements in 2d flexible nanoelectronics: From material perspectives to rf applications," *Flexible and Printed Electronics*, vol. 2, no. 4, p. 043 001, 2017. 16

[76] W. Zhu, M. N. Yogeesh, S. Yang, S. H. Aldave, J.-S. Kim, S. Sonde, L. Tao, N. Lu, and D. Akinwande, "Flexible black phosphorus ambipolar transistors, circuits and am demodulator," *Nano letters*, vol. 15, no. 3, pp. 1883–1890, 2015. 16

[77] Z. Lin, Y. Liu, U. Halim, M. Ding, Y. Liu, Y. Wang, C. Jia, P. Chen, X. Duan, C. Wang, *et al.*, "Solution-processable 2d semiconductors for high-performance large-area electronics," *Nature*, vol. 562, no. 7726, p. 254, 2018. 17

[78] Y. S. Rim, S.-H. Bae, H. Chen, N. De Marco, and Y. Yang, "Recent progress in materials and devices toward printable and flexible sensors," *Advanced Materials*, vol. 28, no. 22, pp. 4415–4440, 2016. 17, 19

[79] B. L. Danforth and E. R. Dickey, "Uv-curable top coat protection against mechanical abrasion for atomic layer deposition (ald) thin film barrier coatings," *Surface and Coatings Technology*, vol. 241, pp. 142–147, 2014. 18

[80] Y.-Y. Lin, R. D. Evans, E. Welch, B.-N. Hsu, A. C. Madison, and R. B. Fair, "Low voltage electrowetting-on-dielectric platform using multi-layer insulators," *Sensors and Actuators B: Chemical*, vol. 150, no. 1, pp. 465–470, 2010. 19

[81] R. P. Ortiz, A. Facchetti, and T. J. Marks, "High-k organic, inorganic, and hybrid dielectrics for low-voltage organic field-effect transistors," *Chemical reviews*, vol. 110, no. 1, pp. 205–239, 2009. 19

[82] D. Yu, Y.-Q. Yang, Z. Chen, Y. Tao, and Y.-F. Liu, "Recent progress on thin-film encapsulation technologies for organic electronic devices," *Optics Communications*, vol. 362, pp. 43–49, 2016. 20

[83] F. Garnier, R. Hajlaoui, A. Yassar, and P. Srivastava, "All-polymer field-effect transistor realized by printing techniques," *Science*, vol. 265, no. 5179, pp. 1684–1686, 1994. 21

[84] Z. Bao, Y. Feng, A. Dodabalapur, V. Raju, and A. J. Lovinger, "High-performance plastic transistors fabricated by printing techniques," *Chemistry of Materials*, vol. 9, no. 6, pp. 1299–1301, 1997. 21

[85] H. Sirringhaus, T. Kawase, R. Friend, T. Shimoda, M. Inbasekaran, W. Wu, and E. Woo, "High-resolution inkjet printing of all-polymer transistor circuits," *Science*, vol. 290, no. 5499, pp. 2123–2126, 2000. 21, 60

[86] Y. Aleeva and B. Pignataro, "Recent advances in upscalable wet methods and ink formulations for printed electronics," *Journal of Materials Chemistry C*, vol. 2, no. 32, pp. 6436–6453, 2014. 22

[87] W. J. Hyun, E. B. Secor, M. C. Hersam, C. D. Frisbie, and L. F. Francis, "High-resolution patterning of graphene by screen printing with a silicon stencil for highly flexible printed electronics," *Advanced Materials*, vol. 27, no. 1, pp. 109–115, 2015. 23

[88] X. Cao, H. Chen, X. Gu, B. Liu, W. Wang, Y. Cao, F. Wu, and C. Zhou, "Screen printing as a scalable and low-cost approach for rigid and flexible thin-film transistors using separated carbon nanotubes," *ACS nano*, vol. 8, no. 12, pp. 12 769–12 776, 2014. 23

[89] A. E. Ostfeld, I. Deckman, A. M. Gaikwad, C. M. Lochner, and A. C. Arias, "Screen printed passive components for flexible power electronics," *Scientific reports*, vol. 5, p. 15 959, 2015. 23

[90] J. Suikkola, T. Björninen, M. Mosallaei, T. Kankkunen, P. Iso-Ketola, L. Ukkonen, J. Vanhala, and M. Mäntysalo, "Screen-printing fabrication and characterization of stretchable electronics," *Scientific reports*, vol. 6, p. 25 784, 2016. 23

[91] J. Chang, X. Zhang, T. Ge, and J. Zhou, "Fully printed electronics on flexible substrates: High gain amplifiers and dac," *Organic Electronics*, vol. 15, no. 3, pp. 701–710, 2014. 23

[92] D. Numakura, "Advanced screen printing" practical approaches for printable & flexible electronics"," in *2008 3rd International Microsystems, Packaging, Assembly & Circuits Technology Conference*, IEEE, 2008, pp. 205–208. 23

[93] G.-K. Lau and M. Shrestha, "Ink-jet printing of micro-electro-mechanical systems (mems)," *Micromachines*, vol. 8, no. 6, p. 194, 2017. 23

[94] M. Ha, J.-W. T. Seo, P. L. Prabhumirashi, W. Zhang, M. L. Geier, M. J. Renn, C. H. Kim, M. C. Hersam, and C. D. Frisbie, "Aerosol jet printed, low voltage, electrolyte gated carbon nanotube ring oscillators with sub-5 μs stage delays," *Nano letters*, vol. 13, no. 3, pp. 954–960, 2013. 24

[95] D. McManus, S. Vranic, F. Withers, V. Sanchez-Romaguera, M. Macucci, H. Yang, R. Sorrentino, K. Parvez, S.-K. Son, G. Iannaccone, *et al.*, "Water-based and biocompatible 2d crystal inks for all-inkjet-printed heterostructures," *Nature nanotechnology*, vol. 12, no. 4, p. 343, 2017. 24

[96] H. Minemawari, T. Yamada, H. Matsui, J. Tsutsumi, S. Haas, R. Chiba, R. Kumai, and T. Hasegawa, "Inkjet printing of single-crystal films," *Nature*, vol. 475, no. 7356, p. 364, 2011. 24

[97] G. Grau, J. Cen, H. Kang, R. Kitsomboonloha, W. J. Scheideler, and V. Subramanian, "Gravure-printed electronics: Recent progress in tooling development, understanding of printing physics, and realization of printed devices," *Flexible and Printed Electronics*, vol. 1, no. 2, p. 023 002, 2016. 25

[98] P. H. Lau, K. Takei, C. Wang, Y. Ju, J. Kim, Z. Yu, T. Takahashi, G. Cho, and A. Javey, "Fully printed, high performance carbon nanotube thin-film transistors on flexible substrates," *Nano letters*, vol. 13, no. 8, pp. 3864–3869, 2013. 25, 60, 110

[99] H. Yan, Z. Chen, Y. Zheng, C. Newman, J. R. Quinn, F. Dötz, M. Kastler, and A. Facchetti, "A high-mobility electron-transporting polymer for printed transistors," *Nature*, vol. 457, no. 7230, p. 679, 2009. 25

[100] H. Zhu, B. B. Narakathu, Z. Fang, A. T. Aijazi, M. Joyce, M. Atashbar, and L. Hu, "A gravure printed antenna on shape-stable transparent nanopaper," *Nanoscale*, vol. 6, no. 15, pp. 9110–9115, 2014. 25

[101] G. Hernandez-Sosa, N. Bornemann, I. Ringle, M. Agari, E. Dörsam, N. Mechau, and U. Lemmer, "Rheological and drying considerations for uniformly gravure-printed layers: Towards large-area flexible organic light-emitting diodes," *Advanced Functional Materials*, vol. 23, no. 25, pp. 3164–3171, 2013. 25

[102] F. C. Krebs, "Fabrication and processing of polymer solar cells: A review of printing and coating techniques," *Solar energy materials and solar cells*, vol. 93, no. 4, pp. 394–412, 2009. 26

[103] S. Kim, H. Sojoudi, H. Zhao, D. Mariappan, G. H. McKinley, K. K. Gleason, and A. J. Hart, "Ultrathin high-resolution flexographic printing using nanoporous stamps," *Science advances*, vol. 2, no. 12, e1601660, 2016. 25

[104] C.-Y. Lo, O.-H. Huttunen, J. Hiitola-Keinanen, J. Petaja, H. Fujita, and H. Toshiyoshi, "Mems-controlled paper-like transmissive flexible display," *Journal of Microelectromechanical Systems*, vol. 19, no. 2, pp. 410–418, 2010. 26

[105] J. Olkkonen, K. Lehtinen, and T. Erho, "Flexographically printed fluidic structures in paper," *Analytical chemistry*, vol. 82, no. 24, pp. 10 246–10 250, 2010. 26

[106] O. Akbulut, A. A. Yu, and F. Stellacci, "Fabrication of biomolecular devices via supramolecular contact-based approaches," *Chemical Society Reviews*, vol. 39, no. 1, pp. 30–37, 2010. 27

[107] C. Thibault, C. Severac, E. Trévisiol, and C. Vieu, "Microtransfer molding of hydrophobic dendrimer," *Microelectronic engineering*, vol. 83, no. 4-9, pp. 1513–1516, 2006. 26

[108] F. Hua, Y. Sun, A. Gaur, M. A. Meitl, L. Bilhaut, L. Rotkina, J. Wang, P. Geil, M. Shim, J. A. Rogers, *et al.*, "Polymer imprint lithography with molecular-scale resolution," *Nano letters*, vol. 4, no. 12, pp. 2467–2471, 2004. 26

[109] H. Yang, W. R. Leow, T. Wang, J. Wang, J. Yu, K. He, D. Qi, C. Wan, and X. Chen, "3d printed photoresponsive devices based on shape memory composites," *Advanced Materials*, vol. 29, no. 33, p. 1 701 627, 2017. 27

[110] H. Ota, S. Emaminejad, Y. Gao, A. Zhao, E. Wu, S. Challa, K. Chen, H. M. Fahad, A. K. Jha, D. Kiriya, *et al.*, "Application of 3d printing for smart objects with embedded electronic sensors and systems," *Advanced Materials Technologies*, vol. 1, no. 1, p. 1 600 013, 2016. 27

[111] H. Yang, D. Qi, Z. Liu, B. K. Chandran, T. Wang, J. Yu, and X. Chen, "Soft thermal sensor with mechanical adaptability," *Advanced Materials*, vol. 28, no. 41, pp. 9175–9181, 2016. 27

[112] H. Yang, W. R. Leow, and X. Chen, "3d printing of flexible electronic devices," *Small Methods*, vol. 2, no. 1, p. 1 700 259, 2018. 27

[113] M. Miyasaka, "Flexible microelectronics becoming a reality with suftla transfer technology," *Journal of the Society for Information Display*, vol. 15, no. 7, pp. 479–484, 2007. 28, 29

[114] J. Haq, S. Ageno, G. B. Raupp, B. D. Vogt, and D. Loy, "Temporary bond-debond process for manufacture of flexible electronics: Impact of adhesive and carrier properties on performance," *Journal of Applied Physics*, vol. 108, no. 11, p. 114 917, 2010. 29

[115] M.-V. Ko, C.-y. Im, I. Lee, J.-h. Lee, S. Kim, W.-E. Hong, and J.-S. Ro, "10.4 l: Late-news paper: Joule heating induced lift-off technology for large area flexible amoled displays," in *SID Symposium Digest of Technical Papers*, Wiley Online Library, vol. 42, 2011, pp. 118–120. 29

[116] C.-C. Lee, J.-C. Ho, K.-J. Chen, M.-H. Yeh, Y.-Z. Lee, and J. Chen, "Highly flexible amoled integrated with ultrathin on-cell touch panel," in *2016 IEEE Photonics Conference (IPC)*, IEEE, 2016, pp. 665–666. 29

[117] S. Y. Chou, P. R. Krauss, W. Zhang, L. Guo, and L. Zhuang, "Sub-10 nm imprint lithography and applications," *Journal of Vacuum Science & Technology B: Microelectronics and Nanometer Structures Processing, Measurement, and Phenomena*, vol. 15, no. 6, pp. 2897–2904, 1997. 30

[118] Z. Jin, L. Gao, Q. Zhou, and J. Wang, "High-performance flexible ultraviolet photoconductors based on solution-processed ultrathin zno/au nanoparticle composite films," *Scientific reports*, vol. 4, p. 4268, 2014. 30

[119] C.-L. Hsu, H.-H. Li, and T.-J. Hsueh, "Water-and humidity-enhanced uv detector by using p-type la-doped zno nanowires on flexible polyimide substrate," *ACS applied materials & interfaces*, vol. 5, no. 21, pp. 11 142–11 151, 2013. 30, 31

[120] X. Hu, X. Zhang, L. Liang, J. Bao, S. Li, W. Yang, and Y. Xie, "High-performance flexible broadband photodetector based on organolead halide perovskite," *Advanced Functional Materials*, vol. 24, no. 46, pp. 7373–7380, 2014. 30

[121] J.-H. Seo, K. Zhang, M. Kim, D. Zhao, H. Yang, W. Zhou, and Z. Ma, "Flexible phototransistors based on single-crystalline silicon nanomembranes," *Advanced Optical Materials*, vol. 4, no. 1, pp. 120–125, 2016. 31

[122] Z. Zheng, L. Gan, J. Zhang, F. Zhuge, and T. Zhai, "An enhanced uv–vis–nir an d flexible photodetector based on electrospun zno nanowire array/pbs quantum dots film heterostructure," *Advanced Science*, vol. 4, no. 3, p. 1 600 316, 2017. 31

[123] H. Chang, Z. Sun, M. Saito, Q. Yuan, H. Zhang, J. Li, Z. Wang, T. Fujita, F. Ding, Z. Zheng, *et al.*, "Regulating infrared photoresponses in reduced graphene oxide phototransistors by defect and atomic structure control," *Acs Nano*, vol. 7, no. 7, pp. 6310–6320, 2013. 31

[124] N. Liu, H. Tian, G. Schwartz, J. B.-H. Tok, T.-L. Ren, and Z. Bao, "Large-area, transparent, and flexible infrared photodetector fabricated using pn junctions formed by n-doping chemical vapor deposition grown graphene," *Nano letters*, vol. 14, no. 7, pp. 3702–3708, 2014. 31

[125] Y. Tao, X. Wu, W. Wang, and J. Wang, "Flexible photodetector from ultraviolet to near infrared based on a sns 2 nanosheet microsphere film," *Journal of Materials Chemistry C*, vol. 3, no. 6, pp. 1347–1353, 2015. 31

[126] G. Azzellino, A. Grimoldi, M. Binda, M. Caironi, D. Natali, and M. Sampietro, "Fully inkjet-printed organic photodetectors with high quantum yield," *Advanced Materials*, vol. 25, no. 47, pp. 6829–6833, 2013. 31

[127] T. Q. Trung and N.-E. Lee, "Flexible and stretchable physical sensor integrated platforms for wearable human-activity monitoringand personal healthcare," *Advanced materials*, vol. 28, no. 22, pp. 4338–4372, 2016. 31

[128] N. T. Tien, Y. G. Seol, L. H. A. Dao, H. Y. Noh, and N.-E. Lee, "Utilizing highly crystalline pyroelectric material as functional gate dielectric in organic thin-film transistors," *Advanced Materials*, vol. 21, no. 8, pp. 910–915, 2009. 31

[129] L. Gao, Y. Zhang, V. Malyarchuk, L. Jia, K.-I. Jang, R. C. Webb, H. Fu, Y. Shi, G. Zhou, L. Shi, *et al.*, "Epidermal photonic devices for quantitative imaging of temperature and thermal transport characteristics of the skin," *Nature communications*, vol. 5, p. 4938, 2014. 31

[130] R. C. Webb, A. P. Bonifas, A. Behnaz, Y. Zhang, K. J. Yu, H. Cheng, M. Shi, Z. Bian, Z. Liu, Y.-S. Kim, *et al.*, "Ultrathin conformal devices for precise and continuous thermal characterization of human skin," *Nature materials*, vol. 12, no. 10, p. 938, 2013. 31

[131] J.-H. Lee, H.-J. Yoon, T. Y. Kim, M. K. Gupta, J. H. Lee, W. Seung, H. Ryu, and S.-W. Kim, "Micropatterned p (vdf-trfe) film-based piezoelectric nanogenerators for highly sensitive self-powered pressure sensors," *Advanced Functional Materials*, vol. 25, no. 21, pp. 3203–3209, 2015. 31

[132] J. Zhou, Y. Gu, P. Fei, W. Mai, Y. Gao, R. Yang, G. Bao, and Z. L. Wang, "Flexible piezotronic strain sensor," *Nano letters*, vol. 8, no. 9, pp. 3035–3040, 2008. 31

[133] H. C. Lim, B. Schulkin, M. Pulickal, S. Liu, R. Petrova, G. Thomas, S. Wagner, K. Sidhu, and J. F. Federici, "Flexible membrane pressure sensor," *Sensors and Actuators A: Physical*, vol. 119, no. 2, pp. 332–335, 2005. 31

[134] D. J. Lipomi, M. Vosgueritchian, B. C. Tee, S. L. Hellstrom, J. A. Lee, C. H. Fox, and Z. Bao, "Skin-like pressure and strain sensors based on transparent elastic films of carbon nanotubes," *Nature nanotechnology*, vol. 6, no. 12, p. 788, 2011. 32, 33, 58, 84, 85, 98, 99

[135] S.-E. Zhu, M. Krishna Ghatkesar, C. Zhang, and G. Janssen, "Graphene based piezoresistive pressure sensor," *Applied Physics Letters*, vol. 102, no. 16, p. 161 904, 2013. 32

[136] S. C. Mannsfeld, B. C. Tee, R. M. Stoltenberg, C. V. H. Chen, S. Barman, B. V. Muir, A. N. Sokolov, C. Reese, and Z. Bao, "Highly sensitive flexible pressure sensors with microstructured rubber dielectric layers," *Nature materials*, vol. 9, no. 10, p. 859, 2010. 32

[137] F. Faridbod, M. R. Ganjali, and M. Hosseini, "Lanthanide materials as chemosensors," in *Lanthanide-Based Multifunctional Materials*, Elsevier, 2018, pp. 411–454. 32

[138] K. Takei, W. Gao, C. Wang, and A. Javey, "Physical and chemical sensing with electronic skin," *Proceedings of the IEEE*, 2019. 32

[139] W.-D. Huang, H. Cao, S. Deb, M. Chiao, and J.-C. Chiao, "A flexible ph sensor based on the iridium oxide sensing film," *Sensors and Actuators A: Physical*, vol. 169, no. 1, pp. 1–11, 2011. 32

[140] Q. He, Z. Zeng, Z. Yin, H. Li, S. Wu, X. Huang, and H. Zhang, "Fabrication of flexible mos2 thin-film transistor arrays for practical gas-sensing applications," *Small*, vol. 8, no. 19, pp. 2994–2999, 2012. 32

[141] K. Melzer, V. D. Bhatt, T. Schuster, E. Jaworska, K. Maksymiuk, A. Michalska, P. Lugli, and G. Scarpa, "Flexible electrolyte-gated ion-selective sensors based on carbon nanotube networks," *IEEE Sensors Journal*, vol. 15, no. 6, pp. 3127–3134, 2014. 32

[142] W. Gao, H. Y. Nyein, Z. Shahpar, H. M. Fahad, K. Chen, S. Emaminejad, Y. Gao, L.-C. Tai, H. Ota, E. Wu, *et al.*, "Wearable microsensor array for multiplexed heavy metal monitoring of body fluids," *Acs Sensors*, vol. 1, no. 7, pp. 866–874, 2016. 32

[143] W. Gao, S. Emaminejad, H. Y. Y. Nyein, S. Challa, K. Chen, A. Peck, H. M. Fahad, H. Ota, H. Shiraki, D. Kiriya, *et al.*, "Fully integrated wearable sensor arrays for multiplexed in situ perspiration analysis," *Nature*, vol. 529, no. 7587, p. 509, 2016. 32, 33, 84, 116

[144] S. Nakata, M. Shiomi, Y. Fujita, T. Arie, S. Akita, and K. Takei, "A wearable ph sensor with high sensitivity based on a flexible charge-coupled device," *Nature Electronics*, vol. 1, no. 11, p. 596, 2018. 32

[145] J. Choi, R. Ghaffari, L. B. Baker, and J. A. Rogers, "Skin-interfaced systems for sweat collection and analytics," *Science advances*, vol. 4, no. 2, eaar3921, 2018. 33

[146] R. Dahiya, "E-skin: From humanoids to humans," *Proceedings of the IEEE*, vol. 107, no. 2, pp. 247–252, 2019. 33

[147] S. Wang, J. Xu, W. Wang, G.-J. N. Wang, R. Rastak, F. Molina-Lopez, J. W. Chung, S. Niu, V. R. Feig, J. Lopez, *et al.*, "Skin electronics from scalable fabrication of an intrinsically stretchable transistor array," *Nature*, vol. 555, no. 7694, p. 83, 2018. 33

[148] D. Yamamoto, S. Nakata, K. Kanao, T. Arie, S. Akita, and K. Takei, "A planar, multisensing wearable health monitoring device integrated with acceleration, temperature, and electrocardiogram sensors," *Advanced Materials Technologies*, vol. 2, no. 7, p. 1 700 057, 2017. 33

[149] Z. L. Wang and J. Song, "Piezoelectric nanogenerators based on zinc oxide nanowire arrays," *Science*, vol. 312, no. 5771, pp. 242–246, 2006. 34

[150] M.-Y. Choi, D. Choi, M.-J. Jin, I. Kim, S.-H. Kim, J.-Y. Choi, S. Y. Lee, J. M. Kim, and S.-W. Kim, "Mechanically powered transparent flexible charge-generating nanodevices with piezoelectric zno nanorods," *Advanced Materials*, vol. 21, no. 21, pp. 2185–2189, 2009. 34

[151] F.-R. Fan, Z.-Q. Tian, and Z. L. Wang, "Flexible triboelectric generator," *Nano energy*, vol. 1, no. 2, pp. 328–334, 2012. 34, 100

[152] A. Gregg, R. Blieden, A. Chang, and H. Ng, "Performance analysis of large scale, amorphous silicon, photovoltaic power systems," in *Conference Record of the Thirty-first IEEE Photovoltaic Specialists Conference, 2005.*, IEEE, 2005, pp. 1615–1618. 35

[153] P. Jackson, D. Hariskos, E. Lotter, S. Paetel, R. Wuerz, R. Menner, W. Wischmann, and M. Powalla, "New world record efficiency for cu (in, ga) se2 thin-film solar cells beyond 20%," *Progress in Photovoltaics: Research and Applications*, vol. 19, no. 7, pp. 894–897, 2011. 35

[154] A. Chirilă, S. Buecheler, F. Pianezzi, P. Bloesch, C. Gretener, A. R. Uhl, C. Fella, L. Kranz, J. Perrenoud, S. Seyrling, *et al.*, "Highly efficient cu (in, ga) se 2 solar cells grown on flexible polymer films," *Nature materials*, vol. 10, no. 11, p. 857, 2011. 35

[155] M. Pagliaro, R. Ciriminna, and G. Palmisano, "Flexible solar cells," *ChemSusChem: Chemistry & Sustainability Energy & Materials*, vol. 1, no. 11, pp. 880–891, 2008. 35

[156] S.-I. Na, S.-S. Kim, J. Jo, and D.-Y. Kim, "Efficient and flexible ito-free organic solar cells using highly conductive polymer anodes," *Advanced Materials*, vol. 20, no. 21, pp. 4061–4067, 2008. 35

[157] T. Kim, J.-H. Kim, T. E. Kang, C. Lee, H. Kang, M. Shin, C. Wang, B. Ma, U. Jeong, T.-S. Kim, *et al.*, "Flexible, highly efficient all-polymer solar cells," *Nature communications*, vol. 6, p. 8547, 2015. 35

[158] J. Huang, C.-Z. Li, C.-C. Chueh, S.-Q. Liu, J.-S. Yu, and A. K.-Y. Jen, "10.4% power conversion efficiency of ito-free organic photovoltaics through enhanced light trapping configuration," *Advanced Energy Materials*, vol. 5, no. 15, p. 1 500 406, 2015. 35

[159] A. S. Subbiah, N. Mathews, S. Mhaisalkar, and S. K. Sarkar, "Novel plasma-assisted low-temperature-processed sno2 thin films for efficient flexible perovskite photovoltaics," *ACS Energy Letters*, vol. 3, no. 7, pp. 1482–1491, 2018. 35

[160] W. Qu, M. Ploetner, and W.-J. Fischer, "Microfabrication of thermoelectric generators on flexible foil substrates as a power source for autonomous microsystems," *Journal of Micromechanics and Microengineering*, vol. 11, no. 2, p. 146, 2001. 35

[161] S. J. Kim, J. H. We, and B. J. Cho, "A wearable thermoelectric generator fabricated on a glass fabric," *Energy & Environmental Science*, vol. 7, no. 6, pp. 1959–1965, 2014. 35

[162] P. A. Penz, J. Sampsell, and D. Collins, "A plastic lcd design with high reliability and color-free readability," *IEEE Transactions on Electron Devices*, vol. 32, no. 11, pp. 2206–2213, 1985. 36

[163] J.-H. Hong, J. M. Shin, G. M. Kim, H. Joo, G. S. Park, I. B. Hwang, M. W. Kim, W.-S. Park, H. Y. Chu, and S. Kim, "9.1-inch stretchable amoled display based on ltps technology," *Journal of the Society for Information Display*, vol. 25, no. 3, pp. 194–199, 2017. 37

[164] Y. Liu, H. Wang, W. Zhao, M. Zhang, H. Qin, and Y. Xie, "Flexible, stretchable sensors for wearable health monitoring: Sensing mechanisms, materials, fabrication strategies and features," *Sensors*, vol. 18, no. 2, p. 645, 2018. 39

[165] S.-W. Hwang, H. Tao, D.-H. Kim, H. Cheng, J.-K. Song, E. Rill, M. A. Brenckle, B. Panilaitis, S. M. Won, Y.-S. Kim, *et al.*, "A physically transient form of silicon electronics," *Science*, vol. 337, no. 6102, pp. 1640–1644, 2012. 43, 44, 58

[166] C. J. Bettinger and Z. Bao, "Organic thin-film transistors fabricated on resorbable biomaterial substrates," *Advanced materials*, vol. 22, no. 5, pp. 651–655, 2010. 43

[167] X. Huang, Y. Liu, S.-W. Hwang, S.-K. Kang, D. Patnaik, J. F. Cortes, and J. A. Rogers, "Biodegradable materials for multilayer transient printed circuit boards," *Advanced Materials*, vol. 26, no. 43, pp. 7371–7377, 2014. 43

[168] S. Greengard, "Vanishing electronics," *Communications of the ACM*, vol. 56, no. 5, pp. 20–22, 2013. 43

[169] A. Mahdavi, L. Ferreira, C. Sundback, J. W. Nichol, E. P. Chan, D. J. Carter, C. J. Bettinger, S. Patanavanich, L. Chignozha, E. Ben-Joseph, *et al.*, "A biodegradable and biocompatible gecko-inspired tissue adhesive," *Proceedings of the National Academy of Sciences*, vol. 105, no. 7, pp. 2307–2312, 2008. 43

[170] M. Irimia-Vladu, P. A. Troshin, M. Reisinger, L. Shmygleva, Y. Kanbur, G. Schwabegger, M. Bodea, R. Schwödiauer, A. Mumyatov, J. W. Fergus, *et al.*, "Biocompatible and biodegradable materials for organic field-effect transistors," *Advanced Functional Materials*, vol. 20, no. 23, pp. 4069–4076, 2010. 43

[171] C. Dagdeviren, S.-W. Hwang, Y. Su, S. Kim, H. Cheng, O. Gur, R. Haney, F. G. Omenetto, Y. Huang, and J. A. Rogers, "Transient, biocompatible electronics and energy harvesters based on zno," *Small*, vol. 9, no. 20, pp. 3398–3404, 2013. 43

[172] C. H. Lee, J.-W. Jeong, Y. Liu, Y. Zhang, Y. Shi, S.-K. Kang, J. Kim, J. S. Kim, N. Y. Lee, B. H. Kim, *et al.*, "Materials and wireless microfluidic systems for electronics capable of chemical dissolution on demand," *Advanced Functional Materials*, vol. 25, no. 9, pp. 1338–1343, 2015. 43

[173] S.-W. Hwang, X. Huang, J.-H. Seo, J.-K. Song, S. Kim, S. Hage-Ali, H.-J. Chung, H. Tao, F. G. Omenetto, Z. Ma, *et al.*, "Materials for bioresorbable radio frequency electronics," *Advanced Materials*, vol. 25, no. 26, pp. 3526–3531, 2013. 43

[174] S. H. Jin, S.-K. Kang, I.-T. Cho, S. Y. Han, H. U. Chung, D. J. Lee, J. Shin, G. W. Baek, T.-i. Kim, J.-H. Lee, *et al.*, "Water-soluble thin film transistors and circuits based on amorphous indium–gallium–zinc oxide," *ACS applied materials & interfaces*, vol. 7, no. 15, pp. 8268–8274, 2015. 43

[175] S.-K. Kang, G. Park, K. Kim, S.-W. Hwang, H. Cheng, J. Shin, S. Chung, M. Kim, L. Yin, J. C. Lee, *et al.*, "Dissolution chemistry and biocompatibility of silicon-and germanium-based semiconductors for transient electronics," *ACS applied materials & interfaces*, vol. 7, no. 17, pp. 9297–9305, 2015. 43

[176] S.-K. Kang, S.-W. Hwang, H. Cheng, S. Yu, B. H. Kim, J.-H. Kim, Y. Huang, and J. A. Rogers, "Dissolution behaviors and applications of silicon oxides and nitrides in transient electronics," *Advanced Functional Materials*, vol. 24, no. 28, pp. 4427–4434, 2014. 43

[177] L. Yin, H. Cheng, S. Mao, R. Haasch, Y. Liu, X. Xie, S.-W. Hwang, H. Jain, S.-K. Kang, Y. Su, *et al.*, "Dissolvable metals for transient electronics," *Advanced Functional Materials*, vol. 24, no. 5, pp. 645–658, 2014. 43

[178] S.-K. Kang, S.-W. Hwang, S. Yu, J.-H. Seo, E. A. Corbin, J. Shin, D. S. Wie, R. Bashir, Z. Ma, and J. A. Rogers, "Biodegradable thin metal foils and spin-on glass materials for transient electronics," *Advanced Functional Materials*, vol. 25, no. 12, pp. 1789–1797, 2015. 43

[179] H. L. Hernandez, S.-K. Kang, O. P. Lee, S.-W. Hwang, J. A. Kaitz, B. Inci, C. W. Park, S. Chung, N. R. Sottos, J. S. Moore, *et al.*, "Triggered transience of metastable poly (phthalaldehyde) for transient electronics," *Advanced Materials*, vol. 26, no. 45, pp. 7637–7642, 2014. 43

[180] S.-W. Hwang, C. H. Lee, H. Cheng, J.-W. Jeong, S.-K. Kang, J.-H. Kim, J. Shin, J. Yang, Z. Liu, G. A. Ameer, *et al.*, "Biodegradable elastomers and silicon nanomembranes/nanoribbons for stretchable, transient electronics, and biosensors," *Nano letters*, vol. 15, no. 5, pp. 2801–2808, 2015. 43

[181] S.-W. Hwang, S.-K. Kang, X. Huang, M. A. Brenckle, F. G. Omenetto, and J. A. Rogers, "Materials for programmed, functional transformation in transient electronic systems," *Advanced Materials*, vol. 27, no. 1, pp. 47–52, 2015. 43

[182] R. J. Moon, A. Martini, J. Nairn, J. Simonsen, and J. Youngblood, "Cellulose nanomaterials review: Structure, properties and nanocomposites," *Chemical Society Reviews*, vol. 40, no. 7, pp. 3941–3994, 2011. 43

[183] Y. Zhou, C. Fuentes-Hernandez, T. M. Khan, J.-C. Liu, J. Hsu, J. W. Shim, A. Dindar, J. P. Youngblood, R. J. Moon, and B. Kippelen, "Recyclable organic solar cells on cellulose nanocrystal substrates," *Scientific reports*, vol. 3, p. 1536, 2013. 43, 44

[184] M. Nogi, M. Karakawa, N. Komoda, H. Yagyu, and T. T. Nge, "Transparent conductive nanofiber paper for foldable solar cells," *Scientific reports*, vol. 5, p. 17 254, 2015. 44

[185] S. Mun, L. Zhai, S.-K. Min, Y. Yun, and J. Kim, "Flexible and transparent strain sensor made with silver nanowire–coated cellulose," *Journal of Intelligent Material Systems and Structures*, vol. 27, no. 8, pp. 1011–1018, 2016. 44

[186] E. Najafabadi, Y. Zhou, K. Knauer, C. Fuentes-Hernandez, and B. Kippelen, "Efficient organic light-emitting diodes fabricated on cellulose nanocrystal substrates," *Applied Physics Letters*, vol. 105, no. 6, 124_1, 2014. 44

[187] H. Yagyu, T. Saito, A. Isogai, H. Koga, and M. Nogi, "Chemical modification of cellulose nanofibers for the production of highly thermal resistant and optically transparent nanopaper for paper devices," *ACS applied materials & interfaces*, vol. 7, no. 39, pp. 22 012–22 017, 2015. 44

[188] M.-C. Hsieh, C. Kim, M. Nogi, and K. Suganuma, "Electrically conductive lines on cellulose nanopaper for flexible electrical devices," *Nanoscale*, vol. 5, no. 19, pp. 9289–9295, 2013. 44

[189] S. Selvarasah, S. Chao, C.-L. Chen, S. Sridhar, A. Busnaina, A. Khademhosseini, and M. Dokmeci, "A reusable high aspect ratio parylene-c shadow mask technology for diverse micropatterning applications," *Sensors and Actuators A: Physical*, vol. 145, pp. 306–315, 2008. 44

[190] X. Huang, Y. Liu, H. Cheng, W.-J. Shin, J. A. Fan, Z. Liu, C.-J. Lu, G.-W. Kong, K. Chen, D. Patnaik, *et al.*, "Materials and designs for wireless epidermal sensors of hydration and strain," *Advanced Functional Materials*, vol. 24, no. 25, pp. 3846–3854, 2014. 45

[191] H. Wang, A. Chakraborty, and C. Luo, "Fabrication of au micropatterns on vertical si sidewalls using flexible pdms shadow masks," *Journal of Micromechanics and Microengineering*, vol. 20, no. 12, p. 127 001, 2010. 45

[192] M. Zheng, W. Li, M. Xu, N. Xu, P. Chen, M. Han, and B. Xie, "Strain sensors based on chromium nanoparticle arrays," *Nanoscale*, vol. 6, no. 8, pp. 3930–3933, 2014. 53, 58

[193] T. Yamada, Y. Hayamizu, Y. Yamamoto, Y. Yomogida, A. Izadi-Najafabadi, D. N. Futaba, and K. Hata, "A stretchable carbon nanotube strain sensor for human-motion detection," *Nature nanotechnology*, vol. 6, no. 5, p. 296, 2011. 53, 58, 84, 85, 98

[194] O. Kanoun, C. Müller, A. Benchirouf, A. Sanli, T. Dinh, A. Al-Hamry, L. Bu, C. Gerlach, and A. Bouhamed, "Flexible carbon nanotube films for high performance strain sensors," *Sensors*, vol. 14, no. 6, pp. 10 042–10 071, 2014. 53

[195] M. Huth, "Granular metals: From electronic correlations to strain-sensing applications," *Journal of Applied Physics*, vol. 107, no. 11, p. 113 709, 2010. 53

[196] J. Herrmann, K.-H. Müller, T. Reda, G. Baxter, B. d. Raguse, G. De Groot, R. Chai, M. Roberts, and L. Wieczorek, "Nanoparticle films as sensitive strain gauges," *Applied Physics Letters*, vol. 91, no. 18, p. 183 105, 2007. 53, 58

[197] I. Beloborodov, A. Lopatin, V. Vinokur, and K. Efetov, "Granular electronic systems," *Reviews of Modern Physics*, vol. 79, no. 2, p. 469, 2007. 53

[198] B. Abeles, P. Sheng, M. Coutts, and Y. Arie, "Structural and electrical properties of granular metal films," *Advances in Physics*, vol. 24, no. 3, pp. 407–461, 1975. 53

[199] T. Ji, S. Jung, and V. K. Varadan, "Field-controllable flexible strain sensors using pentacene semiconductors," *IEEE Electron Device Letters*, vol. 28, no. 12, pp. 1105–1107, 2007. 58, 84, 85

[200] G. Latessa, F. Brunetti, A. Reale, G. Saggio, and A. Di Carlo, "Piezoresistive behaviour of flexible pedot: Pss based sensors," *Sensors and Actuators B: Chemical*, vol. 139, no. 2, pp. 304–309, 2009. 58

[201] J. Tanner, D. Mousadakos, K. Giannakopoulos, E. Skotadis, and D. Tsoukalas, "High strain sensitivity controlled by the surface density of platinum nanoparticles," *Nanotechnology*, vol. 23, no. 28, p. 285 501, 2012. 58, 84, 85

[202] N. M. Sangeetha, N. Decorde, B. Viallet, G. Viau, and L. Ressier, "Nanoparticle-based strain gauges fabricated by convective self assembly: Strain sensitivity and hysteresis with respect to nanoparticle sizes," *The Journal of Physical Chemistry C*, vol. 117, no. 4, pp. 1935–1940, 2013. 58

[203] J. Lee, S. Kim, J. Lee, D. Yang, B. C. Park, S. Ryu, and I. Park, "A stretchable strain sensor based on a metal nanoparticle thin film for human motion detection," *Nanoscale*, vol. 6, no. 20, pp. 11 932–11 939, 2014. 58, 85

[204] W. Wu, "Inorganic nanomaterials for printed electronics: A review," *Nanoscale*, vol. 9, no. 22, pp. 7342–7372, 2017. 60

[205] Y. Zheng, Z. He, Y. Gao, and J. Liu, "Direct desktop printed-circuits-on-paper flexible electronics," *Scientific reports*, vol. 3, p. 1786, 2013. 60, 84, 85

[206] S. G. R. Bade, J. Li, X. Shan, Y. Ling, Y. Tian, T. Dilbeck, T. Besara, T. Geske, H. Gao, B. Ma, *et al.*, "Fully printed halide perovskite light-emitting diodes with silver nanowire electrodes," *ACS nano*, vol. 10, no. 2, pp. 1795–1801, 2015. 60

[207] E. B. Secor, P. L. Prabhumirashi, K. Puntambekar, M. L. Geier, and M. C. Hersam, "Inkjet printing of high conductivity, flexible graphene patterns," *The journal of physical chemistry letters*, vol. 4, no. 8, pp. 1347–1351, 2013. 60

[208] S. M. Sze and K. K. Ng, *Physics of semiconductor devices*. John wiley & sons, 2006. 61, 78, 106

[209] M. I. Nugraha, H. Matsui, S. Z. Bisri, M. Sytnyk, W. Heiss, M. A. Loi, and J. Takeya, "Tunable doping in pbs nanocrystal field-effect transistors using surface molecular dipoles," *APL Materials*, vol. 4, no. 11, p. 116 105, 2016. 61

[210] M. I. Nugraha, R. Häusermann, S. Z. Bisri, H. Matsui, M. Sytnyk, W. Heiss, J. Takeya, and M. A. Loi, "High mobility and low density of trap states in dual-solid-gated pbs nanocrystal field-effect transistors," *Advanced Materials*, vol. 27, no. 12, pp. 2107–2112, 2015. 61, 78, 106

[211] X.-H. Zhang, S. P. Tiwari, and B. Kippelen, "Pentacene organic field-effect transistors with polymeric dielectric interfaces: Performance and stability," *Organic Electronics*, vol. 10, no. 6, pp. 1133–1140, 2009. 61

[212] J. Du, Z. Du, J.-S. Hu, Z. Pan, Q. Shen, J. Sun, D. Long, H. Dong, L. Sun, X. Zhong, *et al.*, "Zn–cu–in–se quantum dot solar cells with a certified power conversion efficiency of 11.6%," *Journal of the American Chemical Society*, vol. 138, no. 12, pp. 4201–4209, 2016. 61

[213] Y. Zhou, D. Benetti, Z. Fan, H. Zhao, D. Ma, A. O. Govorov, A. Vomiero, and F. Rosei, "Near infrared, highly efficient luminescent solar concentrators," *Advanced Energy Materials*, vol. 6, no. 11, p. 1 501 913, 2016. 61

[214] Q. Xiong, F. I. Chowdhury, and X. Wang, "Filter-free narrowband photodetectors employing colloidal quantum dots," *IEEE Journal of Selected Topics in Quantum Electronics*, vol. 24, no. 2, pp. 1–6, 2017. 61

[215] L. Meng, Q. Xu, S. Fan, C. R. Dick, and X. Wang, "Field-effect enhanced triboelectric colloidal quantum dot flexible sensor," *Applied Physics Letters*, vol. 111, no. 18, p. 183 103, 2017. 61, 80, 111

[216] A. G. Shulga, V. Derenskyi, J. M. Salazar-Rios, D. N. Dirin, M. Fritsch, M. V. Kovalenko, U. Scherf, and M. A. Loi, "An all-solution-based hybrid cmos-like quantum dot/carbon nanotube inverter," *Advanced Materials*, vol. 29, no. 35, p. 1 701 764, 2017. 61

[217] F. Dubois, B. Mahler, B. Dubertret, E. Doris, and C. Mioskowski, "A versatile strategy for quantum dot ligand exchange," *Journal of the American Chemical Society*, vol. 129, no. 3, pp. 482–483, 2007. 61

[218] R. Wang, X. Wu, K. Xu, W. Zhou, Y. Shang, H. Tang, H. Chen, and Z. Ning, "Highly efficient inverted structural quantum dot solar cells," *Advanced Materials*, vol. 30, no. 7, p. 1 704 882, 2018. 61

[219] V. Sukhovatkin, S. Hinds, L. Brzozowski, and E. H. Sargent, "Colloidal quantum-dot photodetectors exploiting multiexciton generation," *Science*, vol. 324, no. 5934, pp. 1542–1544, 2009. 61

[220] Q. Xu, L. Meng, T. Zeng, K. Sinha, C. Dick, and X. Wang, "On-chip colloidal quantum dot devices with a cmos compatible architecture for near-infrared light sensing," *Optics letters*, vol. 44, no. 2, pp. 463–466, 2019. 61

[221] J. Tang, K. W. Kemp, S. Hoogland, K. S. Jeong, H. Liu, L. Levina, M. Furukawa, X. Wang, R. Debnath, D. Cha, *et al.*, "Colloidal-quantum-dot photovoltaics using atomic-ligand passivation," *Nature materials*, vol. 10, no. 10, p. 765, 2011. 61, 70, 81, 99, 118

[222] M. Liu, O. Voznyy, R. Sabatini, F. P. G. de Arquer, R. Munir, A. H. Balawi, X. Lan, F. Fan, G. Walters, A. R. Kirmani, *et al.*, "Hybrid organic–inorganic inks flatten the energy landscape in colloidal quantum dot solids," *Nature materials*, vol. 16, no. 2, p. 258, 2017. 62

[223] Q. Lin, H. J. Yun, W. Liu, H.-J. Song, N. S. Makarov, O. Isaienko, T. Nakotte, G. Chen, H. Luo, V. I. Klimov, *et al.*, "Phase-transfer ligand exchange of lead chalcogenide quantum dots for direct deposition of thick, highly conductive films," *Journal of the American Chemical Society*, vol. 139, no. 19, pp. 6644–6653, 2017. 62

[224] D. M. Balazs, N. Rizkia, H.-H. Fang, D. N. Dirin, J. Momand, B. J. Kooi, M. V. Kovalenko, and M. A. Loi, "Colloidal quantum dot inks for single-step-fabricated field-effect transistors: The importance of postdeposition ligand removal," *ACS applied materials & interfaces*, vol. 10, no. 6, pp. 5626–5632, 2018. 62

[225] T. P. Osedach, N. Zhao, T. L. Andrew, P. R. Brown, D. D. Wanger, D. B. Strasfeld, L.-Y. Chang, M. G. Bawendi, and V. Bulovic, "Bias-stress effect in 1, 2-ethanedithiol-treated pbs quantum dot field-effect transistors," *ACS nano*, vol. 6, no. 4, pp. 3121–3127, 2012. 62, 68

[226] S. Masala, V. Adinolfi, J.-P. Sun, S. D. Gobbo, O. Voznyy, I. J. Kramer, I. G. Hill, and E. H. Sargent, "The silicon: Colloidal quantum dot heterojunction," *Advanced Materials*, vol. 27, no. 45, pp. 7445–7450, 2015. 62

[227] X. Xie, H. Chung, C. Sow, and A. Wee, "Oxide growth and its dielectrical properties on alkylsilated native-sio2/si surface," *Chemical physics letters*, vol. 388, no. 4-6, pp. 446–451, 2004. 64

[228] J. Choi, Y. Kim, J. W. Jo, J. Kim, B. Sun, G. Walters, F. P. Garcıa de Arquer, R. Quintero-Bermudez, Y. Li, C. S. Tan, *et al.*, "Chloride passivation of zno electrodes improves charge extraction in colloidal quantum dot photovoltaics," *Advanced Materials*, vol. 29, no. 33, p. 1 702 350, 2017. 64

[229] G. Gu, M. G. Kane, J. E. Doty, and A. H. Firester, "Electron traps and hysteresis in pentacene-based organic thin-film transistors," *Applied Physics Letters*, vol. 87, no. 24, p. 243 512, 2005. 73

[230] H. Lin and S. Tiwari, "Localized charge trapping due to adsorption in nanotube field-effect transistor and its field-mediated transport," *Applied physics letters*, vol. 89, no. 7, p. 073 507, 2006. 73

[231] D. V. Talapin and C. B. Murray, "PbSe Nanocrystal Solids for N-and P-channel Thin Film Field-effect Transistors," *Science*, vol. 310, no. 5745, pp. 86–89, 2005. 78

[232] D. M. Balazs, D. N. Dirin, H.-H. Fang, L. Protesescu, G. H. ten Brink, B. J. Kooi, M. V. Kovalenko, and M. A. Loi, "Counterion-mediated Ligand Exchange for PbS Colloidal Quantum Dot Superlattices," *ACS nano*, vol. 9, no. 12, pp. 11 951–11 959, 2015. 78, 106

[233] J. Yin, P. Hu, J. Luo, L. Wang, M. F. Cohen, and C.-J. Zhong, "Molecularly mediated thin film assembly of nanoparticles on flexible devices: Electrical conductivity versus device strains in different gas/vapor environment," *ACS nano*, vol. 5, no. 8, pp. 6516–6526, 2011. 84, 145

[234] C. Mattmann, F. Clemens, and G. Tröster, "Sensor for measuring strain in textile," *Sensors*, vol. 8, no. 6, pp. 3719–3732, 2008. 84

[235] C. Cochrane, V. Koncar, M. Lewandowski, and C. Dufour, "Design and development of a flexible strain sensor for textile structures based on a conductive polymer composite," *Sensors*, vol. 7, no. 4, pp. 473–492, 2007. 84

[236] W. Honda, S. Harada, T. Arie, S. Akita, and K. Takei, "Wearable, human-interactive, health-monitoring, wireless devices fabricated by macroscale printing techniques," *Advanced Functional Materials*, vol. 24, no. 22, pp. 3299–3304, 2014. 84

[237] S. M. Mahpeykar, Q. Xiong, J. Wei, L. Meng, B. K. Russell, P. Hermansen, A. V. Singhal, and X. Wang, "Stretchable hexagonal diffraction gratings as optical diffusers for in situ tunable broadband photon management," *Advanced Optical Materials*, vol. 4, no. 7, pp. 1106–1114, 2016. 84

[238] D.-H. Kim, N. Lu, R. Ma, Y.-S. Kim, R.-H. Kim, S. Wang, J. Wu, S. M. Won, H. Tao, A. Islam, *et al.*, "Epidermal electronics," *science*, vol. 333, no. 6044, pp. 838–843, 2011. 84, 99

[239] W. Dobie, P. Isaac, and G. O. Gale, "Electrical resistance strain gauges," *American Journal of Physics*, vol. 18, pp. 117–118, 1950. 84

[240] Y. Joo, J. Byun, N. Seong, J. Ha, H. Kim, S. Kim, T. Kim, H. Im, D. Kim, and Y. Hong, "Silver nanowire-embedded pdms with a multiscale structure for a highly sensitive and robust flexible pressure sensor," *Nanoscale*, vol. 7, no. 14, pp. 6208–6215, 2015. 85

[241] N. Luo, W. Dai, C. Li, Z. Zhou, L. Lu, C. C. Poon, S.-C. Chen, Y. Zhang, and N. Zhao, "Flexible piezoresistive sensor patch enabling ultralow power cuffless blood pressure measurement," *Advanced Functional Materials*, vol. 26, no. 8, pp. 1178–1187, 2016. 85

[242] Y.-C. Lai, B.-W. Ye, C.-F. Lu, C.-T. Chen, M.-H. Jao, W.-F. Su, W.-Y. Hung, T.-Y. Lin, and Y.-F. Chen, "Extraordinarily sensitive and low-voltage operational cloth-based electronic skin for wearable sensing and multifunctional integration uses: A tactile-induced insulating-to-conducting transition," *Advanced Functional Materials*, vol. 26, no. 8, pp. 1286–1295, 2016. 85

[243] T. Someya, T. Sekitani, S. Iba, Y. Kato, H. Kawaguchi, and T. Sakurai, "A large-area, flexible pressure sensor matrix with organic field-effect transistors for artificial skin applications," *Proceedings of the National Academy of Sciences*, vol. 101, no. 27, pp. 9966–9970, 2004. 85

[244] J. Wang, J. Jiu, M. Nogi, T. Sugahara, S. Nagao, H. Koga, P. He, and K. Suganuma, "A highly sensitive and flexible pressure sensor with electrodes and elastomeric interlayer containing silver nanowires," *Nanoscale*, vol. 7, no. 7, pp. 2926–2932, 2015. 85

[245] X.-Z. Jiang, Y.-J. Sun, Z. Fan, and T.-Y. Zhang, "Integrated flexible, waterproof, transparent, and self-powered tactile sensing panel," *ACS nano*, vol. 10, no. 8, pp. 7696–7704, 2016. 85, 100

[246] L. Tang and N. Y. Lee, "A facile route for irreversible bonding of plastic-pdms hybrid microdevices at room temperature," *Lab on a Chip*, vol. 10, no. 10, pp. 1274–1280, 2010. 91

[247] D.-H. Kim, J.-H. Ahn, W. M. Choi, H.-S. Kim, T.-H. Kim, J. Song, Y. Y. Huang, Z. Liu, C. Lu, and J. A. Rogers, "Stretchable and foldable silicon integrated circuits," *Science*, vol. 320, no. 5875, pp. 507–511, 2008. 99

[248] L. Meng, S. Fan, S. M. Mahpeykar, and X. Wang, "Digital microelectromechanical sensor with an engineered polydimethylsiloxane (pdms) bridge structure," *Nanoscale*, vol. 9, no. 3, pp. 1257–1262, 2017. 99

[249] S. Lee, A. Reuveny, J. Reeder, S. Lee, H. Jin, Q. Liu, T. Yokota, T. Sekitani, T. Isoyama, Y. Abe, *et al.*, "A transparent bending-insensitive pressure sensor," *Nature nanotechnology*, vol. 11, no. 5, p. 472, 2016. 99

[250] Y. Yamamoto, S. Harada, D. Yamamoto, W. Honda, T. Arie, S. Akita, and K. Takei, "Printed multifunctional flexible device with an integrated motion sensor for health care monitoring," *Science advances*, vol. 2, no. 11, e1601473, 2016. 99

[251] M. Koo, K.-I. Park, S. H. Lee, M. Suh, D. Y. Jeon, J. W. Choi, K. Kang, and K. J. Lee, "Bendable inorganic thin-film battery for fully flexible electronic systems," *Nano letters*, vol. 12, no. 9, pp. 4810–4816, 2012. 99

[252] I. Graz, M. Kaltenbrunner, C. Keplinger, R. Schwödiauer, S. Bauer, S. P. Lacour, and S. Wagner, "Flexible ferroelectret field-effect transistor for large-area sensor skins and microphones," *Applied physics letters*, vol. 89, no. 7, p. 073 501, 2006. 99

[253] C.-S. Kim, B. K. Kang, J. H. Jung, M. J. Lee, H. B. Kim, S. S. Oh, S. H. Jang, H. J. Lee, H. Kastuyoshi, and J. K. Shin, "Active matrix touch sensor perceiving liquid crystal capacitance with amorphous silicon thin film transistors," *Japanese Journal of Applied Physics*, vol. 49, no. 3S, p. 03CC03, 2010. 99

[254] H.-K. Kim, S. Lee, and K.-S. Yun, "Capacitive tactile sensor array for touch screen application," *Sensors and Actuators A: Physical*, vol. 165, no. 1, pp. 2–7, 2011. 99

[255] E.-S. Choi, M.-H. Jeong, K. W. Choi, C. Lim, and S.-B. Lee, "Flexible and transparent touch sensor using single-wall carbon nanotube thin-films," in *2010 3rd International Nanoelectronics Conference (INEC)*, IEEE, 2010, pp. 718–719. 99

[256] J. Lee, P. Lee, H. B. Lee, S. Hong, I. Lee, J. Yeo, S. S. Lee, T.-S. Kim, D. Lee, and S. H. Ko, "Room-temperature nanosoldering of a very long metal nanowire network by conducting-polymer-assisted joining for a flexible touch-panel application," *Advanced Functional Materials*, vol. 23, no. 34, pp. 4171–4176, 2013. 99

[257] E. H. Sargent, "Colloidal quantum dot solar cells," *Nature photonics*, vol. 6, no. 3, p. 133, 2012. 99

[258] W.-k. Koh, S. R. Saudari, A. T. Fafarman, C. R. Kagan, and C. B. Murray, "Thiocyanate-capped pbs nanocubes: Ambipolar transport enables quantum dot based circuits on a flexible substrate," *Nano letters*, vol. 11, no. 11, pp. 4764–4767, 2011. 99

[259] Y. Shirasaki, G. J. Supran, M. G. Bawendi, and V. Bulović, "Emergence of colloidal quantum-dot light-emitting technologies," *Nature photonics*, vol. 7, no. 1, p. 13, 2013. 99

[260] X. Dai, Z. Zhang, Y. Jin, Y. Niu, H. Cao, X. Liang, L. Chen, J. Wang, and X. Peng, "Solution-processed, high-performance light-emitting diodes based on quantum dots," *Nature*, vol. 515, no. 7525, p. 96, 2014. 99

[261] V. Wood, M. J. Panzer, J. Chen, M. S. Bradley, J. E. Halpert, M. G. Bawendi, and V. Bulović, "Inkjet-printed quantum dot–polymer composites for full-color ac-driven displays," *Advanced Materials*, vol. 21, no. 21, pp. 2151–2155, 2009. 99

[262] D. K. Kim, Y. Lai, B. T. Diroll, C. B. Murray, and C. R. Kagan, "Flexible and low-voltage integrated circuits constructed from high-performance nanocrystal transistors," *Nature communications*, vol. 3, p. 1216, 2012. 100

[263] B. Meng, W. Tang, Z.-h. Too, X. Zhang, M. Han, W. Liu, and H. Zhang, "A transparent single-friction-surface triboelectric generator and self-powered touch sensor," *Energy & Environmental Science*, vol. 6, no. 11, pp. 3235–3240, 2013. 100

[264] J. Chen, G. Zhu, J. Yang, Q. Jing, P. Bai, W. Yang, X. Qi, Y. Su, and Z. L. Wang, "Personalized keystroke dynamics for self-powered human–machine interfacing," *ACS nano*, vol. 9, no. 1, pp. 105–116, 2015. 100

[265] S. W. Thomas III, S. J. Vella, G. K. Kaufman, and G. M. Whitesides, "Patterns of electrostatic charge and discharge in contact electrification," *Angewandte Chemie International Edition*, vol. 47, no. 35, pp. 6654–6656, 2008. 106

[266] K.-E. Byun, Y. Cho, M. Seol, S. Kim, S.-W. Kim, H.-J. Shin, S. Park, and S. Hwang, "Control of triboelectrification by engineering surface dipole and surface electronic state," *ACS applied materials & interfaces*, vol. 8, no. 28, pp. 18 519–18 525, 2016. 106

[267] H. Y. Li, L. Su, S. Y. Kuang, C. F. Pan, G. Zhu, and Z. L. Wang, "Significant enhancement of triboelectric charge density by fluorinated surface modification in nanoscale for converting mechanical energy," *Advanced Functional Materials*, vol. 25, no. 35, pp. 5691–5697, 2015. 106

[268] Y. H. Ko, G. Nagaraju, and J. S. Yu, "Multi-stacked pdms-based triboelectric generators with conductive textile for efficient energy harvesting," *RSC Advances*, vol. 5, no. 9, pp. 6437–6442, 2015. 110

[269] L. Meng, Q. Xu, L. Dan, and X. Wang, "Triboelectric flexible sensors employing single-walled carbon nanotube field-effect transistors," in *2018 International Flexible Electronics Technology Conference (IFETC)*, IEEE, 2018, pp. 1–2. 110

[270] J. Xu, O. Voznyy, M. Liu, A. R. Kirmani, G. Walters, R. Munir, M. Abdelsamie, A. H. Proppe, A. Sarkar, F. P. G. de Arquer, *et al.*, "2d matrix engineering for homogeneous quantum dot coupling in photovoltaic solids," *Nature nanotechnology*, vol. 13, no. 6, p. 456, 2018. 118

Appendix A

Mechanical theories for flexible electronic devices

Regarding the mechanical properties, materials can be generally divided into to categories, ductile materials and brittle materials. Ductile material refers to a material which will plastically deform when subjected stress. Unlike ductile material, a brittle material will break without significant plastic deformation when stress applied. The ductile materials can be divided into very ductile materials and moderately ductile materials. It should be noted that, paper, as a popular substrate material for flexible electronic devices, is a moderately ductile material.

In mechanical theories, ones usually utilize the σ (stress) vs. ϵ (strain) curve to illustrate materials' basic mechanical properties. Strain is a measure of deformation relative to its original length. It can be expressed as:

$$\epsilon = \frac{\Delta l}{l} \tag{A.1}$$

The stress is actually the internal force induced by the strain. In an elastic material, the stress and strain can be related by Young's modulus:

$$\sigma = Y\epsilon \tag{A.2}$$

Where Y is Young's modulus and the stress and strain are both uniaxial.

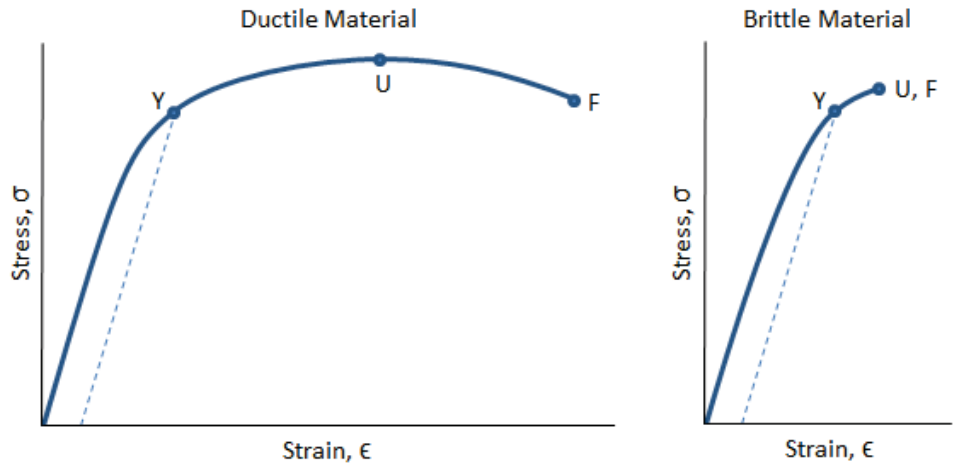

Figure A.1: stess-strain curves of typical ductile and brittle materials

As shown in Fig. A.1, it can be seen that at first, both material will go through a linear region, in which the Young's modulus can be calculated by the slope. The U points beyond the linear region represents the ultimate tensile stress, which means it is the largest stress this material can reach. Brittle materials will fail at this point. However, ductile material will fail after this point.

The model could be a little bit more complex, if we consider a 2D condition. A uniaxial strain will affect another axis. Usually, the two strains on two perpendicular axis will be opposite. The relation between these two strains can be described as:

$$\nu = -\frac{d\epsilon_{trans}}{d\epsilon_{axial}} \tag{A.3}$$

The commercially available strain sensors, strain gauges, are usually characterized by bending strain. According to the previous report[233], the strain on a bended substrate with the bending radius r can be calculated as shown in Fig. A.2. At relax condition, the length of the substrate can be expressed as L and the thickness is t. After being bent on a stainless steel block with a radius of r, the condition of the substrate is shown as the bottom graph in Fig. A.2. It is common to assume that the centre of the substrate will not be stretched or compressed. The length of the central line is still L. However, the top is stretched and the bottom is compressed. The top of the substrate

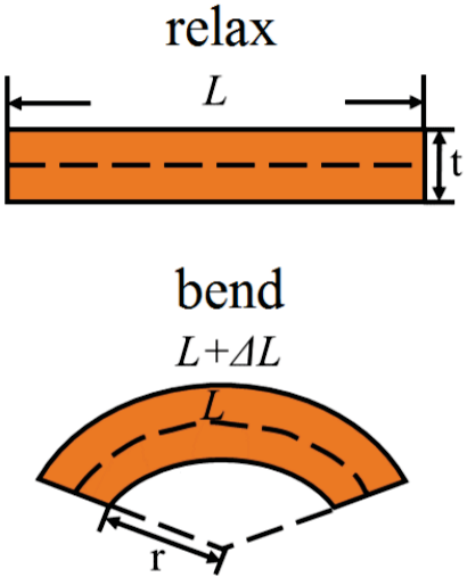

Figure A.2: Illustration of bending strain calculation.

is stretched to $L + \Delta L$. The top and bottom of the substrate are bended to radius of $r + t/2$ and $r + t$. Thus we can get equations as below:

$$\frac{t/2}{r + t/2} = \frac{L + \Delta L}{r + t} \tag{A.4}$$

It is derived to get:

$$\frac{t/2}{r + t/2} = \frac{\Delta L}{L} \tag{A.5}$$

$$\epsilon = \frac{t/2}{r + t/2} \tag{A.6}$$

Where ϵ represents the strain of the top. The calculated results are shown in the table below.

Bending radius	**top surface strain**
2.0 cm	0.498%
1.5 cm	0.662%
1.3 cm	0.763%
1.2 cm	0.826%

Table A.1: Calculated results of the relation between top surface strain and bending radius.

Appendix B

Experimental setups

B.1 CQD synthesis

PbS CQDs were synthesized in a three-neck flask as shown in B.1. The lead oleate precursor was heated by a digitally controlled heating mantle. The thermometer should be in the solution through one neck. Another neck was connected by the nitrogen/vacuum pipeline while the pipeline was connected to a Schlenk line, which enables fast switch between nitrogen and vacuum. The other neck was used in injection.

As stated before, to get fast switching between nitrogen and vacuum, a Schlenk line (Fig. B.2) was utilized. The Schlenk line has two glass pipelines, one for nitrogen and the other one for vaccum. There are several two-way switches between them. These switches can make fast switch between these two pipelines.

B.2 Electrical measurement setup

All the electrical measurements including bending electrical measurements and FET measurements were performed on a Wentworth probe station as shown in Fig. B.3. The probe station has a gold-coated chuck on which one can create a gate contact. Two Keithley 2400 were applied to perform all the 2-terminal and 3-terminal testing. They can apply voltage and test current simultaneously.

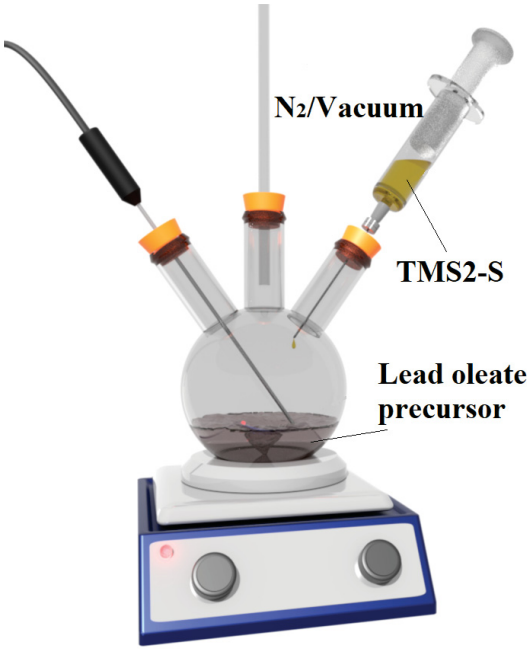

Figure B.1: CQD synthesis experimental setup.

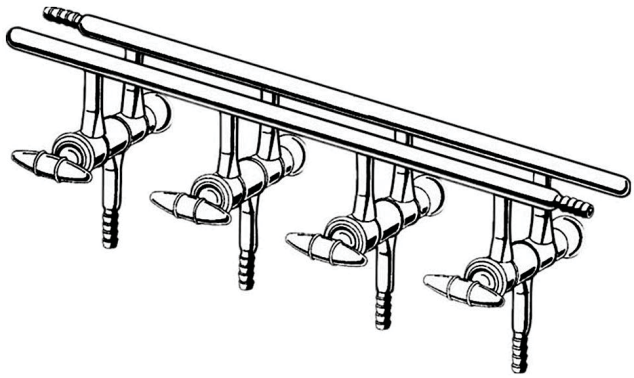

Figure B.2: Schematic of a Schlenk line.

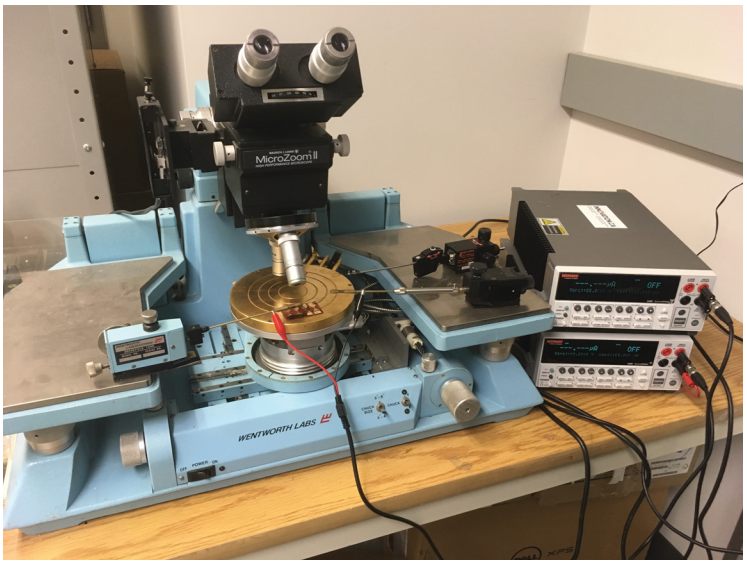

Figure B.3: Picture of the Wentworth probe station and Keithley 2400 sourcemeters.

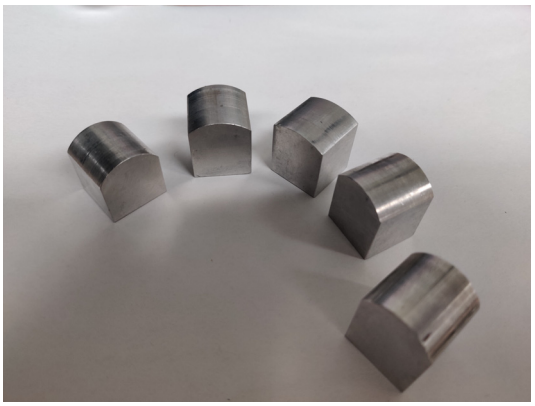

Figure B.4: Picture of the steel blocks in bending testing.

The blocks used in bending testing are shown in Fig. B.4. Top surfaces of these blocks are curved with different radius. If the device was tightly attached onto the top surface, it can be bent to a certain radius.